

THE UNIVERSITY OF CHICAGO

BEHAVIORAL AND ELECTROPHYSIOLOGICAL INVESTIGATION OF EARLY VISUAL PROCESSING IN

THE FLY

A DISSERTATION SUBMITTED TO

THE FACULTY OF THE DIVISION OF THE BIOLOGICAL SCIENCES

AND THE PRITZKER SCHOOL OF MEDICINE

IN CANDIDACY FOR THE DEGREE OF

DOCTOR OF PHILOSOPHY

BIOLOGY

BY

JOHN C. TUTHILL

CHICAGO, ILLINOIS

MARCH 2012

UMI Number: 3499800

All rights reserved

INFORMATION TO ALL USERS

The quality of this reproduction is dependent on the quality of the copy submitted.

In the unlikely event that the author did not send a complete manuscript and there are missing pages, these will be noted. Also, if material had to be removed, a note will indicate the deletion.



UMI 3499800

Copyright 2012 by ProQuest LLC.

All rights reserved. This edition of the work is protected against unauthorized copying under Title 17, United States Code.



ProQuest LLC.  
789 East Eisenhower Parkway  
P.O. Box 1346  
Ann Arbor, MI 48106 - 1346

**Copyright © 2012 by John Tuthill  
All Rights Reserved**

## Table of Contents

<b>List of figures .....</b>	v
<b>List of tables.....</b>	vii
<b>Acknowledgements.....</b>	viii
<b>Chapter 1. Introduction.....</b>	1
Anatomy.....	4
Electrophysiology.....	11
Behavior .....	23
<b>Chapter 2.</b>	
<b>Neural correlates of illusory motion perception in <i>Drosophila</i> .....</b>	32
Abstract.....	32
Introduction .....	32
Results.....	34
Discussion.....	52
Materials and methods.....	59
<b>Chapter 3.</b>	
<b>Behavioral function of a novel class of wide-field neurons in the <i>Drosophila</i> lamina .....</b>	68
Abstract.....	68

Introduction .....	68
Results.....	72
Discussion.....	94
Materials and methods.....	96
<b>Chapter 4.</b>	
<b>Electrophysiological characterization of a wide-field neuron in the <i>Drosophila</i> lamina .....</b>	<b>99</b>
Abstract.....	99
Introduction .....	99
Results.....	101
Discussion.....	116
Materials and methods.....	121
<b>Chapter 5. Concluding remarks.....</b>	<b>126</b>
<b>References .....</b>	<b>136</b>

## List of figures

1.1	Gross anatomy of the fly visual system	2
1.2	Neuron classes of the fly lamina	5
1.3	Electrophysiology of fly photoreceptors	13
1.4	Electrophysiology of fly lamina monopolar cells	15
1.5	Visual behavior in flies	26
2.1	Fly responses to reverse-phi motion	35
2.2	Restricting motion stimuli to narrow windows	37
2.3	Expanding reverse-phi stimuli	38
2.4	Modeling fly responses to reverse-phi motion	40
2.5	Varying properties of the EMD model	42
2.6	Walking behavior of flies in 2-photon imaging experiments	44
2.7	2-photon imaging of reverse-phi responses in the lobula plate	46
2.8	Independently varying stimulus flicker and velocity	48
2.9	Raw data from independent flicker imaging experiments	49
2.10	Bilateral comparison of standard and reverse-phi motion	51
2.11	Proposed alterations to the EMD model	56
2.12	Raw data from bilateral comparison imaging experiments	65
3.1	Anatomy of wide-field neurons	73
3.2	Silencing wide-field neurons alters optomotor behavior	76
3.3	Motion nulling	78
3.3	Motion nulling (cont.)	79
3.4	Other optomotor behaviors	80
3.5	Responses to laterally restricted motion stimuli	82

3.6	Orientation toward a static flicker stimulus	<b>83</b>
3.7	Small-field orientation responses	<b>84</b>
3.8	Steering responses to oscillating optic-flow fields	<b>87</b>
3.9	Fly responses to ON/OFF stimuli	<b>89</b>
3.10	TrpA1 activation of wide-field neurons: optomotor responses	<b>92</b>
3.11	Small-field responses following wide-field neuron activation	<b>93</b>
4.1	Targeted patch-clamp recordings from wide-field neurons	<b>101</b>
4.2	Spontaneous oscillations in wide-field neurons	<b>102</b>
4.3	Light-evoked properties of wide-field neurons	<b>103</b>
4.4	Spatial receptive fields	<b>104</b>
4.5	Asymmetry of receptive fields	<b>106</b>
4.6	Absence of motion selectivity	<b>107</b>
4.7	Flight increases wide-field neuron gain	<b>108</b>
4.8	Octopamine changes wide-field neuron response properties	<b>109</b>
4.9	Modulation of intrinsic spiking by octopamine	<b>111</b>
4.10	Octopamine alters responses to light decrements	<b>112</b>
4.11	Octopamine increases the rate of adaptation	<b>113</b>
4.12	Octopamine increases selectivity for higher frequencies	<b>114</b>
4.13	A computational model of wide-field neuron feedback	<b>115</b>

## **List of tables**

3.1	Mean turn amplitude values	<b>91</b>
-----	----------------------------	-----------

## Acknowledgements

Two people directly contributed data to this thesis: Aljoscha Nern built the two Split-GAL4 driver lines for the lamina wide-field cell, and characterized its anatomy, and Eugenia Chiappe performed the 2-photon calcium imaging experiments. I am grateful to the Janelia Fly Core for help with fly care, Tyler Ofstad for building the w+ (DL); UAS-kir2.1 effector stock, and Barret Pfeiffer for constructing many genetic constructs. I received useful technical assistance from many people, including Niko Kladt, Johannes Seelig, Parvez Ahammad, Frank Midgley, Jinyang Liu, Magnus Karlsson, Dale Cabaniss, and Tanya Tabachnik. I am particularly grateful to Gabe Murphy, Mehmet Fisek, Rachel Wilson, Eugenia Chiappe and Vivek Jayaraman for assistance in developing the electrophysiology preparation. This work benefited greatly from discussions with many people, including Aljoscha Nern, Eugenia Chiappe, Vivek Jayaraman, Gerry Rubin, Bart Borghuis, Gabe Murphy, Matt Smear, Martin Lankheet, Hans van Hateren, Niko Kladt, Tyler Ofstad, Eric Hoopfer, Stephen Huston, Katie von Reyn, Gwyneth Card, Gaby Maimon, Michael Dickinson, Arjun Bharioke, Shaul Druckmann, Mitya Chklovskii, and Jeremy Freeman. I would like to thank Kevin Moses for recruiting me to the Janelia/U-Chicago graduate program. I am also indebted to my graduate committee for their encouragement and guidance, particularly Melina Hale for providing me with space and support in her lab during my time in Chicago. I owe a great deal to my two scientific role models, Arpiar Saunders and Ben Ewen-Campen, who inspire me every day with their beautiful minds and bodies. And, finally, this thesis is dedicated to my wonderful girlfriend, Sarah J. Bard, whose pacifying presence was essential to the completion of this work.

# Chapter 1

## Introduction

From a human perspective, the eye of a fly is a peculiar structure. Unlike the camera-like design of vertebrates, the fly eye consists of many hundreds of lenses (Fig. 1.1A). This unfamiliar optical architecture has invited much speculation about its function. In 1695, van Leeuwenhoek, looking at an insect cornea through a microscope, conjectured that the many lenses of the fly eye formed multiple images of the external world (Land and Nilsson, 2002). However, van Leeuwenhoek's observations were misleading, and we now know that each lens focuses light from distinct points in visual space onto small groups of neighboring photoreceptors (Exner, 1891). The fly's brain then integrates the information across these receptors, forming an internal representation of the external environment. Therefore, despite outward appearances, visual processing in the fly eye is highly similar to that of the vertebrate eye (Sanes and Zipursky, 2010).

The *Drosophila* eye is composed of ~750 discrete visual units, called "ommatidia", which collectively sample 85% of visual space (Fig. 1.1). A lens within each ommatidium focuses light onto 8 primary photo-sensitive neurons that can be divided into two classes: the outer (R1-R6) and inner (R7-R8) photoreceptors. The outer photoreceptors express a single opsin, and are therefore achromatic, while the inner photoreceptors express a mixture of four opsins and are thought to underlie color vision.

The first stage of neural integration in the fly visual system is the lamina, where the outer photoreceptor axons terminate (Fig. 1.1C). Six photoreceptors sampling the same point in visual space project to the same lamina column, or "cartridge". The lamina, as well as the subsequent

visual neuropils, the medulla and lobula complex, are organized retinotopically—each visual cartridge represents a discrete sample of the visual world,  $\sim 5^\circ$  in *Drosophila* (Heisenberg and Wolf, 1984).

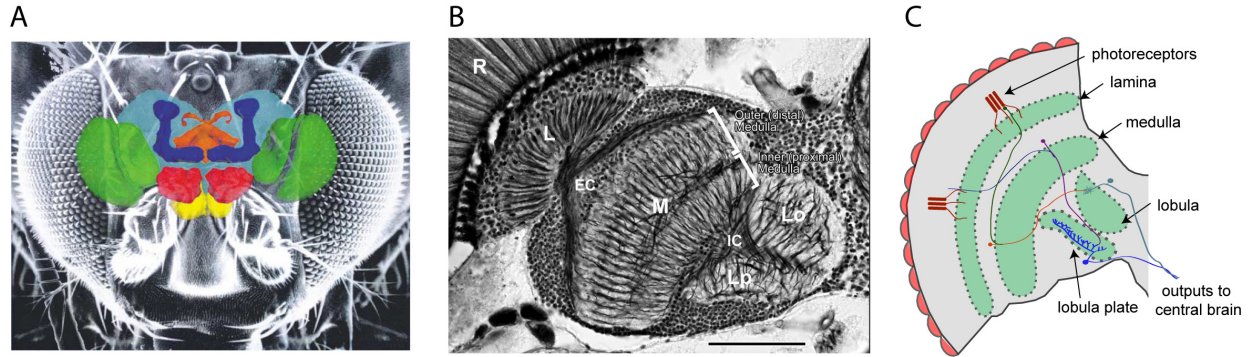


**Fig. 1.1.** Gross anatomy of the fly visual system. **(A)** A simplified model of the *Drosophila* brain superimposed on the fly head. Green, optic lobes; yellow, suboesophageal ganglion; red, antennal lobes; blue, mushroom bodies; orange, central complex. Modified from Heisenberg (2003). **(B)** A horizontal section of the *Drosophila* visual system stained by the Bodian method, demonstrating the columnar organization of the optic lobes. R, photoreceptors; L, lamina; EC, external chiasm; M, medulla; IC, internal chiasm; Lo, lobula; Lp, lobula plate. Modified from Takemura et al., (2008). **(C)** Schematic model of the fly optic lobe.

In addition to the photoreceptor axons, each lamina cartridge contains 11 anatomically identifiable neuron types (Fig. 2.1A). Eight of these neuronal classes are columnar—they occur in each lamina column. Five of the columnar neurons are the lamina monopolar cells L1-L5, which have cell bodies along the distal lamina and send processes toward the central brain, into the medulla. The largest of these, L1, L2, and L3, are known as the large lamina monopolar cells, or LMCs. The LMCs receive direct synaptic input from the R1-R6 photoreceptors, but L4 and L5 do not. Two centrifugal neurons, C2 and C3, project centripetally into the lamina, as does the basket cell T1. The other three lamina cell types, which span multiple columns, are the

amacrine cell and two lamina wide-field neurons, one of which was not previously described (lawf2).

It is due to this simple and elegant architecture that the fly lamina has emerged as an important model circuit for the study of neural anatomy and development. In particular, the simple and repetitive topography of the fly compound eye is highly amenable to studies of developmental patterning (Ting and Lee, 2007). Many of the principles and molecules that govern neuronal differentiation, growth, and axon targeting were identified in the *Drosophila* lamina (Clandinin and Feldheim, 2009). The tools developed to understand fly development can now be applied to understanding the function of neural circuits (Olsen and Wilson, 2008). Here, again, the small number of cell types and well-defined anatomical architecture of the lamina make it an appealing entry point for the study of neural computation.

Setting experimental practicality aside, the lamina is also an attractive system from a purely aesthetic perspective. Cajal and Sanchez (1915) were the first to describe the remarkable homology of the lamina across distantly-related species. Comparative studies of insects and crustaceans revealed that all of the same basic lamina cell types are present in these two lineages, despite the fact that they diverged half a billion years ago (Osorio and Bacon, 1994). The remarkable conservation of specific lamina cell types (Strausfeld and Nassel, 1980) , and even their electrophysiological properties (Wang-Bennett and Glantz, 1987), suggests that the lamina is a highly derived and well-engineered circuit. Modern *Drosophila* genetic tools now offer the opportunity of understanding what features of this small but intricate layer of the fly brain make it so universally successful.

This chapter is intended to provide an introduction to our current understanding of the fly lamina. It is divided into three sections: Anatomy, Electrophysiology, and Behavior. Throughout this discussion, I will treat the “fly visual system” as a singular entity. However, the experiments will be drawn from work in several different fly species. While most of the anatomy and behavior discussed here was conducted in the genetic model organism, *Drosophila Melanogaster*, most of the electrophysiological recordings were obtained from larger flies, such as the housefly, *Musca Domestica*, and the blowfly, *Calliphora vicina*. Although there are certainly important differences between these species, including size, behavior, and ecology, here they are lumped together for the sake of clarity.

## **Anatomy**

### **History**

The earliest descriptions of individual neurons in the insect optic lobes were by Kenyon (1897), who filled several neurons in the bee lamina (or “outer fibrillar mass”, as he called it) with the Golgi method. From these, he was the first to notice the inner and outer optic chiasms, which reverse the retinotopic organization along the antero-posterior axis of the eye. Vigier (1907; 1908) extended the observations of Kenyon by examining the convergence of photoreceptors and monopolar cells in the lamina (Fig. 1.2B). His observations presaged the elegant neural superposition principle, which was not confirmed until 60 years later (discussed below).

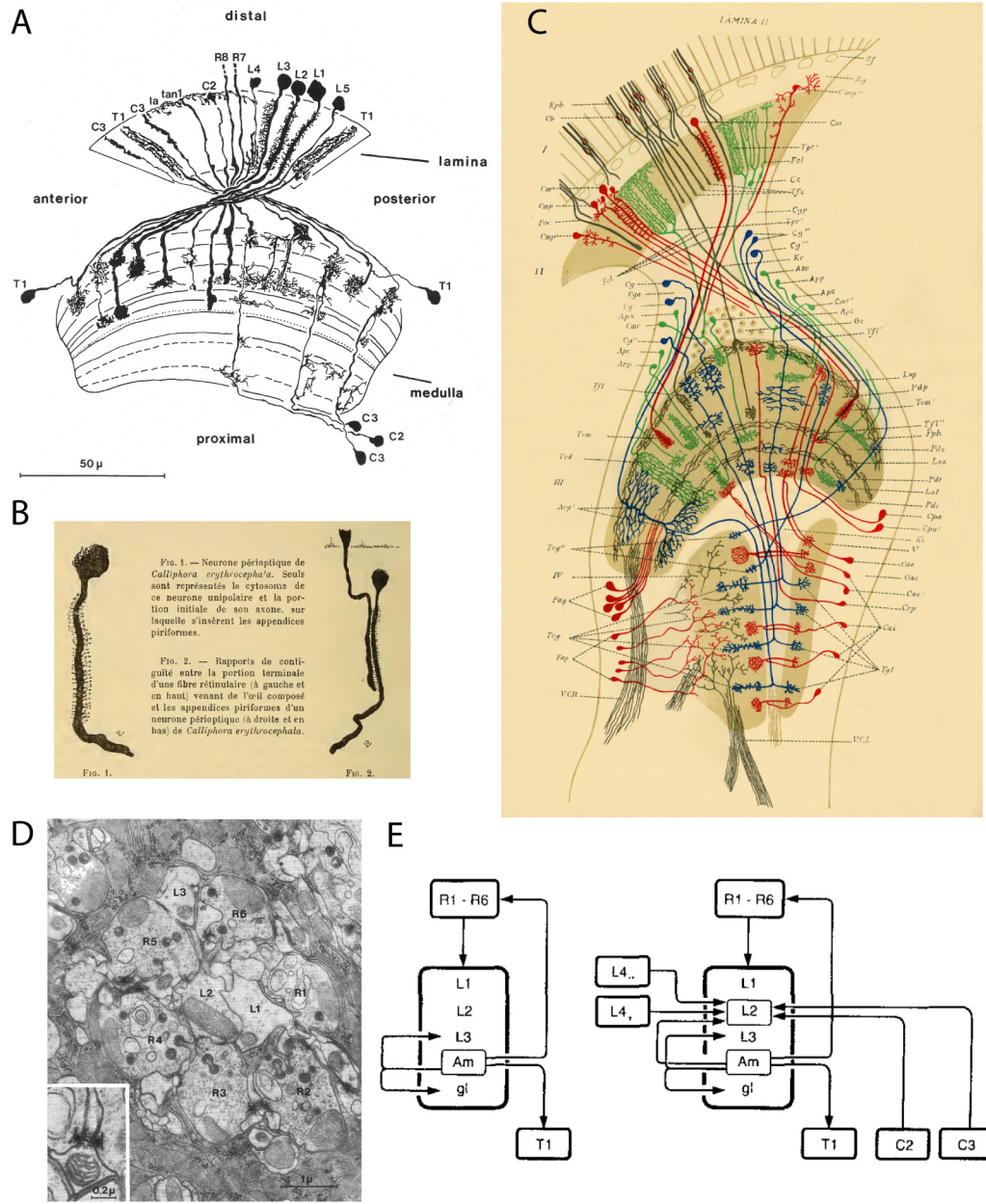


**Fig. 1.2.** Neuron classes of the fly lamina. **(A)** The 11 lamina cell types revealed by Golgi impregnation (from Fischbach and Dittrich, 1989). **(B)** The first Golgi fill of a photoreceptor and a lamina monopolar cell, showing their close proximity in the fly lamina (from Vigier, 1908) **(C)** Golgi fills of many neuron types in the visual system of the blue fly. From Cajal and Sanchez (1915) **(D)** A tangential cross-section of a lamina cartridge by electron microscopy. R1-R6, photoreceptors; L1-L3, lamina monopolar cells. Inset shows two synapses at a T-shaped ribbon (from Heisenberg and Wolf, 1984) **(E)** Lamina pathways with strong synaptic connectivity. (left) Pathways consisting of more than 20 synapses. (right) Pathways represented by more than 8 synapses (from Meinertzhagen and Sorra, 2001).

These initial studies were followed by the comprehensive anatomical descriptions of Ramon y Cajal, who wrote several brief papers on the anatomy of the fly eye (e.g., Cajal, 1910) before publishing a landmark book about the insect nervous system in 1915 (Cajal and Sanchez, 1915). In this treatise, Cajal and Sanchez used the Golgi and reduced silver techniques to identify and trace dozens of unique cell types in the insect optic lobes (Fig. 1.2C). In addition to outlining the basic structure of the fly eye, they also described the high stereotypy of individual neuron classes across disparate insect species, and noted the remarkable similarities between the invertebrate and vertebrate retinas.

Cajal and Sanchez's description of the insect optic lobes informed much of fly neuroanatomy for the next half century. During this period, most of the remaining cell classes in the insect lamina were identified and classified using the Golgi technique (reviewed by Strausfeld, 1976). At the same time, electron microscopic methods began to resolve the synaptic ultrastructure of lamina neurons (reviewed by Shaw, 1984). Finally, in 1989, a comprehensive Golgi study of the *Drosophila* visual system was published (Fischbach and Dittrich, 1989), followed by a complete electron microscope (EM) reconstruction of all the synapses in a single lamina column (Meinertzhagen and O'Neil, 1991). These two resources made the *Drosophila* lamina the most anatomically characterized neural structure other than *C. elegans* (White et al., 1986).

### **The Architecture of the Fly Lamina**

The *Drosophila* brain consists of ~200,000 neurons within a volume of ~1 mm<sup>3</sup>. About a third of these neurons reside within the optic lobes, mainly in the medulla (Strausfeld, 1976). The lamina, by comparison to the medulla, contains a relatively small number of neurons. A lamina cartridge contains 12 neuronal classes and ~1250 synapses, confined within a cylindrical

structure with an approximate diameter of 5  $\mu\text{m}$  and depth of 25  $\mu\text{m}$ . In addition to neurons, each cartridge contains several types of glial cells, including the marginal glia, which enshroud the entire lamina cartridge, and the epithelial glia, which extend throughout the depth of the neuropil (Edwards and Meinertzhagen, 2010). In addition to the columnar organization of the optic lobes, there are three important features that distinguish the fly eye from similar circuits:

1. Unlike the apposition eyes of many other arthropods, the fly lamina is organized according to the so-called “neural superposition” principle (Braitenberg, 1967; Kirschfeld, 1967). Each lamina cartridge receives input from six photoreceptors that are looking at the same point in visual space. However, because the photoreceptors within a single ommatidium all have different optical axes, six photoreceptors from six different ommatidia but all looking at the same point in space, but from six different ommatidia, project to the same lamina cartridge. This clever wiring scheme increases signal-to-noise by averaging six independent measurements from each pixel of the visual world.
2. The lamina is connected to the secondary neuropil of the visual system, the medulla, by fibers that run through a chiasm which inverts the retinotopy of the neuropil along the antero-posterior axis. Therefore, a photon that strikes the anterior visual field will be represented in the posterior medulla. A similar inverting chiasm occurs between the medulla and the tertiary compartments of the visual system, the lobula and lobula plate.
3. In the insect nervous system, cell bodies are anatomically segregated from neuronal processes (e.g., Fig. 1.1B). In the optic lobes, large masses of entangled neuropil containing axons and dendrites are covered by numerous cell bodies; these regions are called the cell-body “cortex”, or “rind”.

Two electron microscopy reconstructions of a *Drosophila* lamina cartridge have provided a nearly complete description of synaptic connectivity in the lamina (Fig. 2D,E; Meinertzhagen and O'Neil, 1991; Rivera-Alba, 2011; Rivera-Alba et al., 2011). These efforts have also served as an important testing ground for EM image acquisition and image segmentation techniques (Chklovskii et al., 2010). It is important to keep in mind that although these reconstructions are “complete”, there are many sources of error. First, not all synapses can be unambiguously identified and attributed to specific neuron types using EM. Natural variability is also large, and not all synapses seen in one column are present in the next (Meinertzhagen and O'Neil, 1991). Finally, the size of photoreceptors and LMCs, as well as the numbers of synapses between them, varies drastically as a function of circadian cycle (Gorska-Andrzejak et al., 2005; Meinertzhagen and Pyza, 1999; Pyza and Meinertzhagen, 1999; Weber et al., 2009). All of these error sources indicate that absolute synapse counts are probably less meaningful than relative synaptic weights.

Below is a list of the basic connectivity features of the *Drosophila* lamina, derived from Meinertzhagen and O'Neil (1991) and Rivera-Alba (2011). Characterization of neurotransmitter phenotypes is taken from Table 2 in Kolodziejczyk et al. (2008).

Axons of the six outer photoreceptors (R1-R6) terminate in each lamina cartridge, while the inner photoreceptors (R7-R8) bypass the lamina and project directly to the medulla (Gao et al., 2008). Photoreceptors form tetrad synapses with four of five possible postsynaptic partners: L1, L2, L3, the amacrine cell, and the epithelial glia. The majority of photoreceptor synapses are onto L1, L2, and the amacrine cell, which each receive ~260 synapses total from R1-R6. L3 and the epithelial glia each receive about 2/3 fewer. The photoreceptors receive small numbers of

feedback synapses (< 10) from several lamina neurons, including L2, L4, C3, and the amacrine cell. There are also several reports of electrical coupling between fly photoreceptors (Ribi, 1978; Shaw and Stowe, 1982; van Hateren, 1986).

L1, L3, and L5 are entirely postsynaptic in the lamina. L1 may release glutamate and acetylcholine, while there is only evidence for glutamate release in L3.

L2 is primarily postsynaptic, but also reciprocally contacts L4 collaterals which arise from neighboring cartridges in the +X (+30°) and -Y (-30°) directions. L2 likely uses glutamate as a neurotransmitter, and possibly also acetylcholine.

L4 receives synapses primarily from L2 and the amacrine cell. The L4 collateral branches are pre-synaptic to most neurons in the cartridges they project to, including the photoreceptors. L4 may release acetylcholine.

The amacrine cells are both pre- and post-synaptic, connecting with most cell types in the lamina. They are probably glutamatergic.

T1 is exclusively postsynaptic in the lamina, with its main input coming from the amacrine cell. The membrane between T1 and the amacrine cell is also thicker and darker, suggesting possible electrical coupling.

C2 synapses are concentrated in the distal lamina, primarily onto L2 and the amacrine cell. C2 is also postsynaptic to several neurons. C2 is thought to release GABA.

C3 is presynaptic to L1, L2, the amacrine cell and the epithelial glia, with synapses concentrated in the distal lamina. It is also postsynaptic to several neurons in the central lamina. Like C2, C3 is probably GABAergic.

The two lamina wide-field neurons make large numbers of synapses onto the amacrine cell and L3, and form additional synapses onto L2, the epithelial glia, C2, and the photoreceptors.

Lamina glial cells are postsynaptic, with large numbers of synapses from the photoreceptors and the amacrine cell.

## **Outlook**

From an anatomical perspective, the fly lamina is one of the most heavily studied pieces of neuropil in any animal. Extensive Golgi studies and complete EM reconstructions have described the basic columnar neurons and their synaptic connectivity patterns. More recent EM reconstructions have also identified the targets of lamina neurons in the medulla (Takemura et al., 2008). The largest gaps in our current understanding of synaptic connectivity in the lamina are the multi-columnar neurons, such as the wide-field and amacrine cells. We will learn more about these cell types as larger-scale EM reconstructions become more feasible (Chklovskii et al., 2010).

In addition to EM, genetic tools have permitted characterization of individual cell types in the *Drosophila* visual system through stochastic labeling (Varija Raghu et al., 2011) and immunocytochemistry (Kolodziejczyk et al., 2008). Improved genetic reagents should improve the reliability of these approaches (Pfeiffer et al., 2008; Pfeiffer et al., 2010). In the future, quantitative RNA sequencing could also be used to understand the complements of ion channels and neurotransmitters used by individual neuron types (Schulz et al., 2006).

## Electrophysiology

### Photoreceptors

Photoreceptors are the primary sensory neurons that convert the currency of the visual world, photons, into the currency of the nervous system, electrical potentials. Among metazoans, photoreceptors come in two flavors, ciliary and microvillar, depending on which part of the cell forms the photoreceptive membrane (Arendt, 2003). Microvillar photoreceptors are more common in invertebrate species, and have many performance advantages—they exhibit high single-photon sensitivity, fast temporal resolution, and a large dynamic range. Ciliary photoreceptors, found in most vertebrate species, are slower and less sensitive, which may be why most vertebrates have a duplex retina with rods for low light levels and cones for daylight (Fain et al., 2010).

In *Drosophila*, each of the ~750 ommatidia contains 8 photoreceptor cells. Six of these (the outer photoreceptors: R1-R6) express a single blue and UV-sensitive rhodopsin (Rh1), while the two inner photoreceptors (R7 and R8) express a complex pattern of rhodopsins that divide ommatidia into two subtypes: “pale” and “yellow”. Yellow-type ommatidia express the UV-sensitive Rh4 in R7 and green-sensitive Rh6 in R8, while pale-type ommatidia express UV-sensitive Rh3 in R7 and blue-sensitive Rh5 in R8. The two subtypes are stochastically distributed throughout the eye, but occur in a stereotyped ratio of 70% yellow and 30% pale (Cook and Desplan, 2001).

Similar to the mammalian rod and cone, a fly photoreceptor codes the number of photons arriving within the window of visual space it views. When a single rhodopsin molecule in the

photoreceptive membrane absorbs a photon, it undergoes a conformational change to metarhodopsin. This process, called photo-isomerization, is coupled to the opening of cation channels in the photoreceptor membrane through a complex second messenger cascade (Hardie and Raghu, 2001). The phototransduction cascade is understood in exquisite detail (Hardie and Postma, 2008), having been the first sensory modality in any animal to be subjected to detailed genetic analysis (Pak et al., 1969).

Within a photoreceptor, a single photo-isomerization produces a discrete increase in the membrane potential ( $\sim 1$  mV) called a quantum bump (Dodge et al., 1968). Individual quantum bumps are visible in dark-adapted photoreceptors exposed to dim light (Fuortes and Yeandle, 1964). As in vertebrate vision (Hecht et al., 1942), such discrete events are large enough to produce a detectable response in postsynaptic cells, and allow the visual system to approach the limits of acuity set by photon catch (Dubs et al., 1981). At higher light intensities, quantum bumps combine additively to generate a continuous and noisy signal (Fig. 1.3A, B).

Photoreceptors must squeeze the  $10^9$  range of light intensities encountered in the natural world within a 70 mV dynamic range. To accomplish this, photoreceptors continuously adapt to the background luminance, resulting in a unique intensity-response curve at each background (Fig. 1.3C). Three specific adaptation mechanisms have been identified in fly photoreceptors. The first is the 'intracellular pupil', consisting of small pigment granules which reduce the amount of light that reaches the photoreceptor (Kirschfeld and Franceschini, 1969). Pigment migration can reduce light flux through the photoreceptive waveguide by a factor of 100 (Franceschini, 1972). A second mechanism is hyperpolarization of the photoreceptor due to an electrogenic Na<sup>+</sup>/K<sup>+</sup> transporter during strong light adaptation (Jansonius, 1990; Uusitalo et al.,

1995a). The third mechanism is a K<sup>+</sup> conductance called *Shaker* (Hardie et al., 1991), whose rapid inactivation prevents saturation and improves signal-to-noise under light adapted conditions (Niven et al., 2003).

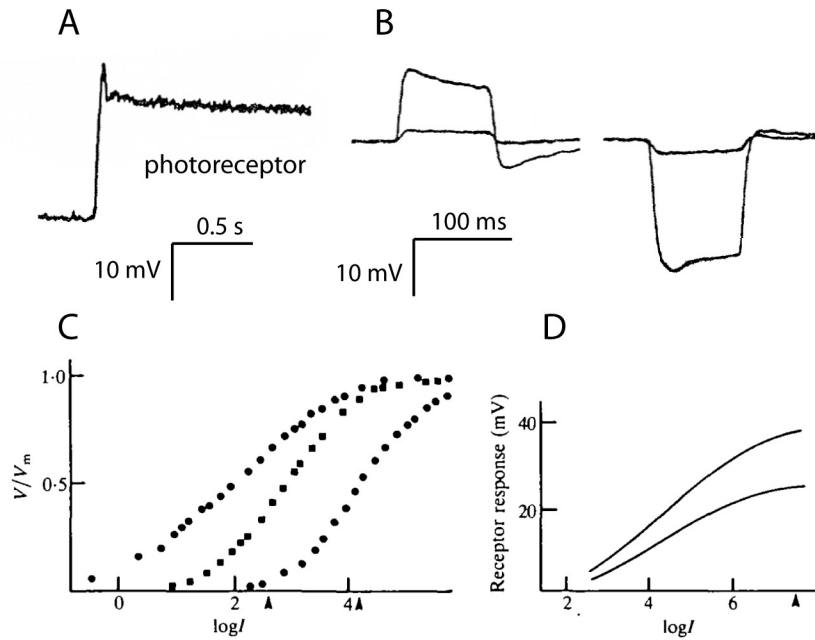


**Fig. 1.3.** Electrophysiology of fly photoreceptors. **(A)** Electrophysiological responses of a dark-adapted fly photoreceptor to the onset of a background intensity of  $5 \times 10^5$  photons  $s^{-1}$ . **(B)** Average photoreceptor response to 100 ms pulse increments (left) and decrements (right) about this background intensity. **(C)** Intensity-response curves of photoreceptors. The left-most curve is a dark-adapted cell, while the others were light-adapted at intensities indicated by the arrowheads. **(D)** Light adaptation in the photoreceptors maximizes sensitivity and minimizes non-linear summation. Plot shows the range of photoreceptor responses generated by signals of average natural contrast over a large range of mean light intensities. The arrowhead indicates the mean intensity of a bright sunny day. The response is maintained close to the optimal 50% level at daylight levels. A and B are modified from Laughlin et al. (1987), C and D are from Laughlin (1989).

Another important factor that extends the operational range of fly photoreceptors is non-linear summation of voltage signals (Laughlin, 1989). Non-linear summation results from the activation of parallel conductance channels in the photoreceptor membrane. As response amplitude increases, open channels generate progressively less current; this effect can be

thought of as a self-shunting of the receptor potential. The result is that the photoreceptor's sensitivity to small intensity changes decreases as amplitude rises.

The two fundamental components of the photoreceptor signal, (1) adaptation that reduces sensitivity to bright light and (2) a non-linear relationship between stimulus and response, are roughly equivalent to a logarithmic transformation of the incoming light signal (Laughlin, 1987).

This relationship is particularly advantageous for vision because it scales light signals proportional to the mean intensity. Such dynamic scaling allows photoreceptors to encode an invariant property of natural images—contrast. Contrast is defined as the variance about the mean light intensity,  $\Delta I/I$ , where  $\Delta I$  is the difference between an object and the mean luminance level (Shapley and Enroth-Cugell, 1984). In fly photoreceptors, equal contrasts produce approximately equal responses, independent of the mean light intensity (Fig. 3D; Zettler, 1969). The visual system operates at extraordinarily diverse light levels, from dim starlight to bright sunlight—photoreceptor contrast coding is an effective method of representing visual scenes irrespective of the mean illumination level.

### **The large lamina monopolar cells (LMCs)**

The outer photoreceptors, R1-R6, send axons to the secondary optic neuropil, the lamina. As described above, the lamina contains over a dozen anatomically defined cell types arranged in a columnar organization. However, thorough electrophysiological characterization has been performed on only a handful of these neuron classes. In particular, the large lamina monopolar cells (LMCs) L1, L2 and L3 have been studied in great detail in larger flies. Here, I will review our understanding of visual processing in the LMCs.

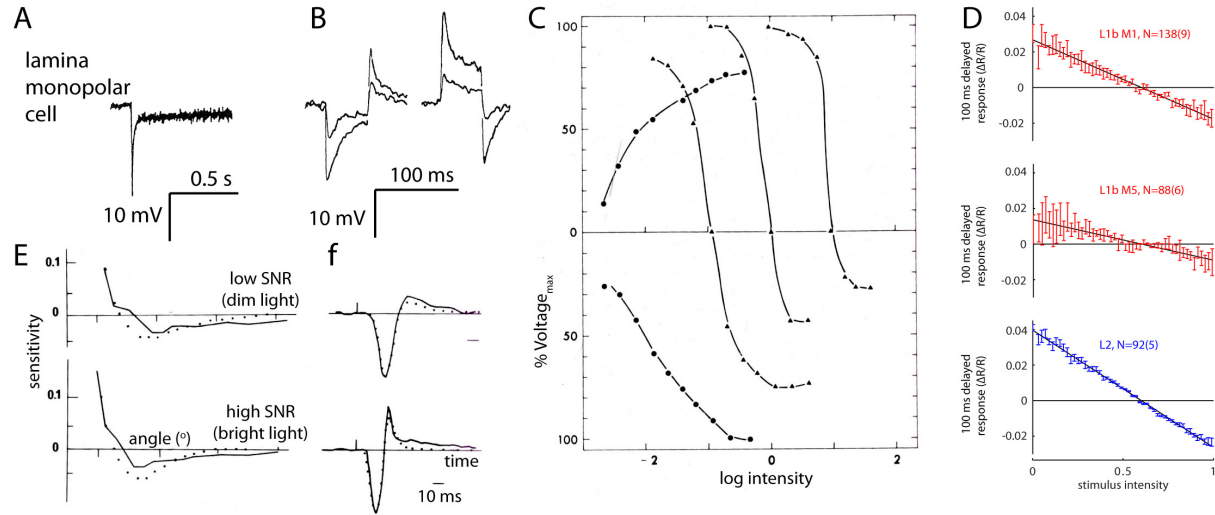


**Fig. 1.4.** Electrophysiology of fly lamina monopolar cells. **(A)** Electrophysiological responses of a dark-adapted lamina monopolar cell (LMC) to the onset of a background intensity of  $5 \times 10^5$  photons  $s^{-1}$ . **(B)** Average LMC response to 100 ms pulse increments (left) and decrements (right) about this background intensity. Stimuli are the same as in Fig. 1.2A, B. **(C)** Peak response amplitudes to light flashes at four different adaptation states. The left-most curve (circular data-points) is from the dark-adapted state. The other three are light-adapted at the intensity where each curve crosses the abscissa. Data is from Laughlin and Hardie (1978). Figure modified from Laughlin (1984). **(D)** Intensity-response curves (mean  $\pm$  s.e.m.) measured by 2-photon calcium imaging in the axon terminals of L1 and L2. M1 and M5 refer to layers of the medulla in which L1 arborizes; L2 terminates in layer M2 (from Clark et al., 2011). **(E)** Comparison of experimentally measured LMC receptive fields (solid lines) with the theoretical predictions of the predictive coding model (dotted lines). At lower signal-to-noise, the theory predicts that the width of the inhibitory surround should increase and weaken. This relationship is also observed in the physiological data. **(F)** Experimentally measured LMC impulse-response functions (responses to brief light flashes; solid lines) and theoretical expectations (dotted lines). As predicted, temporal inhibition is stronger at higher signal-to-noise. The data from both e and f are from Srinivasan et al. (1982).

LMCs are non-spiking interneurons that invert, amplify, and filter the photoreceptor signal.

They respond to luminance increases with a transient hyperpolarization, and luminance decreases with a transient depolarization (Fig. 4A, B; Autrum et al., 1970; Scholes, 1969)). This inversion of depolarizing photoreceptor input is mediated by a chloride conductance in the LMCs (Hardie, 1987; Zettler and Straka, 1987). Transmitter release at photoreceptor—LMC synapses is tonic even in darkness (Laughlin et al., 1987; Uusitalo et al., 1995a). Through a

series of experiments in dissociated blowfly LMCs, Hardie and colleagues discovered that the neurotransmitter released by photoreceptors is histamine (Hardie, 1989). There are two histamine receptors in *Drosophila*, one of which, hclA or ort (Gengs et al., 2002), is the native receptor on LMCs, while the other, hclB or hisCl1 (Zheng et al., 2002), is restricted to lamina glial cells (Pantazis et al., 2008). Synaptic transmission between photoreceptors and LMCs is abolished in hclA null mutants, while hclB mutants exhibit slower LMC responses, suggesting that histamine-mediated glial signaling contributes to LMC function (Pantazis et al., 2008).

LMCs dramatically amplify photoreceptor signals—in the blowfly, LMC responses are approximately 6 times larger than photoreceptor responses (Laughlin et al., 1987). Amplification promotes accurate transmission by reducing the effects of intrinsic noise and making full use of the LMC response range (Fig. 1.4C). However, excessive amplification at higher intensities could saturate LMC responses, leading to information loss. Information theory suggests that amplification should be matched to the statistical distribution of input amplitudes, in this case the range of contrasts typically encountered by a fly. Comparisons of contrast levels in natural scenes and LMC response amplitudes indicate that LMC amplification is indeed matched to the distribution of contrasts encountered in the natural world (Laughlin, 1981). At daylight intensities, contrast-response curves are steep and sigmoidal, and closely match the distribution of contrast signals encountered in the natural world (Fig. 1.4C).

LMCs extract and enhance photoreceptor contrast signals through a combination of temporal and spatial antagonism. Spatial antagonism, functionally equivalent to lateral inhibition, results from the center-surround structure of the LMC receptive field (Dubs, 1982; Zettler and Jarvilehto, 1972). For example, illuminating a ring of photoreceptors surrounding an LMC's

receptive field produces a weak depolarization that opposes the signal from the center.

Therefore, the net LMC response is the difference between the signal generated in the receptive field center and the average luminance of the surround (Fig. 1.4E).

A much larger contribution to adaptation is produced by temporal antagonism, apparent in the phasic responses to light increments and decrements (Fig. 1.4F). LMC adaptation exhibits both fast (<5 ms) and slow (> 5 ms) components. The source of fast LMC adaptation is unknown, but could be due to pre- or post-synaptic voltage-gated channels (Uusitalo et al., 1995b; Weckstrom et al., 1992), rapid feedback from neighboring neurons (Zheng et al., 2006), or rapid desensitization of postsynaptic histamine receptors (Skingsley et al., 1995). As for slower adaptation, there is some evidence that extracellular field potentials in the lamina shape transmitter release from the photoreceptor terminals (Weckstrom and Laughlin, 2010), consistent with transient changes in the postsynaptic chloride conductance on the same time scale (Laughlin and Osorio, 1989).

Antagonism in LMCs provided an experimental test for an important theory called “predictive coding”, which posited that removing redundant, or predictable, components of a sensory signal could enable neurons to operate with a higher sensitivity and protect relevant signals from intrinsic noise (Barlow, 1961b; Srinivasan et al., 1982). Because neighboring pixels in a natural scene are highly correlated, redundancy can be reduced by subtracting the weighted average of nearby points from a received signal. Temporal predictive coding can function in an analogous manner by providing a weighted mean of previous signals that is then subtracted from the present. A key component of the predictive coding theory is that spatial and temporal weighting functions should depend on the signal-to-noise ratio (SNR) of sensory inputs (Fig.

1.4E, F). At low SNR (i.e., in dim light), random fluctuations render photoreceptor signals unreliable; therefore antagonism should be reduced in amplitude and extended in space or time. Interestingly, both spatial and temporal antagonism in fly LMCs are progressively weakened as light levels decrease, in a manner consistent with the predictive coding framework (Srinivasan et al., 1982).

### **Distinct properties of L1, L2, and L3**

Up to this point, we have lumped L1-L3 into a single group—the LMCs. However, these neuron types likely serve distinct functions, given their distinct anatomical profiles and conserved stereotypy in distantly related species. Indeed, electrophysiological investigations of L1, L2, and L3 have identified several subtle differences. L3 has a higher input resistance (van Hateren and Laughlin, 1990) and rests at a more depolarized potential (-60 mV) than L1 or L2 (-40 mV)(Hardie and Weckstrom, 1990). L1-L3 also differ in their complements of voltage-sensitive conductances. An A-current in L1 and L2 is totally inactivated in the physiological response range, but L3 possesses a slowly-inactivating delayed rectifier which sharpens responses to light decrements(Hardie and Weckstrom, 1990). L3 and L1 can also both respond to light-OFF with an spike-like event superimposed on the depolarizing OFF response— this spike appears to be mediated by voltage-gated sodium channels in the axon (Uusitalo et al., 1995b). L3 exhibits this behavior under physiological conditions, while it is only observed in L1 immediately following a brief hyperpolarization of the resting potential. Finally, of the three LMCs, L2 is most strongly affected by lateral antagonism (Laughlin et al., 1987). Interestingly, L2 also receives synaptic input from L4 collaterals projecting from neighboring cartridges, suggesting a potential circuit for spatial antagonism.

Several recent studies have used 2-photon imaging of genetically-encoded calcium indicators to examine LMC function in *Drosophila*. In the first such example, Reiff et al. (2010) expressed TN-XXL in L2 neurons and imaged from the terminals in the medulla. In dark-adapted flies, they found that calcium responses to light OFF were significantly larger than to light ON. However, brightness increases sharply truncated light OFF calcium transients, resulting in high sensitivity to flickering ON and OFF stimuli. A similar study by Clark et al. (2011), using the same GAL4 line and calcium indicator, found that L2 terminals respond to both light ON and light OFF, though light OFF responses were slightly faster and larger. This group also imaged from the terminals of L1 in layers M1 and M5 in the medulla, and found that these compartments responded similarly to L2, with intracellular calcium levels increasing at light OFF and decreasing at light ON. Finally, they used white-noise contrast stimuli to show that calcium signals in L1 and L2 respond linearly to dynamical light stimuli, but have different adaptation kinetics (Fig. 1.4D). In particular, calcium signals in L2 returned rapidly to baseline after a luminance increase, while L1 retained low calcium levels that decayed more slowly.

Overall, calcium imaging data in *Drosophila* are largely consistent with the electrophysiological recordings from LMCs. The novel feature of these imaging studies is the dramatic rectification in the L2 terminal observed by Reiff et al. (2010), which was much less pronounced in the data of Clark et al. (2011). Although there is no obvious methodological reason for the discrepancy between these two papers, this rectification is not without precedent. In fact, there was previous evidence from sharp-electrode recordings in larger flies that ON and OFF responses are generated at spatially distinct sites. Injecting current in the lamina input regions of LMCs primarily affects ON responses, while current injection in the axon alters OFF responses (Guy

and Srinivasan, 1988; Zettler and Jarvilehto, 1973). Based on this evidence, Guy and Srinivasan (1988) suggested that ON responses are generated at the photoreceptor—LMC synapses in the lamina, while OFF responses arise from the axon or in the LMC terminals in the medulla.

Detailed investigations of L1 and L2 compartmentalization, as well as the contributions of other lamina cell types, will be needed to understand how electrical signals are segregated and transformed within the LMCs.

Based partially on the observed rectification in L2, a recent paper has also argued that L1 and L2 comprise ON and OFF pathways (Joesch et al., 2010). In this study, the authors synaptically silenced L1 and L2 and recorded from downstream motion-sensitive neurons—the lobula plate tangential cells (LPTCs). Joesch et al. found that silencing both L1 and L2 blocked LPTC responses, while restoration of either one or the other pathway reconstituted motion sensitivity. They resolved this discrepancy by demonstrating electrical coupling via gap junctions between L1 and L2, as suggested earlier in the house-fly (Chi and Carlson, 1980).

Finally, they used moving bright and dark edges to show that LPTC neurons are less sensitive to OFF edges when L2 was silenced, and less sensitive to ON edges when L1 was blocked. From these data, the authors concluded that L1 and L2 constitute ON and OFF channels, similar to bipolar cells in the vertebrate retina.

Although physiological investigations of the LMCs have been ongoing for over 40 years (Scholes, 1969), a great deal remains unknown. We know from many sharp-electrode recordings in the fly lamina that luminance signals undergo a basic set of transformations as they pass from photoreceptors to LMCs: log transformation, subtraction of redundant components, and amplification. What is less clear is how light signals are transformed as they pass from lamina to

medulla, and how the parallel pathways of the LMCs differentially contribute to visual processing. Novel approaches using genetic tools in *Drosophila* hold great promise, however parsimonious interpretation of these complex experiments has so far proven difficult.

### **Other lamina cells**

Historically, intracellular recordings in insects have been obtained by random penetration of neurons with high impedance sharp electrodes. The sharp-electrode technique creates a strong bias for larger neurons, which explains why most recordings in the lamina are from the large monopolar cells. For this reason, disproportionate attention has been paid to the LMCs, and very little is known about other cell types in the lamina. However, there are exceptions to this trend.

In the early 1970's Arnett and McCann described two distinct spiking units recorded from the fly lamina/medulla chiasm with tungsten microelectrodes (Arnett, 1971; Arnett, 1972; McCann and Arnett, 1972). The first of these was an "on-off" unit that produced a transient response when a light was switched ON or OFF. The other was a "sustained" unit that produces sustained action potentials when its receptive field was illuminated. These units were later characterized in blowflies, and found to have interesting spatial and temporal properties (Jansonius and van Hateren, 1991; Jansonius and van Hateren, 1993a; Jansonius and van Hateren, 1993b). For example, the on-off unit has a large receptive field (5-7 ommatidia), and adaptation occurs independently in different areas of the receptive field (Jansonius and van Hateren, 1993a). The sustained unit did not exhibit such adaptation, and had a much smaller receptive field (Jansonius and van Hateren, 1993b). Based on lesion experiments, it was determined that these spikes originated from the lamina (Arnett, 1972; Jansonius and van Hateren, unpublished data),

and so were hypothesized to correspond to the lamina neurons L4 and L5. However, further investigation is needed to corroborate these claims.

Intracellular recordings from other neurons in fly lamina are sparse and of generally poor quality due to the leakiness inherent in recording from very small neurons. For example, a single recording from the basket cell, T1, suggests that it responds to light flashes in a manner similar to the other LMCs (Jarvilehto and Zettler, 1973). Douglass and Strausfeld (Douglass and Strausfeld, 1995) managed to record several such examples from lamina neurons, including C2, T1, L4, and L5. However, it is difficult to interpret such single examples, and more physiological data is needed to understand even the most basic functional properties of lamina neurons.

## **Outlook**

Forty years of electrophysiology in the insect lamina has yielded a great deal of knowledge about the transformation of luminance signals between the photoreceptors and the large monopolar cells (LMCs). Several important principles, such as lateral inhibition, matched amplification, and predictive coding, have been elucidated at these synapses. What is lacking, however, is an equivalent understanding of other lamina cell types, and how lamina circuits interact to process visual information. But even if we could reliably record from every cell type in the lamina, this would still not provide a meaningful picture of circuit function. As might be expected for peripheral sensory processing, lamina neurons have very simple response properties—they generally respond to changes in luminance contrast. What will be much more interesting is how the different cell types interact to compress and process visual information, and how they feed into distinct neural pathways. The genetic tools available in *Drosophila* offer the possibility of understanding circuit-level computations. For example, unbiased techniques,

such as visually targeted patch-clamp recordings (Wilson et al., 2004) and imaging of genetically-encoded calcium indicators (Clark et al., 2011; Reiff et al., 2010) in *Drosophila*, could help overcome the sampling bias of blind sharp-electrode recordings. Combining physiology with genetic manipulation of individual cell types is a promising route toward understanding the function of early visual circuits in the fly.

## Behavior

### Fly visual behaviors

Previous studies of fly visual behavior have primarily focused on three basic behaviors: (1) phototaxis: the attraction of an animal to toward a stationary light source, (2) the optomotor response: the tendency of animal to turn in the direction in which the visual panorama rotates (Fig. 1.5D), and (3) object orientation: an animal's tendency to orient toward an object in the absence of other visual stimuli (Fig. 1.5E).

Phototaxis toward a white light source (Fig. 1.5B) was initially described in *Drosophila ampelophila* (Carpenter, 1905), and subsequently investigated in other fly species (Gross, 1913). When given a choice between equiluminant green and ultraviolet light sources, flies will walk toward the UV light (Gao et al., 2008; Hu and Stark, 1977). The adaptive value of positive phototaxis in flies is not entirely clear, although most eukaryotes, including many single-celled organisms, exhibit either positive or negative phototactic behavior (Jekely, 2009).

The optomotor response of flies was first studied by Hecht and Wald (1933; 1934), who measured the visual acuity of *Drosophila* running through a small enclosed tunnel surrounded by a moving visual pattern. Similar studies using rotating cylinders demonstrated that flies tend

to run in circles when surrounded by a rotating visual panorama (Gaffron, 1934; Gavel, 1939).

Soon after the initial descriptions of optomotor behavior, neuroethologists began to apply mathematical and engineering techniques to the study of fly optomotor behavior (Kalmus, 1949). A noteworthy result of this approach was the influential Hassenstein-Reichardt elementary motion detector (EMD) model (Hassenstein and Reichardt, 1956). Many of the predictions of the EMD model, including the dependence of optomotor responses on stimulus temporal frequency, were tested by measuring fly optomotor responses (Fig. 5D; Fermi and Reichardt, 1963; Gotz, 1964). Such experiments were facilitated by the development of the torque meter for measuring both open- and closed-loop tethered flight behaviors (Fig. 1.5C). Similar analyses of walking optomotor responses revealed that local motion detection occurs primarily between neighboring ommatidia at high contrast (Buchner, 1976; Buchner et al., 1978). Optomotor responses are not, however, the simple sum of local motion vectors: for example, a laterally centered expansion stimulus that mimics yaw translation evokes stronger steering responses than the equivalent rotation stimulus (Duistermars et al., 2007a; Tammero et al., 2004).

Object orientation responses were identified by measuring the steering reactions of tethered flying house flies (Fig. 5E; Reichardt and Wenking, 1969). When given closed-loop control over a visual pattern consisting of a single vertical dark stripe, flies tend to keep the stripe in their frontal visual field— this behavior has been termed “stripe fixation”. A similar orientation behavior is seen in freely walking (Horn and Wehner, 1975) or flying (Maimon et al., 2008) flies . Orientation behavior was originally thought to be related to motion-induced course control, which acted by preventing front-to-back motion in the visual field (Poggio and Reichardt, 1976;

Reichardt and Poggio, 1976). However, flies can also maintain arbitrary directions of flight relative to an object (“anti-fixation”; Heisenberg and Wolf, 1979), and are attracted to locally oscillating and flickering stripes (Pick, 1976; Wehrhahn and Hausen, 1980). Therefore, it appears that object tracking does not rely exclusively on simple motion-evoked reflexes, but is more likely a combination of several overlapping visual behaviors (Buchner, 1984; Heisenberg and Wolf, 1984; Reiser and Dickinson, 2010).

Other fly behaviors that require vision are the looming-evoked landing response in flying flies (Borst and Bahde, 1988; Wagner, 1982; Wehrhahn et al., 1981), the escape response (Card and Dickinson, 2008a; Card and Dickinson, 2008b), gap crossing (Pick and Strauss, 2005; Triphan et al., 2010), spatial navigation (Ofstad et al., 2011), courtship (Markow, 1987), and aggression (Baier et al., 2002). However, the visual components of these behaviors have not received the same attention as the photactic, optomotor, and object orientation responses, and at this point little is known about their neural substrates.

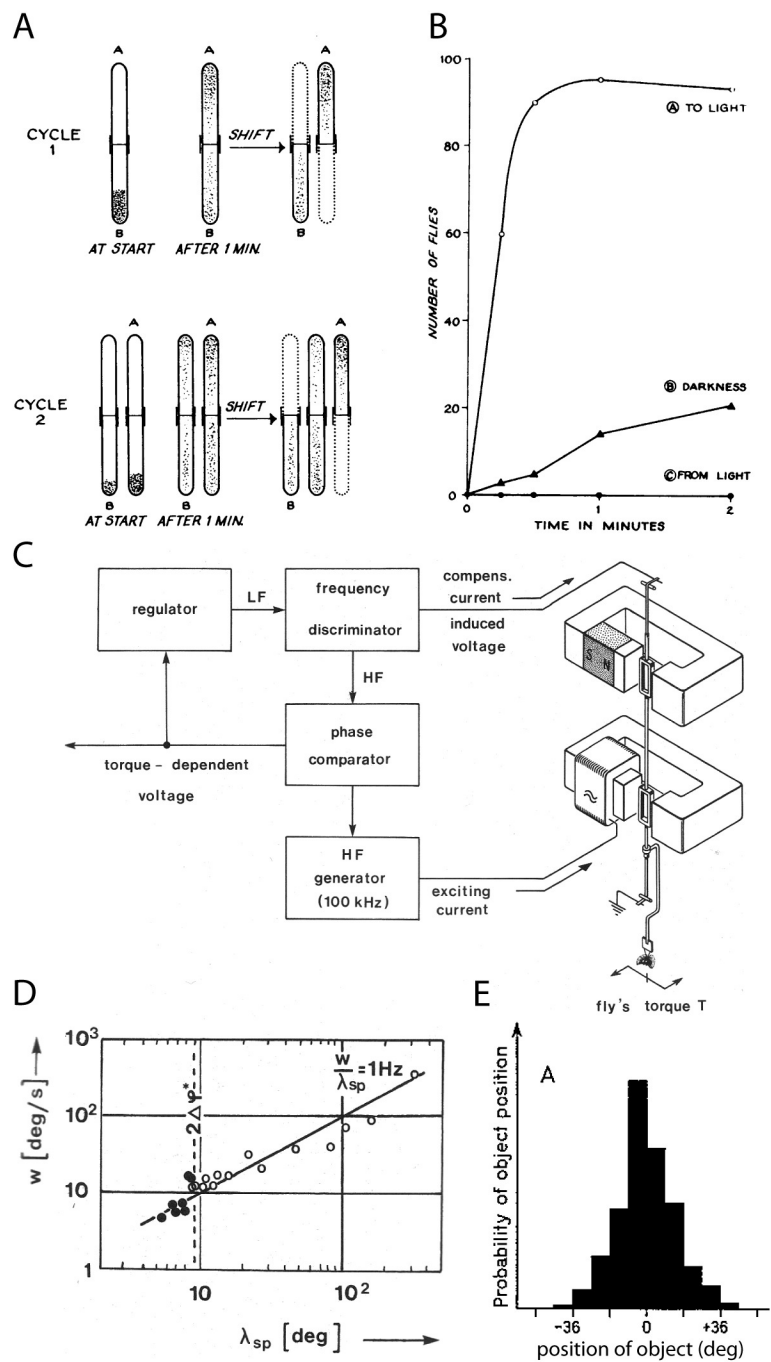
Finally, it should be noted that in addition to the primary eyes, flies have three photosensitive organs called ocelli that form a triangle on the dorsal part of the head. The ocelli are each equipped with a small convex lens, forming a blurred image containing little spatial detail. They are thought to contribute to orientation behaviors such as the dorsal light response, in which the fly aligns its head with sources of brightness (Schuppe and Hengstenberg, 1993). There is also evidence that ocelli may be used in flight stabilization (Parsons et al., 2010; Stange, 1981; Taylor, 1981) and orientation towards edges in walking flies (Wehrhahn, 1984).

**Fig. 1.5. Quantification of fly visual behaviors. (A)** Countercurrent distribution system for fractionating populations of *Drosophila* based on phototaxis behavior. The dotted lines indicate new tubes introduced at the end of each experimental cycle.

Adapted from Benzer (1967)

**(B)** Phototaxis behavior of wild-type flies. The flies start in one end of the tube, and the number of flies that reach the opposite end is measured as a function of time. In A, a light source is present at the opposite end. In B, no light source is present. In C, the light source starts at the same end of the tube as the flies. **(C)** The torque compensator for measuring the flight behavior of tethered flies, designed by Karl Gotz (from Heisenberg and Wolf, 1984). **(D)** Yaw torque behavior recorded at the torque compensator in response to rotating optomotor stimuli. Data points indicate the spatial wavelength ( $\lambda_{sp}$ ) that evoked a maximum torque response across a range of stimulus velocities ( $w$ ). Filled circles show turning against the direction of stimulus motion, while open circles are with stimulus motion. The peak response is evoked by motion at 1 Hz temporal frequency ( $w/\lambda_{sp}$ ). Data are from Gotz (1964). Figure modified from Heisenberg and Wolf (1984).

**(E)** Object orientation recorded at the torque compensator. The fly is given closed-loop control over the position of a 6° dark stripe on a bright background. Histograms depict the probability of stripe position as a function of angular position. Modified from Reichardt and Wenking (1969).



## Genetic dissection of fly visual behaviors

The robustness and easy quantification of fly visual behaviors provided an opportunity for testing the behavioral effects of genetic mutation. For example, many of the early eye mutants exhibited deficits in phototaxis (McEwen, 1918) and optomotor responses (Kalmus, 1943). In the 1960's, Seymour Benzer screened directly for phototactic mutants using a countercurrent device (Fig. 5A, B; Benzer, 1967). The strains isolated and studied by the Benzer lab made a compelling case that mutations in individual genes can modify animal behavior. These discoveries led to the establishment of the behavioral genetics field, in which genetic mutations were used to understand the function of the brain and resulting behaviors.

Behavioral genetics has since been used to probe all of the visual behaviors described above (reviewed by Heisenberg and Wolf, 1984). A notable example is the demonstration that the achromatic photoreceptor pathways (R1-R6) primarily underlie motion detection, while color pathways (R7-R8) contribute to phototaxis (Heisenberg and Buchner, 1977). Studies of anatomical mutants, such as *optomotor-blind*<sup>H31</sup> (*omb*<sup>H31</sup>), confirmed the role of lobula plate neurons in optomotor steering (Heisenberg et al., 1978). Another optomotor-deficient strain, *rol sol*, which possessed greatly reduced optic lobes, could still orient toward visual objects (Wolf and Heisenberg, 1986). Similarly, the mutant *Vam*, which exhibited relatively specific degeneration of L1 and L2, demonstrated no measurable optomotor response, but could orient weakly toward dark stripes (Coombe and Heisenberg, 1986). Such examples suggested that optomotor and orientation behaviors are executed by distinct neural pathways.

## Using binary expression systems

The severity of the phenotypes derived from genetic screens, and the inability to selectively perturb specific circuits, limited the utility of genetic mutants for understanding visual circuits. However, the development of ectopic transgene expression systems, in particular the GAL4-UAS system (Brand and Perrimon, 1993), has fueled a recent renaissance in genetic dissection of *Drosophila* neural circuits.

The first attempt to understand visual system function using these techniques was by Rister et al (Rister et al., 2007). This group measured optomotor responses of tethered flies while they inactivated subsets of lamina neurons. They found that silencing L1 and L2 together abolished optomotor behavior, but silencing one or the other pathway did not disrupt optomotor responses except under certain conditions. Specifically, L1 and L2 appeared to be redundant at high pattern contrast, while neither was sufficient at very low contrasts. At intermediate contrasts, L1 appeared to mediate detection of front-to-back motion, while L2 mediated back-to-front motion. A later study confirmed that silencing the LMCs abolished visual motion detection, while leaving phototaxis intact (Zhu et al., 2009). However, another set of experiments performed with populations of freely walking flies found that silencing L2 affected responses to translational but not rotational motion (Katsov and Clandinin, 2008). Finally, a more recent study concluded that L1 or L2 did not affect behavioral responses to standard moving edges (Clark et al., 2011). Rather, these manipulations produced different effects when flies were tested with moving edges that inverted contrast as they moved— silencing L1 impaired responses to dark-bright edges, and silencing L2 affected responses to bright-dark edges.

## Outlook

A consistent conclusion across these four behavioral studies and the electrophysiological experiments of (Joesch et al., 2010) is that silencing both L1 and L2 with *shibire<sup>ts</sup>* abolishes optomotor behavior. However, silencing L1 or L2 alone has been reported to cause differential responses to front-to-back vs. back-to-front motion (Rister et al., 2007), contrast-inverting edges (Clark et al., 2011), and ON vs. OFF motion stimuli (Joesch et al., 2010). What are we to make of these many and varied results? Though these experiments are each considerable technical achievements, their collective interpretation has proven difficult for a number of reasons.

The GAL4 lines used in all of these studies are not specific to single cell types. It is therefore difficult to definitively ascribe specific functions to single neuron classes. Even where specific GAL4 lines are available, it is important to test multiple driver lines for each cell type due to the possibility of developmental or site-specific expression effects (Pfeiffer et al., 2010).

The efficacy of neural effectors is highly variable, depending on the cell type and the expression vectors used (Thum et al., 2006) . Expressing *shibire<sup>ts</sup>* or tetanus toxin within a GAL4 pattern does not necessarily mean that all the neurons in that pattern are synaptically silent.

Unfortunately, due to the considerable technical challenge of recording from the *Drosophila* lamina, none of these behavioral studies have functionally confirmed that the neurons they are targeting are effectively silenced.

The genetic backgrounds of GAL4 lines are highly variable. Because genetic background can have a large effect on behavior, it is difficult to interpret behavioral experiments conducted

with flies of varying backgrounds (An et al., 2000). Furthermore, the background of most GAL4 lines is relatively poor compared to wild-type flies, rendering complicated behavioral experiments difficult to achieve.

Each of these efforts has employed a different behavioral paradigm with a unique visual display system. For example, the four papers described above quantified tethered flight steering (Rister et al., 2007), head movements of tethered flies (Rister et al., 2007; Zhu et al., 2009), spatial distributions of freely walking flies (Zhu et al., 2009), individual trajectories of freely walking flies (Katsov and Clandinin, 2008), steering of tethered flies walking on an air-supported ball (Clark et al., 2011), and the landing response of tethered flies (Rister et al., 2007; Zhu et al., 2009).

Future studies of the lamina using behavioral genetics must overcome these caveats by (1) using specific GAL4 lines, preferably more than one driver line per cell type, (2) verifying the efficacy of effector expression with electrophysiology, and (3) improving the genetic background of GAL4 lines and using a consistent background across experiments.

### **Plan for Thesis**

While this introduction has focused on the known properties of a handful of lamina neurons, the work presented in this thesis will address (1) the development of new behavioral assays to understand lamina processing, and (2) the behavioral and electrophysiological function of uncharacterized cell types in the *Drosophila* lamina. Chapter 2 will discuss the characterization of a novel behavioral response called reverse-phi, and its implications for early visual processing. Chapter 3 will focus on behavioral genetics experiments targeting a novel cell-type

in the fly lamina, called the lamina wide-field neuron. Chapter 4 will describe electrophysiological recordings from lamina wide-field neurons. Chapter 5 will discuss future directions and provide preliminary data for other lamina cell types.

## Chapter 2

### Neural correlates of illusory motion perception in *Drosophila*

#### Abstract

When the contrast of an image flickers as it moves, humans perceive an illusory reversal in the direction of motion. This classic illusion, called *reverse-phi motion*, has been well-characterized using psychophysics and several models have been proposed to account for its effects. Here, we show that *Drosophila melanogaster* also respond behaviorally to the reverse-phi illusion, and that the illusion is present in dendritic calcium signals of motion-sensitive neurons in the fly lobula plate. These results closely match the predictions of the predominant model of fly motion detection. However, high flicker rates cause an inversion of the reverse-phi behavioral response that is also present in calcium signals of the LPTC dendrites but not predicted by the model. The fly's behavioral and neural responses to the reverse-phi illusion reveal unexpected interactions between motion and flicker signals in the fly visual system, and suggest that a similar correlation-based mechanism underlies visual motion detection across the animal kingdom.

#### Introduction

Among visual organisms, the ability to detect motion is nearly universal. Animals as diverse as beetles (Hassenstein and Reichardt, 1956) and wallabies (Ibbotson and Clifford, 2001) compute visual motion from time-varying patterns of brightness received by an array of photoreceptors. However, the mechanisms by which the visual system detects motion are not well understood

in any animal (Clifford and Ibbotson, 2002). Here, we use a visual illusion to probe the mechanisms of motion detection in the fly, *Drosophila Melanogaster*.

Sequential flashes at neighboring spatial positions cause humans to perceive motion in the direction of the second flash, an effect called *phi* or *apparent* motion (1875). A related phenomenon, reverse-*phi* motion, also relies on sequential luminance changes to evoke a motion percept (Anstis and Rogers, 1975); however, in the reverse-*phi* stimulus, the contrast polarity of the stimulus inverts as it moves, causing a reversal in the direction of perceived motion. For example, when a black random dot pattern turns to white as it moves rightward across a gray background, human subjects perceive leftward motion (Sato, 1989).

The reverse-*phi* effect is not a subtle illusion. Humans exhibit nearly equal sensitivity, and comparable spatial and temporal tuning, for standard and reverse-*phi* motion (Bours et al., 2009). Sensitivity to reverse-*phi* has also been shown for other vertebrates such as primates (Krekkelberg and Albright, 2005) and zebrafish (Orger et al., 2000). Directional responses to reverse-*phi* motion are present in cat striate cortex (Emerson et al., 1987), the nucleus of the optic tract in the wallaby (Ibbotson and Clifford, 2001), and primate area MT (Krekkelberg and Albright, 2005; Livingstone et al., 2001). These psychophysical and neurophysiological data suggest that sensitivity to reverse-*phi* motion may be a common feature of motion detection in the vertebrate visual system, and for this reason, reverse-*phi* has been an important tool for building models of visual motion detection (Adelson and Bergen, 1985; Johnston and Clifford, 1995; Krekelberg and Albright, 2005; Mo and Koch, 2003; Shioiri and Cavanagh, 1990; Wehrhahn and Rapf, 1992).

The prevailing model for motion detection in the fly is the Hassenstein-Reichardt elementary motion detector (or H-R EMD), in which the intensity measured at one photoreceptor is temporally filtered and multiplied with a neighboring intensity signal (Reichardt, 1961). Columnar motion detection circuits compute *local* motion features across the fly eye, which are then integrated to produce *global* motion percepts (Single and Borst, 1998). Anatomically, local motion computations are presumed to be implemented within columnar circuits of the lamina and medulla(Higgins et al., 2004); local motion signals are then integrated by wide-field tangential cells in the lobula plate that encode global motion patterns (Fig. 2.1A).

In this chapter, we examine behavioral and physiological responses to reverse-phi motion as a test of this conceptual framework in a genetic model organism, *Drosophila melanogaster*. We found that flies exhibit *reverse-optomotor* behavioral responses when presented with panoramic reverse-phi motion, and that neurons in the fly lobula plate are also sensitive to this illusion. Further experiments using combinations of motion and flicker stimuli revealed novel aspects of motion computation not explained by the EMD model, and we propose specific modifications to the EMD to explain these results.

## Results

### Responses to panoramic standard and reverse-phi motion

We studied visually-guided behavior in tethered flies suspended in a virtual-reality flight simulator, allowing us to precisely control the fly's visual environment while monitoring her behavior with an optical wingbeat analyzer(Reiser and Dickinson, 2008) (Fig. 2.1B). When faced

with a rotating square-wave intensity stimulus, tethered flies attempt to turn in the direction of motion—a behavior known as the optomotor response (Fig. 2.1D, top row)(Gotz, 1964).

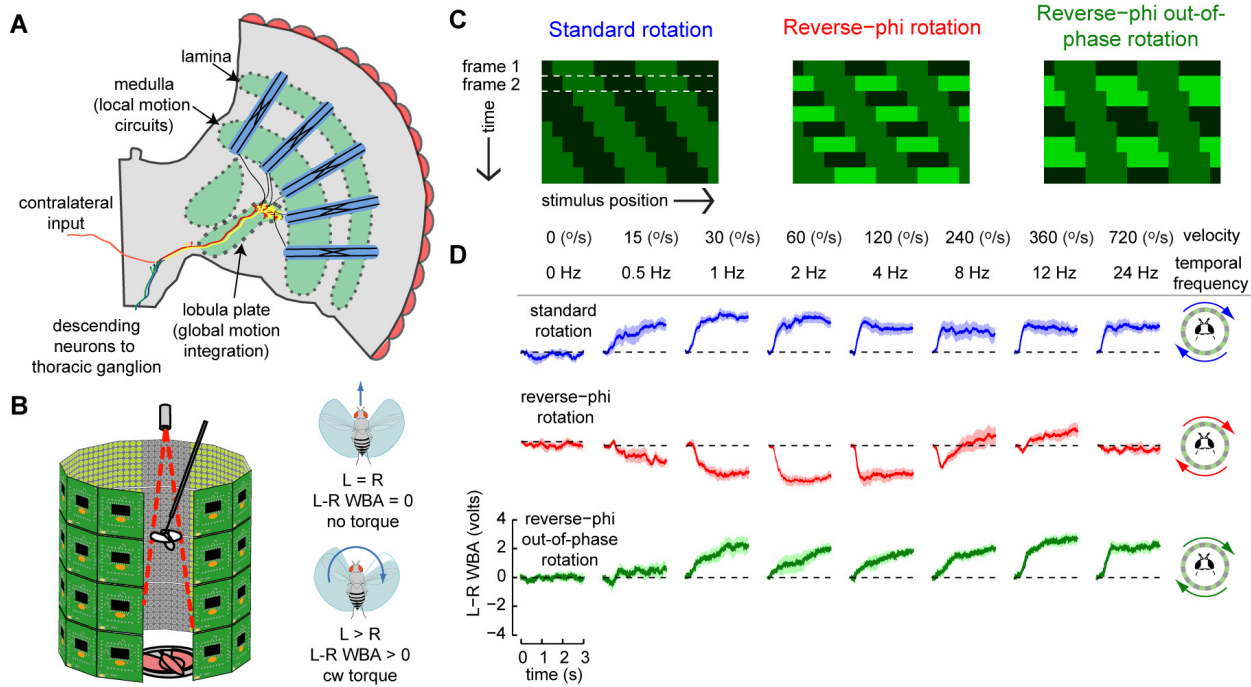


**Fig. 2.1.** Flies faced with panoramic reverse-phi motion exhibit reverse-optomotor responses. **(A)** A schematic model for fly motion vision consists of 2 stages: (1) local motion is computed by columnar circuits within the lamina and medulla, followed by (2) global integration of local motion signals in the lobula plate tangential cells. The output of the LPTCs then control optomotor behavior. **(B)** The fly is suspended within a virtual flight arena where the amplitude and frequency of each wingbeat are tracked by an optical detector. The difference between the two wingbeats (L-R WBA) is proportional to yaw torque. For example, when the amplitude of the left wingbeat is greater than the right, the fly is attempting to steer to the right with clockwise torque. **(C)** Space-time depictions of motion stimuli used in rotation experiments—all three are square-wave patterns moving from top left to bottom right. **(D)** Mean turning behavior of 10 flies ( $\pm$  s.e.m) in response to open-loop rotation of standard (top row), reverse-phi (middle row), and reverse-phi out of phase (bottom row) square-wave gratings ( $\lambda=30^\circ$ ). The speed of reverse-phi out-of-phase stimuli moved at  $\frac{1}{2}$  the speed of the standard and reverse-phi stimuli because motion occurred only in every 2<sup>nd</sup> frame (see space-time plot, C). Flies were presented with motion in both directions (CW and CCW), but responses are combined and plotted for clockwise rotation (see methods for a complete description of data treatment).

In order to determine whether flies perceive the reverse-phi illusion, we first compared optomotor steering behavior to standard and reverse-phi motion stimuli (Fig. 2.1C). The reverse-phi stimulus was similar to the standard stimulus, except that every other stripe alternated between bright and dark as it moved (Fig. 2.1C). Hence, this stimulus contained both motion and flicker components. Rotation of the reverse-phi stimulus evoked *reverse-optomotor* responses—flies steered against the direction of motion (Fig. 2.1D, middle row)—demonstrating that flies respond to the reverse-phi illusion with an inverted optomotor response. The reverse-optomotor response peaked at low stimulus velocities; at higher velocities, flies only transiently turned against the direction of stimulus motion, followed by steering in the opposite direction. Reverse-phi responses were not critically dependent on the global structure of the stimulus. For example, standard and reverse optomotor responses persisted even when the spatial extent of the stimulus was reduced to a narrow window (Fig. 2.2), and responses to translational (Duistermars et al., 2007a; Tammero et al., 2004) standard and reverse-phi stimuli were similar to responses to rotation stimuli in directionality and temporal tuning (Fig. 2.3).

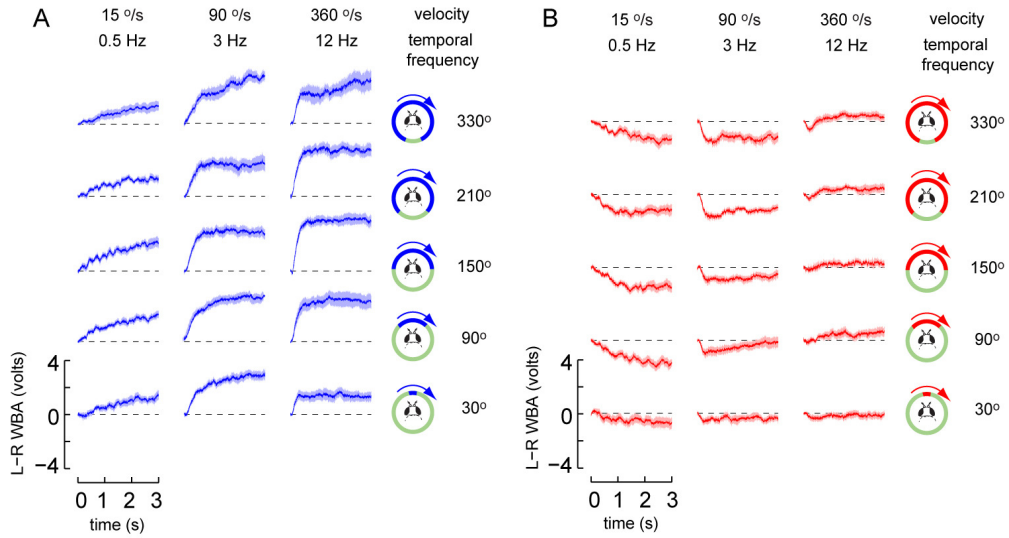
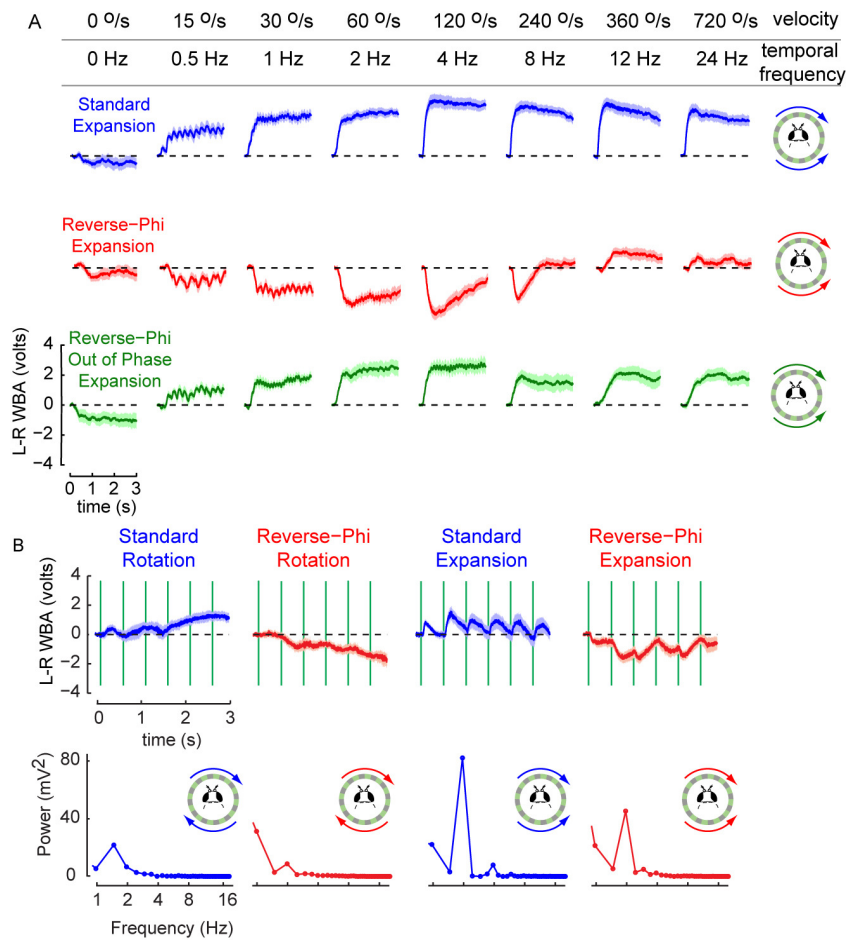


**Fig. 2.2.** Behavioral responses to standard and reverse-phi motion persist at smaller stimulus sizes. Mean turning behavior of 8 flies ( $\pm$  s.e.m) in response to open-loop rotation of **(A)** standard and **(B)** reverse-phi motion stimuli ( $\lambda=30^\circ$ , as in Fig. 2.1). The spatial extent of the motion stimulus was varied from near full-field ( $330^\circ$ ) to a small window ( $30^\circ$ ), and flies were tested at three velocities. Standard optomotor responses were similar across spatial extents, while responses to reverse-phi motion decreased when the stimulus was restricted to a  $30^\circ$  window.

Although tethered flies do not exhibit directional turning responses to pure wide-field flicker stimuli (e.g., Fig. 2.8A, leftmost column), it is possible that adding flicker to a motion stimulus simply interferes with the standard optomotor response. To test whether adding flicker reverses optomotor behavior, we used a third stimulus that we call reverse-phi out-of-phase rotation. This stimulus was similar to the reverse-phi stimulus except that the flicker occurred out of phase with the discrete motion steps (Fig. 2.1C). When flicker was out-of-phase with motion, the reverse-phi illusion was abolished (Fig. 2.1D, bottom row). This result confirms an important feature of fly motion detection—that it is strictly local in both space and time (Buchner, 1976; Reichardt, 1961). Although the discrete motion steps are generated by bars of

alternating intensity, the flies respond as if they were presented with flicker-free standard motion.

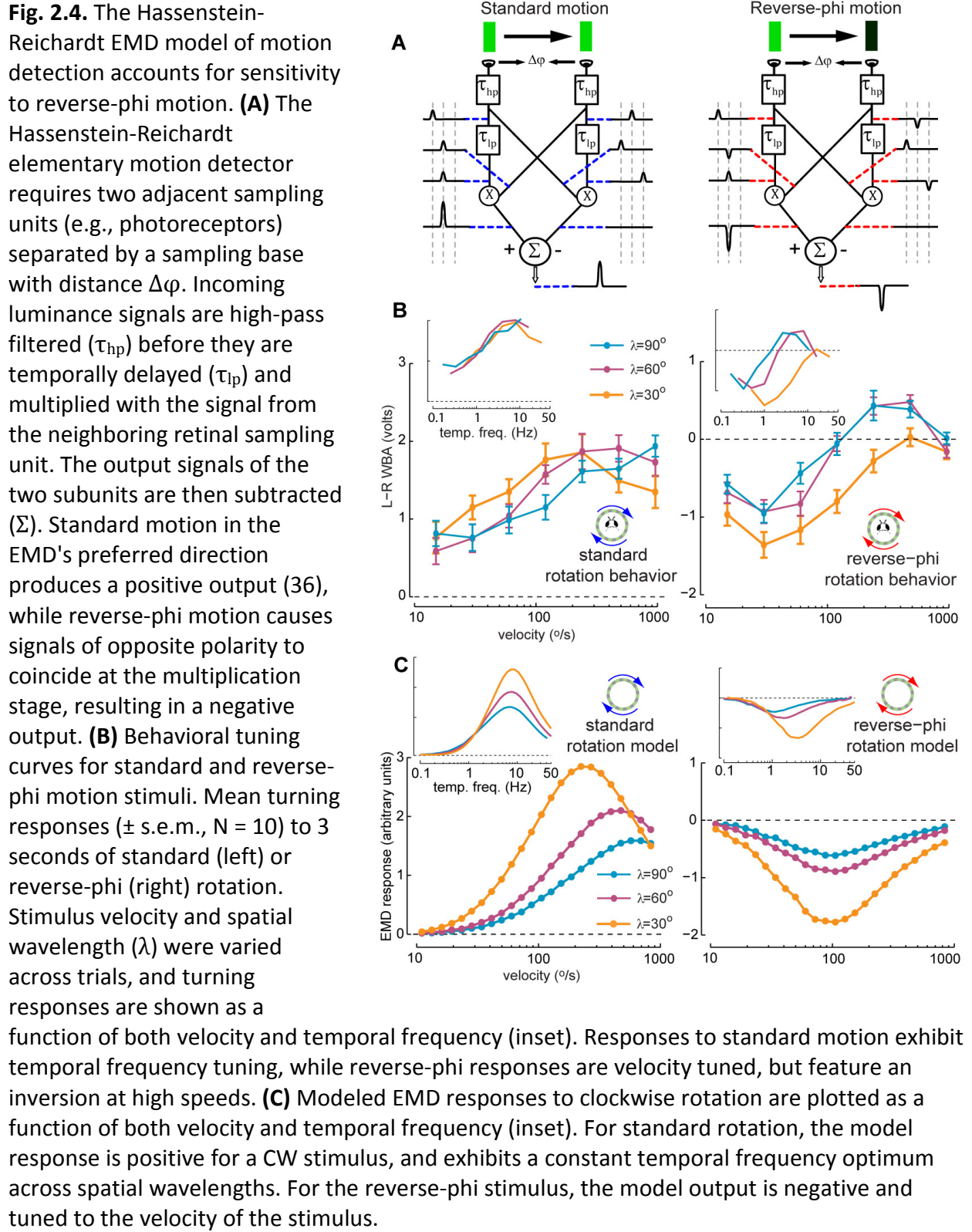
**Fig. 2.3.** Panoramic reverse-phi expansion causes flies to turn toward the focus of expansion (FOE). **(A)** Mean turning behavior of 10 flies ( $\pm$  s.e.m) in response to open-loop expansion of standard (top row), reverse-phi (middle row) and reverse-phi out-of-phase (bottom row) square-wave gratings ( $\lambda=30^\circ$ ). Responses when the focus of expansion was to the right of the fly were inverted and averaged with steering behavior when the focus of expansion was centered to the left. As in Fig. 2.1, the standard optomotor response, here manifested as a turn towards the focus of contraction (FOC), is inverted under the reverse-phi conditions, but not for reverse-phi out-of-phase. **(B)** To examine turning responses to discrete motion impulses, standard and reverse-phi rotation and expansion stimuli were advanced every half second (2 frames/sec). The red and blue traces illustrate fly mean turning behavior ( $\pm$  s.e.m.;  $N = 11$ ), while the green lines denote the motion steps of the visual stimulus. Even these infrequent motion steps induce turning reactions that are in the same direction (positive for standard, negative for reverse-phi) as the responses to the faster stimuli that approximate continuous motion. Shown below are the power spectra of the L-R WBA traces. Note that expansion responses feature much stronger phase locking to both stimuli.



### **Reverse-optomotor responses are largely predicted by the EMD Model**

In the Hassenstein-Reichardt EMD model, the intensity measured at one input (nominally a photoreceptor) is delayed by a first order low-pass filter and multiplied with a neighboring intensity signal (Reichardt, 1961); subtracting the output of the two mirror-symmetrical arms of the EMD results in a directionally selective signal (Fig. 2.4a). Due to the multiplication stage of the EMD model, successive activation of neighboring subunits with signals of opposite polarity results in a negative output (Reichardt, 1961), suggesting a mechanism for the fly's sensitivity to reverse-phi motion (Fig. 2.4A).

To what extent are the behavioral responses to reverse-phi motion accounted for by local motion computation of H-R EMDs? To explicitly test this, we constructed tuning curves comparing optomotor and reverse-optomotor behavior across spatial and temporal stimulus parameters to the tuning curves predicted by modeling. The amplitudes of rotation responses increased with stimulus velocity before decaying at the highest velocities tested (Fig. 2.4B, left). Notably, each curve, corresponding to one spatial period, peaks within a different range of stimulus velocities, but when plotted against temporal frequency (the ratio of angular velocity and spatial wavelength) the curves are clearly tuned to a common range of optimal temporal frequencies (4-16 Hz) across spatial periods (Fig. 2.4B, inset).



In comparison, reverse-phi turning responses were of opposite sign and distinctly tuned to the velocity of the stimulus—they exhibit a velocity optimum centered at 30°/s across spatial periods (Fig. 2.4B, right) and are not tuned to temporal frequency (inset). The velocity-dependence of the reverse-phi tuning curves suggests that reverse-optomotor responses are tuned to the flicker rate of the stimulus which is constant across spatial frequencies. As was shown in Fig. 2.1D, the reverse-phi response inverts at higher velocities; the inversion is absent for the smallest spatial period in this time-averaged response and is quite prominent for the lower spatial period stimuli (Fig. 2.4B).

To compare fly behavior with the predictions of the H-R EMD model, we simulated the response of an EMD (with compound eye optics) to reverse-phi and standard motion stimuli identical to those used in our experiments (see SI for model details). While for standard rotation the EMD model predicts a temporal frequency optimum, for the reverse-phi stimuli the model results exhibit a velocity optimum independent of spatial period (Fig. 2.4C). Varying the time constant of the EMD low-pass and high-pass filter time-constants did not qualitatively affect these results (Fig. 2.5). Overall, the EMD simulation captured most features of standard and reverse-optomotor flight behavior, and provides evidence for a local correlation-based mechanism underlying perception of the reverse-phi illusion. However, the inversion of the reverse-phi response at higher motion rates is strikingly absent from the simulation results of the standard EMD model (but see augmented model in Discussion).

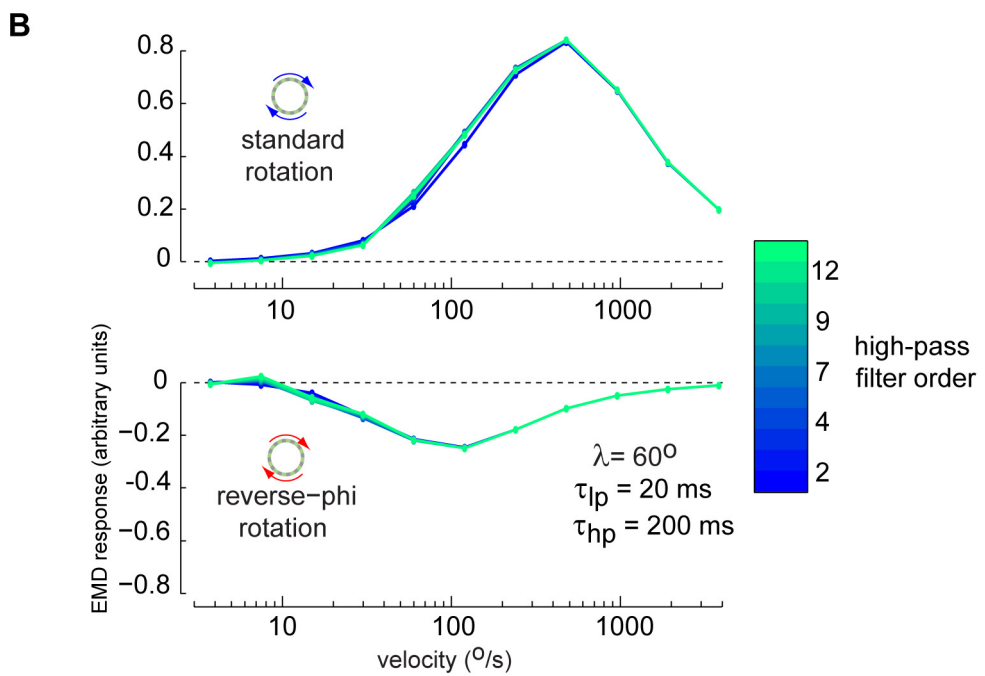
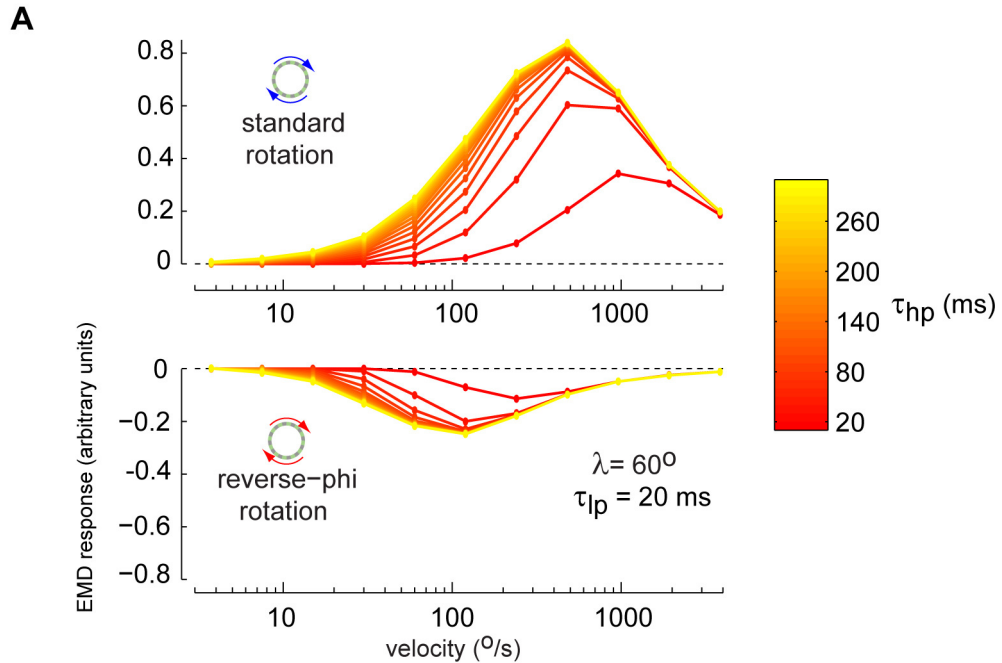


**Fig. 2.5.** Basic modifications to the high-pass filters do not affect the qualitative predictions of the EMD model. **(A)** Varying the time constant of the EMD high-pass filters alters the shape of simulated standard and reverse-phi tuning curves only at very short time constants. The  $\tau_{hp}$  used in all other simulations throughout this manuscript was 200 ms. **(B)** Varying the order of the EMD high-pass filters does not alter the shape of standard and reverse-phi tuning curves (for  $\tau_{hp} = 200$  ms).

### **Responses of a motion-sensitive neuron to reverse-phi motion**

A group of large motion-sensitive neurons in the fly visual system, the lobula plate tangential cells (LPTCs), spatially integrate signals from an array of small-field local directionally selective neurons (Single and Borst, 1998), forming receptive fields that match the complex patterns of global optic flow a fly encounters during self-motion (Borst et al., 2010). Previous studies in blowflies have also shown that the spiking H1 neuron displays directional responses when the eye is stimulated locally (Egelhaaf and Borst, 1992; Egelhaaf et al., 1989; Franceschini et al., 1989). In one case, Egelhaaf and Borst (Egelhaaf and Borst, 1992) used apparent motion stimuli that consisted of sequential brightness changes of same and opposite polarity bars—discrete, local analogs of the standard and reverse-phi motion stimuli used in this study. To test whether responses to reverse-phi are present at the input level of the LPTCs, we optically recorded transient calcium signals from the LPTC dendrites, the site where integration of local EMDs is thought to occur (Borst et al., 2010; Single and Borst, 1998).

Within the LPTC network, the horizontal-system (HS) neurons are required for optomotor behavior in blowflies (Geiger and Nassel, 1981; Hausen and Wehrhahn, 1983). Recently, the response properties of HS neurons have also been characterized in *Drosophila* (Chiappe et al., 2010; Schnell et al., 2010; Seelig et al., 2010), and found to be largely similar to the blowfly. Because HS neurons likely subserve the behaviors measured in our previous experiments, we chose to perform all imaging experiment in the horizontal-system north (HSN) neuron. Since the gain and tuning of LPTCs depends on the behavioral state of the animal (Chiappe et al., 2010; Maimon et al., 2010), we performed all imaging experiments in behaving flies to ensure

that even small neural signatures of the reverse-phi illusion could be observed (Fig. 2.6). We expressed the genetically-encoded calcium indicator gCaMP3.0(Tian et al., 2009) in HS neurons using the GAL4-UAS binary expression system(Brand and Perrimon, 1993), and imaged changes in fluorescence with 2-photon microscopy while flies walked on an air-supported ball within an arena similar to that used in the flight behavior experiments (Fig. 2.7A) (Seelig et al., 2010).

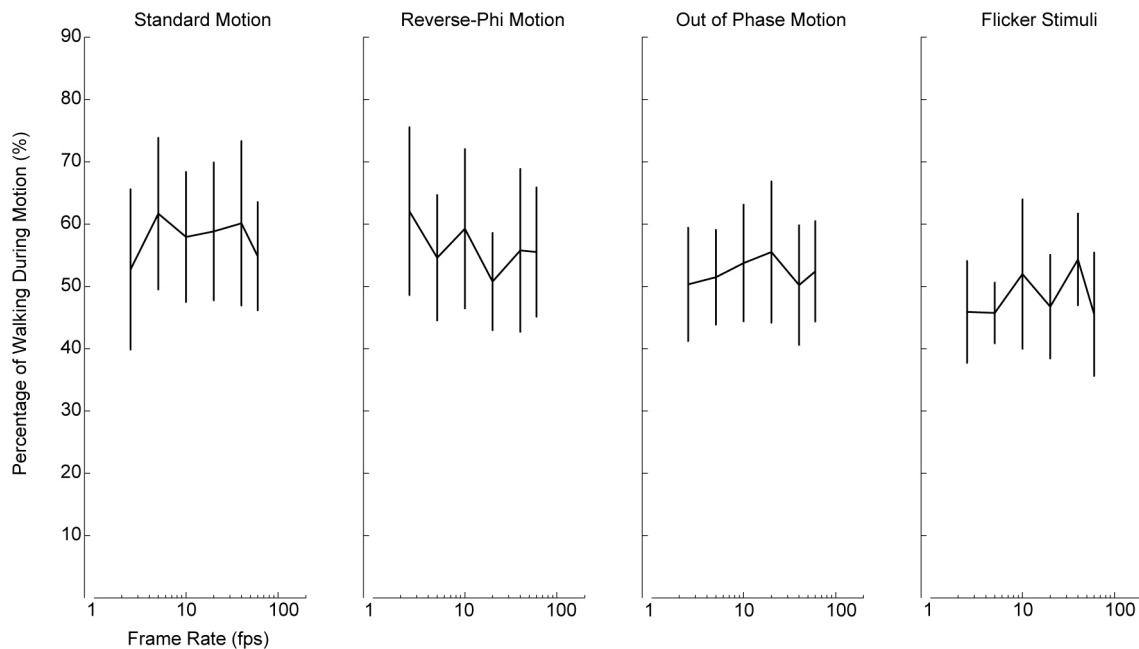


**Fig. 2.6.** Walking behavior of flies remains constant across visual stimuli. We calculated the percentage of time the fly spent walking (velocity  $> 1^{\circ}/s$ ) during stimulus presentation at all different stimulus combinations, i.e. at different stimulus velocities in standard, reverse-phi, reverse-phi out of phase and static flicker. These behavioral measurements correspond to the trials from which the data in Fig. 2.7 were generated.

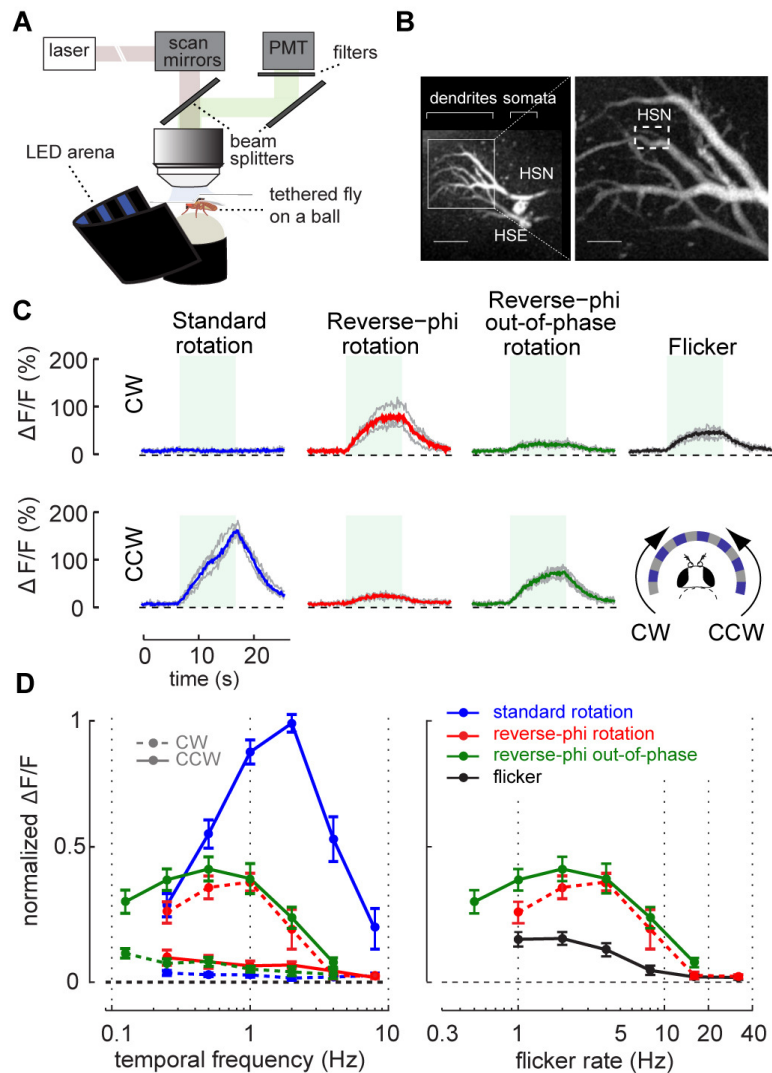
In agreement with previous work (Chiappe et al., 2010; Schnell et al., 2010), HSN in the left lobula plate (Fig. 2.7B) responded to standard motion in its preferred, or counter-clockwise (CCW), direction with an increase in calcium signal. There was no change in calcium signal if the standard motion stimulus was moving clockwise, in the null direction of the left HSN (Fig. 2.7C). In contrast, a reverse-phi stimulus moving in the neuron's null direction (CW) evoked a larger

calcium response than when the stimulus moved in the cell's preferred direction (CCW). When flicker was de-coupled from motion in the reverse-phi out-of-phase stimulus, the neuron responded more strongly to a stimulus moving in its standard preferred direction (CCW). HSN also responded to a non-directional full-field flicker stimulus, in agreement with previous electrophysiological results from blowfly LPTCs(Egelhaaf et al., 1989; Srinivasan and Dvorak, 1980). We attribute the weaker calcium responses to null direction reverse-phi and reverse-phi out-of-phase stimuli to the flicker components of these stimuli (see below).

We further investigated the reverse-phi effect in HSN by presenting the three motion stimuli at several velocities and wide-field flicker at several rates (Fig. 2.7D). We found strong qualitative agreement between the temporal frequency tuning curves we obtained from imaging (Fig. 2.7D, left) and the results of behavior (Figs. 1, 4) and the HR EMD simulation (Fig. 2.4C). For example, flight behavior, EMD simulation, and HSN responses were tuned to higher temporal frequencies for standard motion than reverse-phi motion, although the absolute frequencies of maximum sensitivity were lower in the neuronal response—we attribute this to differences in speed tuning between walking and flying(Chiappe et al., 2010). When we compared the tuning curves obtained with the three stimuli containing flicker (CW reverse-phi, CCW reverse-phi out-of-phase, and wide-field flicker), we found that flicker alone could not account for the observed responses to reverse-phi motion (Fig. 2.7D, right). Interestingly, responses to wide-field flicker were inhibited if motion was also present, as revealed by comparing the responses to null-direction movement of reverse-phi and reverse-phi out-of-phase stimuli with those obtained with wide-field flicker only (Fig. 2.7C,D). Overall, the similarities between flight behavior and HSN responses demonstrate that the reverse-phi illusion is present at the level of the HSN

dendrites, suggesting that small-field motion detectors underlie behavioral sensitivity to the reverse-phi illusion.

**Fig. 2.7.** The lobula plate tangential cell HSN responds to reverse-phi motion with inverted direction selectivity. **(A)** The experimental setup used to record calcium transients from LPTC dendrites consists of a tethered fly walking on an air-supported ball. **(B)** Left: low magnification (scale bar, 25  $\mu$ m) of the left hemisphere of the fly brain (dorsal to the left, midline to the top) with Horizontal System North (HSN) and Equatorial (HSE) neurons labeled with gCaMP3.0. Right: higher magnification view of the dendritic arbors of the HS neurons (scale bar, 7  $\mu$ m), showing the region of interest selected to analyze HSN responses to moving stimuli. **(C)** Example from a single fly of the HSN responses to visual motion stimuli moving at 1 Hz (4-5 repetitions each, individual trials are gray and the mean is depicted in the corresponding color— blue: standard rotation, red: reverse-phi, and green: reverse-phi out-of-phase). The shaded region denotes the onset and duration of the visual stimulation. **(D)** Normalized HSN dendrite responses ( $N = 9$  flies; mean  $\Delta F/F \pm$  s.e.m during the last 0.5 s of the stimulation) to motion (left) and flicker-containing stimuli (right). Flicker rates within the response range of the HSN neuron elicited mean responses that were significantly lower than those induced by either CW reverse-phi motion (right:  $p < 0.001$ , *U*-test, with the sole exception of the lowest flicker rate tested  $p = 0.09$ ), or CCW reverse-phi out-of-phase ( $p < 0.0005$ , *U*-test).



### Temporal deconstruction of the reverse-phi stimulus.

To further explore interactions between motion and flicker, we deconstructed the reverse-phi stimulus into its individual components by independently varying the rates of contrast flicker and motion. In the absence of flicker, flies steered in the direction of stimulus motion (Fig. 2.8A, top row). Reverse-phi optomotor responses were strongest when the flicker rate was equal to the rate of stimulus motion (Fig. 2.8A, red traces). In the three conditions with low flicker rates and high motion velocities, standard optomotor behavior persisted (denoted with blue asterisks), indicating that the illusion is abolished when the standard motion component occurs much more frequently than the reverse-phi steps. Surprisingly, flies also turned against the direction of stimulus motion when the flicker occurred in every other motion step (red asterisks); that is, when the stimulus consisted of equal parts reverse-phi and standard motion. This behavior cannot be explained as the linear combination of the responses to the two stimuli, since when presented in isolation the steering responses to standard motion are larger in amplitude. It is also not captured by the EMD model (green lines in Fig. 2.8A denote predictions of the EMD). Interestingly, in the three cases (denoted with black asterisks) where the combined stimulus flickers at an integer multiple of the motion step rate, the reverse-phi response is abolished, even though flicker always accompanies the motion step. At the higher flicker rates, flies often steered transiently in the direction of the reverse-phi stimulus, followed by a ‘corrective’ steering response in the opposite direction (also seen in Fig. 2.1D), presumably reflecting an adaptive mechanism that is enhanced by flicker. We call this phenomenon the *flicker-mediated inversion*.

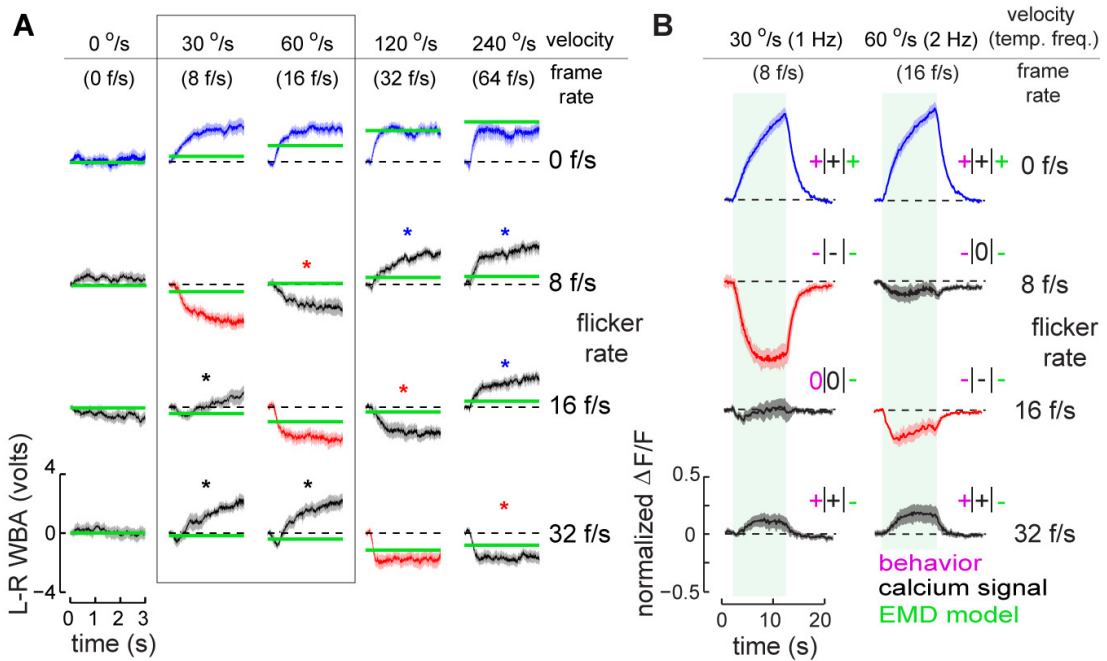
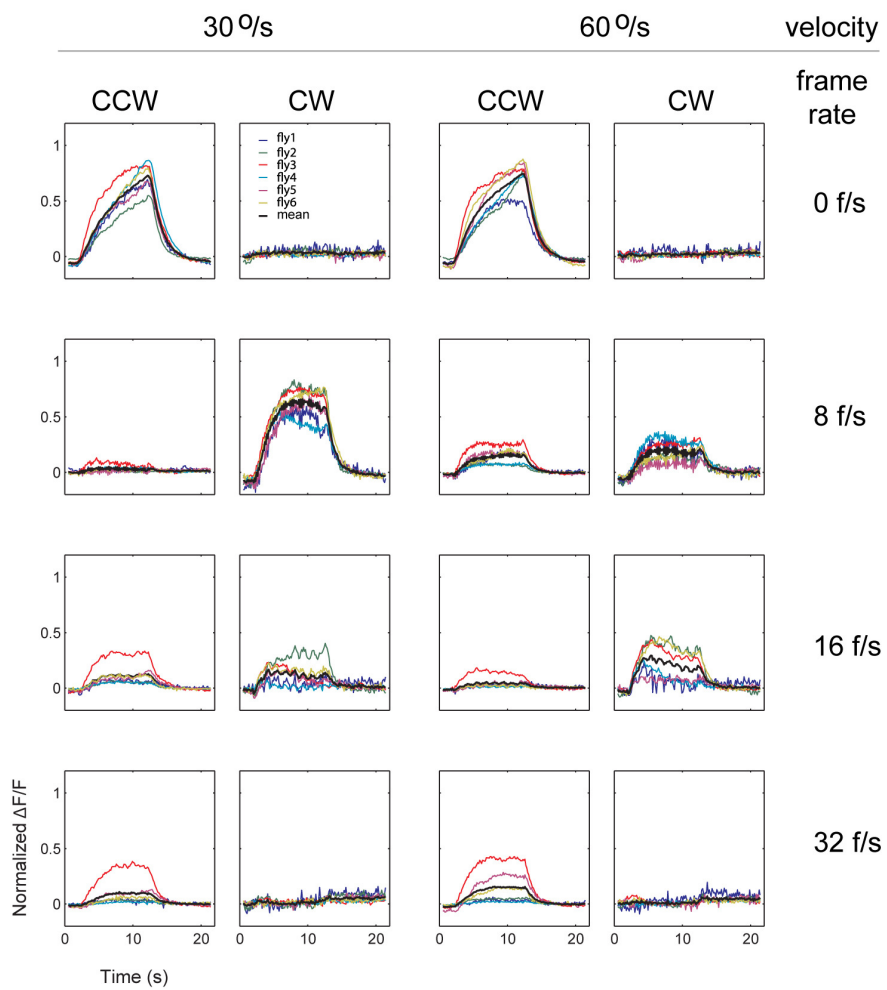


**Fig. 2.8.** Independently varying motion and flicker rates reveals local motion computations not described by the EMD model. **(A)** Mean turning responses ( $\pm$  s.e.m,  $N = 10$  flies) to reverse-phi rotating stimuli in which the velocity and rate of contrast reversal were controlled independently. Rotation occurred at one of 5 velocities and the contrast of the stimulus was inverted at one of 4 flicker rates. Blue traces indicate standard motion (no flicker), red traces reverse-phi (flicker rate is equal to motion frame rate). Blue asterisks denote conditions with low flicker rates and high motion frame rates, black asterisks when the stimulus flickers at an integer multiple of the motion frame rate, and red asterisks when the motion frame rate is twice the flicker rate. Green lines represent the steady-state output of an elementary motion detector simulation (same model parameters as in Fig. 2.4C) to each visual stimulus. **(B)** Normalized HSN dendrite responses ( $\pm$  s.e.m,  $N = 6$  flies) to reverse-phi motion stimuli in which the rate of contrast reversal was independently varied (identical stimuli as in columns 2-3 of A; traces color coded same as in A). To facilitate comparison with the behavioral results, each time series is plotted as CCW responses minus CW responses (calculated from the individual traces in Fig. 2.9). Boxes on the right of each trace show whether HSN calcium transients (black), fly behavior (magenta) and EMD model prediction (green) are significantly greater than (+), less than (-), or not different (0) from zero, measured as the normalized mean response to the same stimulus ( $P < 0.1$ , one-tailed t-test).

Where does the flicker-mediated inversion originate? To test whether it is present in the output of the elementary motion detection circuitry, we performed a subset of the same experimental conditions while imaging calcium transients from the HSN cell dendrites (Fig. 2.8A). As

expected, we observed robust calcium responses to standard motion in the absence of flicker (blue traces), and an opposite direction response when the flicker and motion rates were equal (red traces). Remarkably, in cases where we observed the flicker-mediated inversion in flight behavior (i.e., when the flicker rate was greater than the rate of stimulus motion), we found that calcium accumulation in the HSN dendrites also reflected this inversion (Fig. 2.8B and Fig. 2.9). These data agree with our behavioral results but contradict the predictions of the standard EMD model (Fig. 2.8B, inset). They also demonstrate an unexpected interaction between flicker and motion detection in the fly visual system.

**Fig. 2.9.** HSN dendrites reverse-phi responses peak when contrast flicker occurs in phase with stimulus motion. Normalized mean responses of each HSN dendrite from different flies (indicated in different colors) when the stimulus was moved at 30 and 60 °/s in two different directions (CCW, counter clockwise, and CW, clockwise) during which the flicker rate of the stimulus was changed independently at different rates indicated on the right side of the figure. Fig. 2.8B was obtained from these traces by subtracting CW responses from CCW responses.



### **Bilateral comparison of reverse-phi and standard motion.**

Our results suggest that reverse-phi motion is computed locally. However, in order to generate appropriate behavioral responses, flies integrate local motion signals from across the entire visual field. In order to test global integration of local motion signals, we designed a stimulus in which 90° windows of visual motion were centered laterally on each side of the fly. When faced with a lateral window of standard clockwise rotation, flies exhibited robust optomotor steering similar to full-field optomotor responses (Fig. 2.10a, top row). A lateral window of clockwise reverse-phi motion elicited reverse-optomotor responses (Fig. 2.10a, middle row), but did not result in an inversion of the response at higher speeds; this is due to the fact that a reliable behavioral measurement of the flicker-mediated inversion requires a nearly full-field presentation of the reverse-phi stimulus (e.g., Fig. 2.2).

We then asked whether simultaneous presentation of the standard and reverse-phi patterns would result in an additive combination of standard and reverse-optomotor responses, as suggested by a simple model of integration across both eyes. If this were the case, one would expect that flies would always turn in the direction of standard motion (clockwise), because this pattern elicited larger amplitude steering responses at all velocities (Fig. 2.10a). However, we found that at lower velocities, reverse-optomotor behavior dominated the response (Fig. 2.10a, bottom row). This behavior peaked around the reverse-optomotor optimum observed previously, and inverted as pattern velocity increased, such that at the higher velocities tested flies turned in the direction of the standard rotating pattern. The linear prediction (the sum of

the standard and reverse-optomotor responses, depicted as the gray lines in Fig. 2.10a) cannot account for this paradoxical behavior.

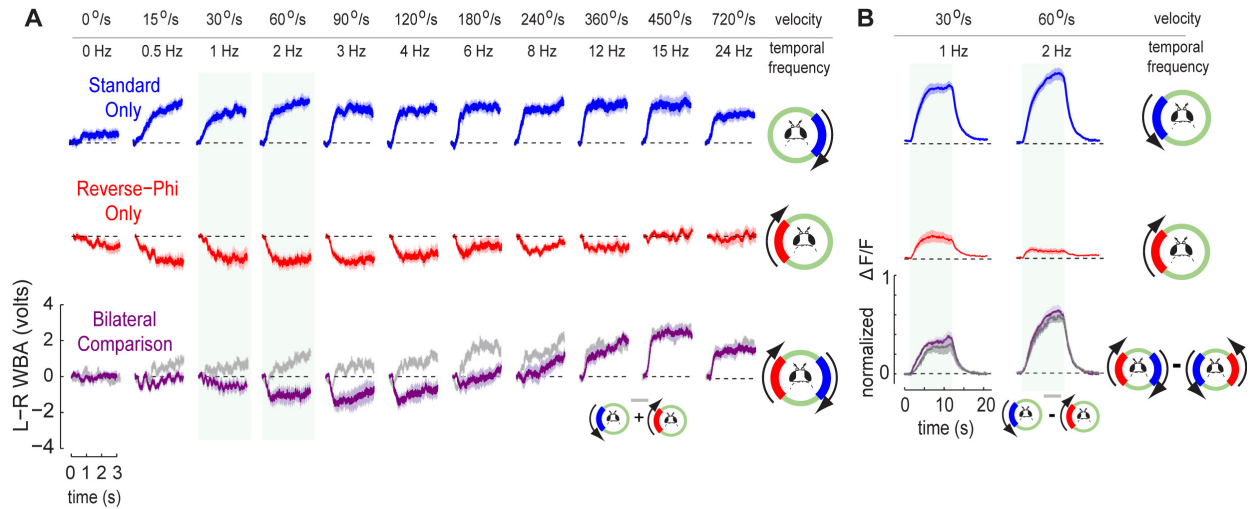


**Fig. 2.10.** Bilateral comparison of standard and reverse-phi motion shows a non-additive integration of motion signals that is not present in the HSN dendritic response. **(A)** Mean turning ( $\pm$  s.e.m.;  $n = 10$  flies) in response to bilateral presentation of standard and reverse-phi rotating patterns. Top row: one side ( $90^\circ$ ) of the arena displayed a standard rotating pattern ( $\lambda=30^\circ$ ), while the rest of the arena was held at a constant intermediate intensity. The same for a reverse-phi pattern (middle row). Bottom row: standard and reverse-phi patterns were presented bilaterally, on opposite sides of the arena, while  $90^\circ$  in front of and behind the fly were held constant. The gray traces in the bottom row represent the sum of the responses to standard and reverse-phi motion alone. **(B)** HSN-dendrite normalized mean responses ( $\pm$  s.e.m.,  $n = 6$  flies) to unilateral and bilateral presentation of reverse-phi and standard motion stimuli, measured in the left lobula plate. Top and middle rows: responses to unilateral presentation of standard (CCW, blue trace) and reverse-phi (CW, red traces). Bottom row: both stimuli were presented simultaneously on opposite sides of the arena. Shown in purple is the response to bilateral presentation of standard and reverse-phi stimuli, plotted as the difference between the two stimulus configurations (CCW response - CW response). For comparison, the differences between the responses to monocular stimulation with standard and reverse-phi stimuli are shown in gray. The individual traces for each condition are shown in Fig. 2.12.

Is the behavioral dominance of the reverse-phi stimulus reflected in the response properties of the HSN neuron? We tested this by imaging calcium signals from HSN dendrites while presenting walking flies with unilateral and bilateral motion stimuli like those in the previous experiment (Fig. 2.10b). When presented ipsilaterally only, standard and reverse-phi motion

excite the cell when moving in the preferred and null directions, respectively. But when the two patterns were presented bilaterally, for example reverse-phi ipsilateral and standard contralateral (both moving CW), the calcium signal of the HSN neuron was not dramatically different from that to unilateral motion. In other words, HSN responses did not reflect the dominance of the reverse-phi stimulus we observed during flight behavior. Although our behavioral data demonstrate that global integration of standard and reverse-phi motion stimuli is not simply additive, this nonlinearity is not evident at the level of the HSN dendrites.

## Discussion

Our results show that *Drosophila melanogaster* exhibit *reverse-optomotor* responses when faced with reverse-phi motion (Figs. 1, 2 and 3), that is they perceive the illusion in much the same way as do vertebrates. HSN dendrites in the lobula plate of walking flies also respond to reverse-phi stimuli with reverse direction selectivity (Fig. 2.7). Behavioral (Figs. 1, 4), physiological (Fig. 2.7), and modeling (Fig. 2.4) data suggest that the reverse-phi illusion is computed at the level of local motion detection circuits, the outputs of which are then integrated at the dendrites of the LPTCs. However, we also identified a flicker-mediated inversion of the reverse-phi illusion (Fig. 2.8A) that is not explained by the classical EMD model. Calcium imaging in the HSN dendrites suggests that this inversion occurs presynaptic to the LPTCs (Fig. 2.8B).

### **The EMD model captures many features of reverse-phi sensitivity.**

Over fifty years ago, Hassenstein and Reichardt used an analog of the reverse-phi stimulus to describe and model motion detection in the *Chlorophanus* beetle (Reichardt, 1961). They

observed that alternately presenting two adjacent bars of the same polarity (On-On) caused the beetles to turn in one direction, but bars of opposite polarity (e.g. On-Off), elicited a turn in the opposite direction. This led them to conclude that motion detection involved multiplication of neighboring luminance signals, and resulted in the formulation of the EMD model, which has since been used to describe motion detection in many animals, including humans (Borst and Egelhaaf, 1989; van Santen and Sperling, 1985).

The EMD and other closely related models based on spatiotemporal correlation such as the Barlow-Levick (Barlow and Levick, 1965) and motion energy models (Adelson and Bergen, 1985), are inherently susceptible to the reverse-phi illusion (Fig. 4A and refs. Bours et al., 2009; Mo and Koch, 2003). In contrast, the primary alternative class of models for motion detection, based on the so-called gradient detector (Srinivasan, 1990), will not detect any directional motion in response to a reverse-phi stimulus without substantial modification (Johnston and Clifford, 1995). Although the neural implementation of spatiotemporal correlation in the fly visual system is currently unknown, the EMD model serves as a useful comparison for our behavioral and physiological data.

A non-intuitive prediction of the EMD model is that responses to reverse-phi motion will peak at a particular velocity. To understand this, it is useful to consider the discrete events that give rise to motion signals. In the case of standard motion, these events are generated by the motion of edges (light-to-dark and dark-to-light transitions) whose arrival rate is determined by the temporal frequency (Reichardt, 1961), defined as the ratio of the angular velocity and spatial period of the stimulus. Above a peak temporal frequency set by the EMD low-pass filter

time constant, response amplitudes are attenuated, producing the characteristic tuning curves shown in Fig. 2.4C. By contrast, the discrete motion events induced by a reverse-phi stimulus are generated by flickering edges that occur at a rate set by the stimulus velocity, independent of spatial frequency. Therefore in the reverse-phi stimulus, the flicker rate serves the same role in specifying the peak response as the temporal frequency does for standard motion stimuli. In agreement with this prediction, behavioral responses to reverse-phi motion exhibit a pronounced velocity optimum, while responses to standard motion peak at a particular temporal frequency (Fig. 2.4B). Overall, the EMD model captures several key features of the data in Figs. 1-3.

#### **Features not captured by the EMD model.**

By combining motion and flicker stimuli, we identified a flicker-mediated inversion of the flies' optomotor response that is not predicted by the canonical EMD model. Under open-loop conditions, the optomotor steering response of the fly saturates rapidly (Fig. 2.1D and Fig. 2.4). However, when presented with reverse-phi stimuli, fly behavioral responses do not immediately saturate, and adaptation occurs more rapidly, particularly at high flicker rates (Fig. 2.1D and 8A). In some cases, rapid adaption leads to a complete inversion of the reverse-optomotor response. This flicker-mediated inversion is apparent in fly optomotor responses to high velocity reverse-phi stimuli (Fig. 2.4B), or when the flicker rate exceeds the rate of stimulus motion (Fig. 2.8). Considering the striking agreement between the behavioral inversion and the calcium signals of the HSN dendrites (Fig. 2.8), it is clear that this rapid adaptation is present in

the LPTC inputs and may be either upstream of local motion detection, or an intimate, and currently enigmatic feature of fly motion detection.

If the standard EMD cannot fully account for the fly's responses to combined motion and flicker stimuli, is there an alternative model that can? One possible explanation for the inversion is that temporal aliasing occurs in the motion detector at high flicker rates. For example, an EMD implemented with a temporal delay line, rather than a first-order low-pass filter, would produce inverted output values at some range of high flicker rates (Fig. 2.11). Inhibitory interneurons in the fly visual system (Sinakevitch and Strausfeld, 2004) could execute such a fixed delay, as in the closely-related Barlow-Levick model (Barlow and Levick, 1965; Mo and Koch, 2003).

Another feature seen in our data (Fig. 2.7D) and previous studies (Egelhaaf et al., 1989; Franceschini et al., 1989) is the weak flicker sensitivity of the LPTC neurons. One potential explanation for this phenomenon is that motion detection circuits are not perfectly balanced, and there is evidence that LPTCs receive antagonistic signals from asymmetric EMDs with opposite preferred directions (Franceschini et al., 1989). Therefore, a model that accounts for both HSN flicker sensitivity and the flicker-mediated inversion is an elaborated EMD that includes asymmetric summation of motion signals and temporal aliasing due to a discrete temporal delay in the motion detector (Fig. 2.11). We presume that the adaptive time course of the behavioral responses (Figs. 1 and 4) are due to temporal adaptation in pre-motion circuits within the lamina and medulla. More complex models consisting of identified neuron types and

biophysically realistic processing (Higgins et al., 2004; Mo and Koch, 2003) may prove useful in elucidating the contribution of adaptation to reverse-phi perception and motion computation.

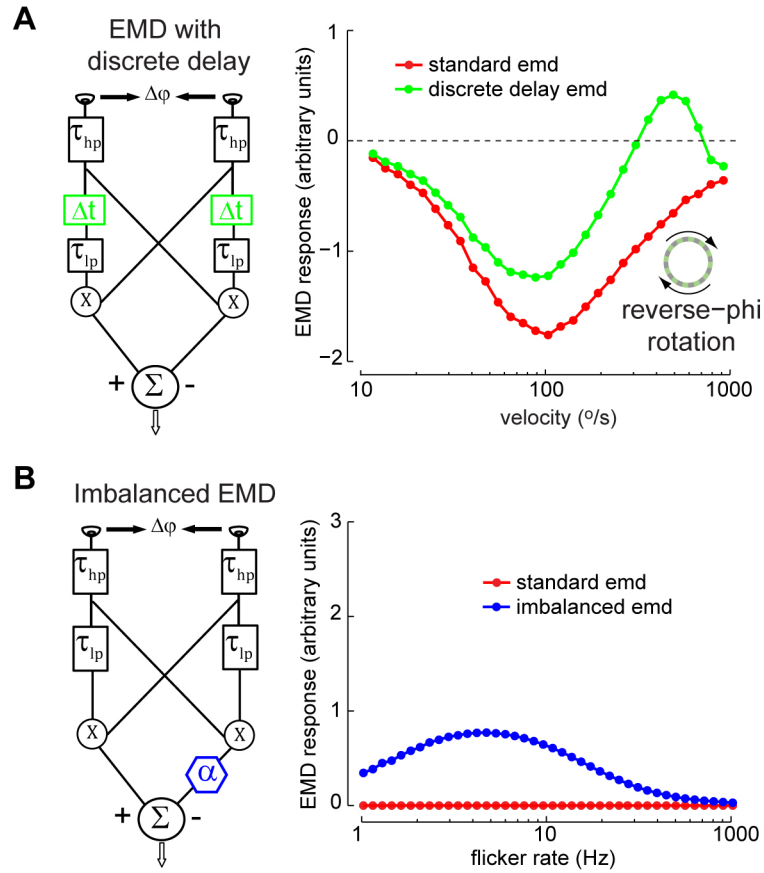


**Fig. 2.11.** Modifications to the EMD model that account for flicker-related phenomena. **(A)** Introducing a short temporal delay into the EMD model ( $\Delta t = 10$  ms) results in an inversion of the reverse-phi response at high velocities ( $\lambda=60^\circ$ ). The parameters of the simulation were identical to the simulation in Fig. 2.4C, except for the presence of the delay. **(B)** Adding a gain factor ( $\alpha$ ) so that the subtraction stage of the EMD becomes unbalanced results in sensitivity to pure flicker stimuli. The visual stimulus was a full-field flicker stimulus consisting of the minimum and maximum intensity values of the reverse-phi stimulus used in all other experiments and simulations. When  $\alpha = 1$ , the EMD is fully balanced (red) and insensitive to flicker, but when the half detectors are even slightly un-balanced ( $\alpha = 1.01$ , blue), the model is flicker-sensitive. All other model parameters were identical to the simulation in Fig. 2.4C. These modifications to the EMD model are shown to support the plausibility of these mechanisms rather than to reproduce the data in the text.

We also discovered that flies simultaneously presented with standard and reverse-phi motion turn in the direction of the reverse-phi stimulus at low velocities, and with the standard motion pattern at higher velocities (Fig. 2.10A), while HSN responses to reverse-phi motion were always lower than those to standard motion, even when presented bilaterally. The bilateral comparison result is not predicted by the relative amplitudes of the EMD model (Fig. 2.4), nor by a linear combination of steering responses to either pattern alone (Fig. 2.10B). Behavioral dominance of reverse-phi motion requires binocular separation of standard and reverse-phi stimuli (data not shown), suggesting that this nonlinear integration occurs independent of, or postsynaptic to the LPTC's. One parsimonious way to explain these data is that some mechanism of global motion integration accounts for preferential orientation to reverse-phi stimuli, and that this mechanism must be based on signals that are qualitatively different from the local inputs to HSN we measure.

### **Reverse-phi motion as a circuit-breaking tool.**

A powerful approach for studying the properties of visual circuits is reverse-correlation-based system identification (Marmarelis and McCann, 1973). However, motion circuits present a particular challenge because motion detection relies on nonlinear interactions and structured spatiotemporal correlations. An important motivation for studying visual illusions like reverse-phi is to identify behavioral and neural phenomena not resolvable with standard reverse-correlation techniques. The reverse-phi illusion promises to be an important tool for dissecting the neural circuitry that underlies motion detection, as demonstrated by two recent papers that employed reverse-phi motion stimuli (Clark et al., 2011; Eichner et al., 2011). The reason

for performing these studies in *Drosophila* is that the molecular genetics toolkit available in flies enables the identification and manipulation of motion circuits (Rister et al., 2007). For example, recent data suggest that signals are rectified into ON and OFF pathways early in the motion pathway (Joesch et al., 2010). One might predict that flies, like humans (Wehrhahn and Rapf, 1992), are not equally sensitive to ON and OFF motion signals. Selectively silencing components of ON or OFF pathways might specifically disrupt sensitivity to reverse-phi motion.

Nearly a century ago, Ramon y Cajal speculated about the remarkably high degree of anatomical similarity between the peripheral visual systems of flies and vertebrates (Cajal and Sanchez, 1915). We now know there are also striking genetic and developmental commonalities that support a common evolutionary origin (Sanes and Zipursky, 2010). Despite 500 million years of evolution, fly and human eyes are also likely performing many of the same neural computations. Many visual illusions are perceived by both humans and insects (Srinivasan, 1993), suggesting that similar neural mechanisms underlie visual processing across the animal kingdom. A further test of this analogy would be to look in humans for the surprising features of reverse-phi perception we identify in this study. Sensitivity to both spatiotemporal correlations (standard motion signals) and anti-correlations (reverse-phi motion) may be part of a common strategy to average out noisy fluctuations in visual inputs, thus allowing movement detection circuits to be maximally sensitive to the most relevant and persistent motion signals in the environment.

## Materials and methods

### Tethered flight experiments.

*Drosophila melanogaster* from our laboratory culture descended from 15 wild females caught in 2009 were reared on standard fly medium and kept in a 25° incubator on a 14 h:10 h light:dark cycle. Gravid females, 3-5 days old, were cold-anesthetized and tethered to a 0.1 mm tungsten wire with UV-activated glue. A drop of glue was placed between the head and thorax at an angle close to natural flight posture (David, 1978). All of the data presented are from head-fixed flies; however, we observed only minor differences between responses of head-free and head-fixed flies.

After at least 30 minutes of recovery, flies were placed within a cylindrical electronic flight simulator. Within the arena, the position of the wings was monitored using a wingbeat analyzer(Gotz, 1987) . The wingbeat amplitudes, frequency, and signals encoding the positions of the display stimuli were sampled at 1 kHz by a DigiData 1440A (Axon Instruments). All data analysis was performed offline in MATLAB (Mathworks, Natick, MA). In all figures showing flight behavior, we follow a convention of plotting the turning response of flies as the left minus right wing beat amplitude (L-R WBA), a measure which is directly proportional to yaw torque (Tammero et al., 2004).

All of the flight behavior experiments used a protocol in which 3 second open-loop trials were interleaved with 5 seconds of closed-loop ‘stripe fixation,’ during which the fly actively controlled the position of a 30° dark stripe against a bright background. The stripe fixation epochs ensured that the flies were actively steering at the onset of each open-loop condition. If

the fly stopped flying during a trial, a small fan automatically delivered a brief wind stimulus to encourage her to resume flight. Trials in which the flight stopped were excluded from subsequent analysis. Within an experiment, each set of conditions was presented as random blocks repeated three times. Trials in which the fly stopped flying were repeated at the end of each block. Therefore, each fly completed each condition at least three times. These data were averaged on a fly-by-fly basis to produce a mean turning response for each condition, and then plotted as the mean  $\pm$  s.e.m. across flies.

For each open-loop condition, the mean response during the 50 ms previous to stimulus onset was subtracted from the subsequent turning response. Half of the conditions (CCW rotation) were inverted and averaged with the corresponding symmetric conditions (CW rotation) on a per-fly basis. The convention in all behavior figures is that rotation is CW (and in Fig. 2.3, the focus of contraction is to the right). Power spectra of L-R WBA time series in Fig. 2.3 were computed from these mean response time series.

We chose to perform all behavioral experiments in flying flies because flight responses are more rapid and repeatable, allowing us to test many (up to 96) stimulus conditions on single flies- this would not have been possible in walking flies, which respond more slowly and with greater variability. Imaging experiments were performed in walking rather than fixed animals because it has been shown that the behavioral state of the fly modulates the velocity coding of LPTC neurons (Chiappe et al., 2010). Previous studies have demonstrated that the yaw optomotor responses of walking and flying flies are comparable in spatial and temporal tuning (Gotz and Wenking, 1973; Gotz, 1964)

### Visual stimuli.

The visual arena consisted of a 32x88 array of green LEDs covering 330° in azimuth and 120° in elevation (Reiser and Dickinson, 2008). In the imaging setup, the LEDs were blue (to prevent bleed-through to the photomultiplier) and its dimensions covered 210° in azimuth and 60° in elevation of the fly's visual field. With the fly on the ball, the subtended angle of elevation was reduced to ~53°. In both setups, each pixel subtends less than a 3.75° visual angle on the fly's retina. The maximum pixel size of each LED is below the inter-ommatidial distance of *Drosophila* (Heisenberg and Wolf, 1984), so single pixel jumps between consecutive frames simulate continuous motion to the fly (except when motion is very slow).

We examined flight behavior in response to three motion stimuli: standard, reverse-phi, and reverse-phi out-of-phase rotation (Fig. 2.1B). The standard rotation stimulus was a square wave grating of alternating bright (intensity 6 out of 7) and intermediate intensity (3/7) stripes with a spatial period,  $\lambda$ , of 30° (one period consists of a dim and a bright bar, each 4 pixels wide). The reverse-phi stimulus (Video S1) was similar except that within each motion step alternating stripes switched between bright (6/7) and dark (1/7) intensity levels, selected to be symmetric with respect to the intensity of the intermediate intensity bars. The maximum intensity (7/7) was approximately  $72 \text{ cdm}^{-2}$  and minimum intensity (1/7) was  $0 \text{ cdm}^{-2}$ , with intermediate grayscale values distributed linearly within this range (Reiser and Dickinson, 2008).

The reverse-phi out-of-phase stimulus was similar to the reverse-phi rotation stimulus except that the contrast flicker occurred *between* and not *within* motion steps. Therefore, motion alternately followed ON and OFF luminance changes (Fig. 2.1B). Importantly, the motion

component of the reverse-phi out-of-phase stimuli was  $\frac{1}{2}$  that of reverse-phi and standard motion stimuli, because motion occurred in every other frame. This probably contributed to the decrement of the response to reverse-phi out-of-phase stimuli compared to standard motion stimuli. We presented each stimulus at one of eight speeds rotating either clockwise (CW) or counterclockwise (CCW), so that a trial block contained 48 unique conditions (Fig. 2.1). Although the mean luminance of the standard and reverse-phi patterns was not identical, optomotor responses of contrast-adapted flies are nearly constant across the range of contrasts used in our experiments (Duistermars et al., 2007a); control experiments confirmed that reverse-phi behavioral responses persisted across a range of contrasts.

In the analogous 2-photon imaging experiments (Fig. 2.7), flies were presented with the visual stimuli described above, with an additional full-field flicker stimulus that consisted of a square wave pattern ( $\lambda = 30^\circ$ ) with a background of intermediate intensity (3/7) and stationary bars which flickered between dark (0/7) and bright (6/7) intensity. This flicker stimulus covered the same spatial extent as the motion stimuli. To construct tuning curves while imaging, we moved these stimuli at six speeds (2, 4, 8, 16, 32, and 64 frames per second).

To build the behavioral tuning curves in Fig. 2.4, we parametrically varied the standard and reverse-phi rotation stimuli. We tested flies with 84 unique conditions: 7 velocities (15, 30, 60, 120, 240, 480, 960°/s), 3 spatial wavelengths ( $\lambda=30^\circ, 60^\circ, 90^\circ$ ), and both directions (Fig. 2.4B). The temporal frequency denoted in Fig. 2.4 is the ratio between the angular velocity and the pattern's spatial period.

To disambiguate the two components of the reverse-phi stimulus we constructed a stimulus similar to the reverse-phi rotation stimulus described above, except that velocity and contrast flicker of the square-wave grating ( $\lambda=30^\circ$ ) were controlled independently (see Video S2 for an example). In the tethered flight experiments of Fig. 2.8A, flies were tested with stimuli rotating in open-loop at one of five velocities and flickering at one of four flicker rates (stimulus details labeled in the figure). In these experiments, motion and flicker always started in phase and then drifted in and out of phase depending on the independent rates of motion and flicker. In the two-photon imaging experiments of Fig. 2.8B, only a subset of these conditions were tested.

We also tested standard, reverse-phi, and reverse-phi out-of-phase stimuli that simulated side-slip translation in flight (Tammero et al., 2004). These patterns were identical to the rotating stimuli ( $\lambda=30^\circ$ ; same intensities) except the frontal and rear hemispheres of the arena rotated in opposite directions, creating a lateral focus of contraction (FOC) and a focus of expansion (FOE) on the opposite side of the arena. We presented 48 conditions: each stimulus at the same eight speeds as in Fig. 2.1, with the FOC positioned on either side of the fly (Fig.3). To examine the characteristics of transient responses to brief motion pulses, we also conducted "impulse-response" experiments (Duistermars et al., 2007a) by stepping the standard and reverse-phi motion stimuli ( $\lambda=30^\circ$ ) at 2 increments ( $3.75^\circ$  each) per second (Fig. 2.3).

### **Two-photon imaging**

A cold-anesthetized female fly (expressing the genetically encoded calcium indicator GCaMP3.0 in HS neurons by using the *R27B03-GAL4* driver from the Rubin laboratory) was tethered and mounted on a custom holder under a dissection microscope where its legs were free to move

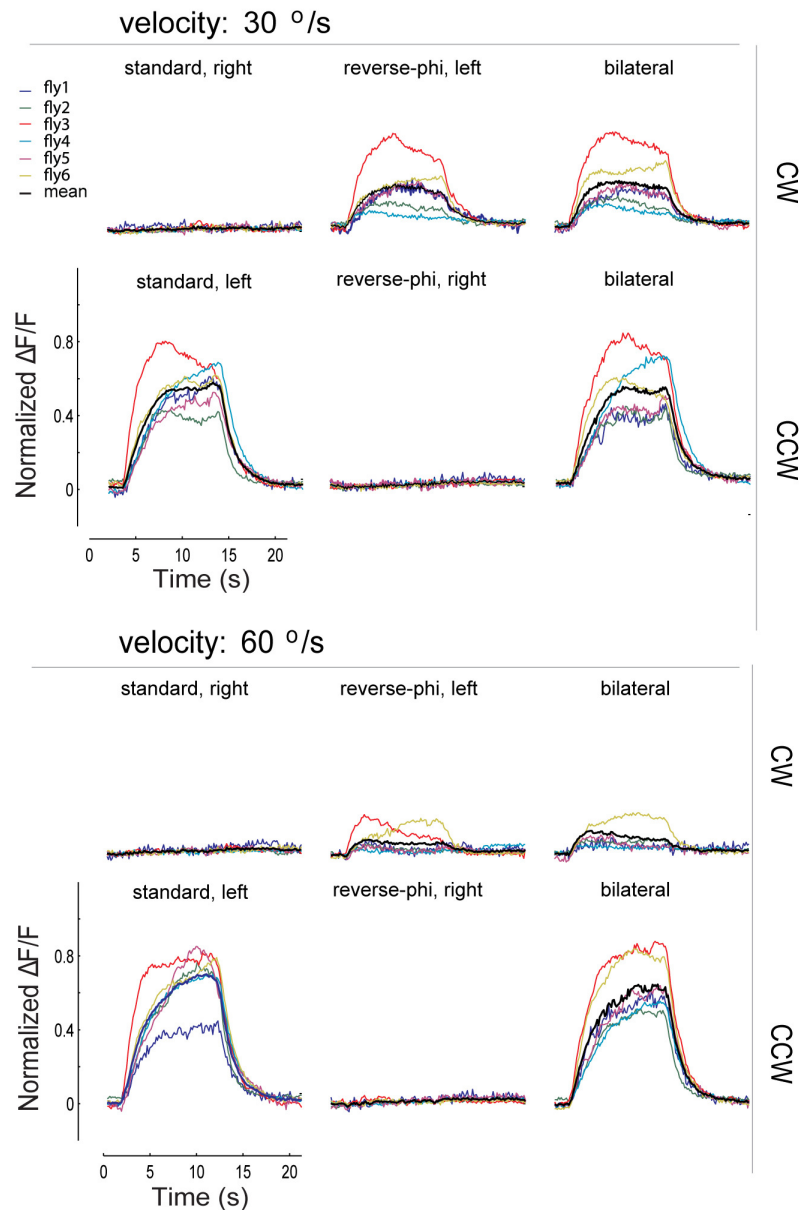
on an air-supported ball (Fig. 2.7A). The percentage of time the animals were walking was nearly constant across visual stimulus conditions (Fig. 2.6). We always imaged from the left lobula plate of the optic lobe and the same region of interest (ROI, Fig. 2.7B) from a highly stereotyped branching segment of the HSN dendrite (Scott et al., 2003), which was selected based on optical access and response strength. Other details of the preparation are described in Seelig et al. (Seelig et al., 2010).

Images were acquired in framescan mode (8 Hz) on a custom-built two-photon microscope (Fig. 2.7A) using ScanImage 3.6 software (Pologruto et al., 2003), an Olympus 40x, 0.9 NA LUMPlanFI/IR objective. During all imaging experiments, single trials consisted of a 5-second period where all pixels in the arena displayed a uniform intermediate intensity followed by 10 seconds of motion in the CW and CCW directions (the preferred and non-preferred or null direction of motion, respectively, for the left side HSN neuron). The trial concluded with 10 seconds of all display pixels illuminated to allow for the complete decay of calcium transients. Trials were repeated at least 4 times per condition.

Analysis of imaging data was performed using custom MATLAB code (Seelig et al., 2010). For all trials, we computed the HSN response as the ratio between the change in fluorescence (i.e., the average pixel value within the selected ROI, Fig. 2.7B) with respect to baseline, and the baseline fluorescence, expressed as a percentage. To allow comparisons across flies, the responses of HSN dendrites were normalized to the maximal responses for each fly and averaged across flies. To construct temporal tuning curves, normalized responses were calculated as the mean of  $\Delta F/F$  during the last 0.5 s of the stimulation. To facilitate comparison with the behavioral

results, in Fig. 2.8, we present the calcium imaging data as the CCW responses minus CW responses. This transformation is a way to obtain bidirectional responses from the calcium signal which is largely rectified. Conceptually it is as if we subtract the preferred direction (PD) response of the right HSN from the PD response of the left HSN. Because we only image from the left HSN, we use the response to the symmetrical presentations of the stimuli as a proxy.

**Fig. 2.12.** HSN dendrites respond similarly to bilateral and unilateral presentations of standard and reverse-phi patterns. Normalized mean responses per fly (indicated in different colors) to ipsilateral reverse-phi (top row) or ipsilateral standard pattern (bottom row) show similar amplitude compared to the responses to bilateral simultaneous presentation of both patterns in the corresponding positions. Patterns and position of the patterns are indicated at the top of each panel, and the direction of pattern motion is indicated at the right of the figure (CCW or CW). Patterns moved at 30 °/s (top) or 60 °/s (bottom). The plots in Fig. 2.10B were obtained from these traces.



## Motion detection model

We modeled the local circuit of the *Drosophila* motion detection system as one Hassenstein-Reichardt Elementary Motion Detector (EMD) beneath simple compound eye optics. For the point-spread function of ommatidial lenses we used Gaussian sampling (Snyder, 1979):

$$L(\theta) = k \exp \left[ \frac{4 \ln 2}{\Delta p^2} \theta^2 \right]$$

where  $k$  is a standardization constant,  $\Delta p$  is the acceptance angle of the photoreceptor ( $5^\circ$ ; Heisenberg and Wolf, 1984) and  $\theta$  is the vector of discrete positions through a pair of ommatidia with increments of  $0.375^\circ$  used an inter-ommatidial angle ( $\Delta\varphi$ ) of  $4.5^\circ$  (Snyder, 1979). The image was formed by the convolution of an intensity signal,  $I(\theta, n)$ , a function of angular position and the discrete sample time ( $n$ ), with the acceptance angle of the ommatidia:

$$R(n) = L(\theta) \otimes I(\theta, n)$$

We used simple ray tracing to simulate the view of the ommatidial pair confronted with our standard cylindrical LED display. The simulated EMD computed the local optic flow field from the retinal image  $R(n)$ .

Our EMD implementation was based on the modifications proposed to capture most of the related experimental phenomena (Borst et al., 2003; Harris and O'Carroll, 2002); the classic model with first-order low pass filter ( $\tau = 20$  ms; selected to match the temporal frequency optimum, TFO, of 8 Hz, Fig. 2.4) to simulate the delayed intensity signal was augmented with a first-order high-pass filter in the input lines to account for neural adaptation ( $\tau = 200$  ms). The response of the EMD,  $M$ , was then computed by multiplying the filtered signal at each position

with the current value of the neighboring signal, and subtracting the result of the mirror symmetric pair (Fig. 2.4B):

$$M(n) = LP(HP(R_1(n))) * HP(R_2(n)) - LP(HP(R_2(n))) * HP(R_1(n))$$

where *HP* and *LP* are the first-order high and low pass filter operators, respectively. Varying the time constant of the *LP* delay filter affects the amplitude and the TFO of the model EMD, but did not qualitatively affect the shape of the tuning curves. Varying the time constant of the *HP* filter over values below 50 ms varied the amplitude and width of the temporal frequency tuning curve, but changes in the range of 50-200 ms had only a negligible effect on the model's tuning (Fig. 2.5). To test whether the biphasic impulse-response functions of higher-order high-pass filters altered the shape of reverse-phi tuning curves, we tested a range of high-pass filter orders (Fig. 2.5B). Spatial integration across an array of simulated EMDs also did not qualitatively change the model results. The model and subsequent modifications (Figs. 4, 5, 8, and 11) were implemented in Simulink and MATLAB (Mathworks, Natick, MA), and presented as steady-state response values. High- and low-pass Butterworth filters were designed with the MATLAB Signal Processing Toolbox and imported into Simulink.

## Chapter 3

### Behavioral function of a novel class of wide-field neurons in the *Drosophila* lamina

#### Abstract

The most peripheral visual neuropil of the fly brain, the lamina, contains a dozen genetically and anatomically defined neuron types. We designed a series of tethered flight experiments to test for behavioral phenotypes following genetic perturbation of neurons in the *Drosophila* lamina. We then used intersectional strategies for ectopic transgene expression to genetically target a novel type of visual feedback neuron, the lamina wide-field cell (lawf2). Silencing lamina wide-field neurons generally decreased the fly's ability to detect low contrast wide-field motion stimuli and reduced tracking of small-field objects. More specifically, this manipulation increased the amplitude of behavioral responses to very slow motion stimuli. These results suggest that wide-field neurons provide low-frequency feedback to the lamina, suppressing behavioral responses to slowly moving visual stimuli and broadly enhancing visual sensitivity.

#### Introduction

Brains are composed of an incredibly diverse assortment of genetically-defined neuron types. A fundamental problem in neuroscience is explaining how these different classes of neurons contribute to animal behavior. Although behavioral screens can identify groups of neurons involved in particular behaviors, a more challenging task has been to relate behavioral phenotypes to the functional properties of individual neuron classes (Luo et al., 2008). Two primary obstacles are (1) specifically perturbing single neuron types and (2) exploring the large parameter space of behaviors to identify the most relevant contributions of those neurons to

defined behaviors. Here we attempt to overcome these obstacles by silencing a specific neuron class in the fly lamina, and searching extensively for behavioral phenotypes by quantifying flight steering in a virtual reality flight simulator.

The *Drosophila* visual system is uniquely suited as a testing ground for cell-type specific dissection of behavior. The fly optic lobes are organized into retinotopic columns, or “cartridges”, each representing a small region of visual space (5°; Heisenberg and Wolf, 1984). In the lamina, each cartridge contains only 8 columnar neuron classes and 4 multi-columnar neurons. The anatomy of the lamina has been described in exquisite detail with both light and electron microscopy (Cajal and Sanchez, 1915; Fischbach and Dittrich, 1989; Meinertzhagen and O’Neil, 1991; Rivera-Alba et al., 2011). Advanced genetic tools for transgene expression and cell-type specific manipulations have also led to a detailed understanding of many developmental processes in the *Drosophila* visual system (Clandinin and Feldheim, 2009). Many of these tools can now be applied to understanding the function of neural circuits, particularly in the context of behavior (Olsen and Wilson, 2008).

Despite this abundance of knowledge and tools, our understanding of cell-type function in the lamina is limited to the two largest columnar neurons, the lamina monopolar cells L1 and L2. L1 and L2 receive direct input from the photoreceptors and have been characterized physiologically in larger flies (Laughlin and Hardie, 1978; Scholes, 1969) and *Drosophila* (Clark et al., 2011; Reiff et al., 2010; Zheng et al., 2006). L1 and L2 are non-spiking neurons that respond to a flash of light with a transient hyperpolarization, and depolarize transiently when the light is terminated (Scholes, 1969). Genetically silencing both L1 and L2 abolishes motion-dependent behaviors, but silencing either neuron class alone has only a marginal effect (Rister et al., 2007).

Differences between the L1 and L2 pathways have been suggested based on behavior (Clark et al., 2011; Rister et al., 2007), or recording from downstream neurons (Joesch et al., 2010). Aside from L1 and L2, however, the functional contributions of other lamina neurons are not well understood.

An important feature of working at the sensory periphery is that all information that enters the nervous system must pass through the sense organs. Therefore, the processing limits of retinal neurons set the upper bounds on visual perception. This has been exploited to constrain, for example, the sensitivity of vertebrate rod photoreceptors (Hecht et al., 1942) and the spectral sensitivities of cones (Wald, 1964). By combining such psychophysical measurements with electrophysiological recordings, there has emerged a general view that the retinas of both vertebrates and invertebrates extract ethologically relevant features of visual scenes (Carandini et al., 2005; Lettvin, 1968). Feature extraction is accomplished by the specific filtering properties of neurons or neural circuits. This filtering is often described in terms of a neuron's receptive field; for example, certain classes of vertebrate retinal ganglion cells respond most strongly to bright or dark edges (Kuffler, 1953).

At the same time, the retina must deal with the significant problem of adaptation—vision operates over an enormous range of light conditions, from bright sunlight to dim starlight. The most peripheral regions of the visual system extract and preserve relevant signals across a vast range of inputs. (Rieke and Rudd, 2009). Retinal neurons deal with input variability by adjusting their sensitivity, or adapting, to the statistical features of light inputs, such as mean light intensity and variability about the mean (Laughlin, 1989; Shapley and Enroth-Cugell, 1984).

Although such gain control is seen throughout the nervous system, the peripheral retina appears to be particularly specialized to encode sensory signals across a large luminance range. If the function of the peripheral retina is to extract and preserve noisy signals across a wide range of light conditions, how do individual neuron types contribute to this purpose? One idea is that different neuron classes represent independent and parallel processing pathways—each cell class separately extracts a unique feature of the visual scene. Similarly, different cell types could also encode redundant features, but feed into functionally segregated pathways. Another possibility is that a small number of feed-forward pathways are modulated by the activity of feedback and local interneurons. Such local processing could serve to enhance the coding capacity of feedforward pathways through mechanisms like predictive gain control and lateral inhibition. The preponderance of local interneurons in the peripheral visual systems of both vertebrates and invertebrates supports this view.

We used the above considerations to develop a comprehensive psychophysical protocol to search for visual phenotypes of lamina neurons. This compact sequence of visual stimuli was designed to test a breadth of existing and novel hypotheses about peripheral visual processing. We applied this behavioral protocol to transgenic flies in which specific neuron classes of the fly lamina were silenced or activated. In this Chapter, we take advantage of this approach to elucidate the function of a novel class of wide-field neurons in the *Drosophila* lamina. We found that wide-field neurons play an important role in suppressing visual sensitivity to low frequency visual motion stimuli, and that silencing these neurons specifically affects a small number of visual behaviors.

## Results

### A novel class of wide-field neurons in the fly lamina

Using a large collection of GAL4 driver lines (Pfeiffer et al., 2008), we identified a new multi-columnar neuron type in the peripheral visual system of *Drosophila* (Fig 1b). We call this neuron type lamina wide-field 2 (lawf2), to differentiate it from a previously described, anatomically similar wide-field neuron (lawf1; Fischbach and Dittrich, 1989). There are ~30 wide-field neurons per eye, and their cell bodies tile the cell body layer of the medulla cortex (Fig. 3.1C). These neurons send axons into the lamina, which branch into wide arborizations that tile the distal lamina, spanning ~10-15 cartridges, or ~40°-60° of visual space (Fig. 3.1A,B). Wide-field neurons receive dendritic input from two layers of the medulla, M1 and M9. The M1 dendritic fields overlap, tiling the medulla, and cover ~20-25 cartridges (Fig. 3.1D, left). In contrast, the processes in layer M9 do not typically overlap, and extend across ~8-10 cartridges (Fig. 3.1D, right). Staining for presynaptic markers indicates that wide-field neurons are presynaptic in the lamina, and potentially release acetylcholine (Fig. 3.1E). Recent evidence from single-cell transcription profiling suggests that L2 and L4 express primarily nicotinic acetylcholine receptors (Takemura et al., 2011), providing a potential substrate for wide-field neuron feedback.

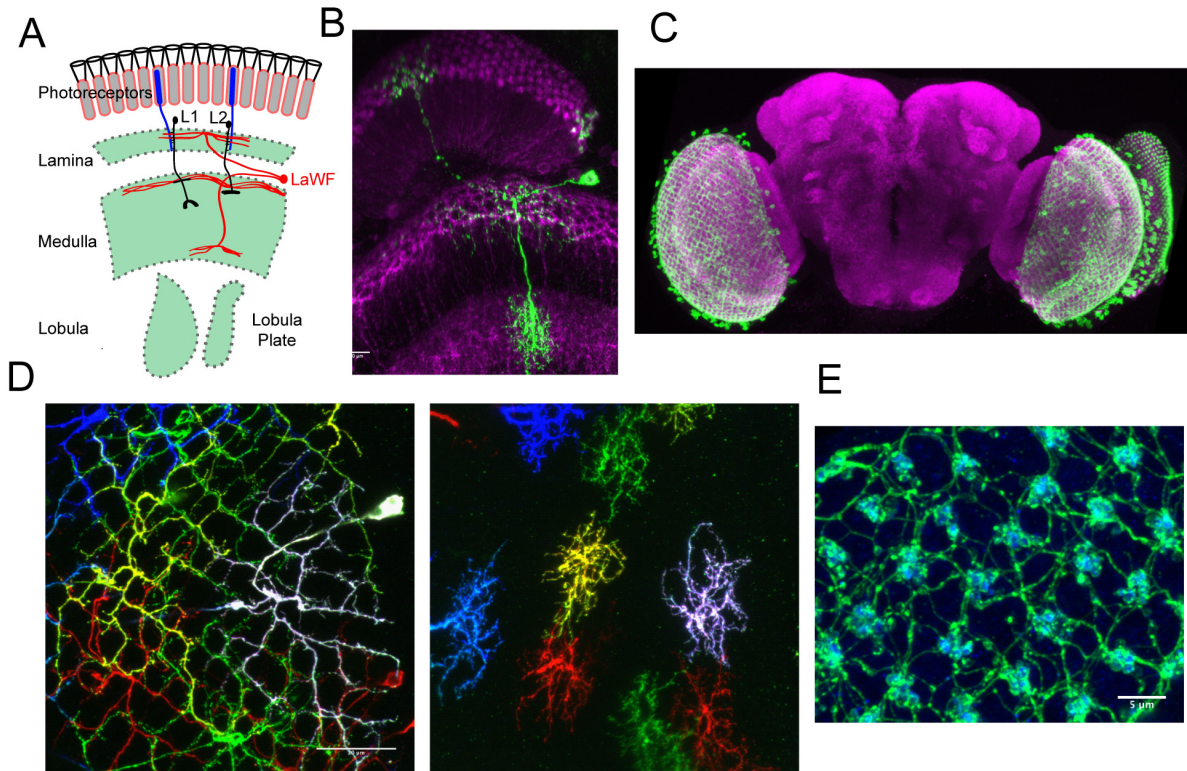


**Fig. 3.1.** Anatomy of a novel wide-field neuron in the *Drosophila* lamina (lawf2) **(A)** A schematic of a single wide-field neuron. Each cell has two dendritic arborizations, each spanning multiple visual columns in layers M1 and M9 of the medulla, and an axonal arborization in the distal lamina. **(B)** A stochastically GFP-labeled wide-field neuron. GAL4 expression is labeled in green with UAS-mcD8::GFP and neuropil is counter-stained in magenta (anti-nc82). **(C)** A confocal image of a highly specific split-GAL4 lines used to target transgene expression to wide-field neurons. **(D)** Multi-color stochastic labeling of the Split-Gal4 pattern in C. Each wide-field neuron within the pattern is labeled with a different color. (Left) arborizations in later M1 of the medulla, illustrating the overlap of dendritic processes. (Right) Non-overlapping dendrites in layer M1. **(E)** Antibody staining against choline acetyltransferase (ChAT) in blue overlaps with GFP-labeling of wide-field neurons (green) in the lamina, suggesting that wide-field neurons release acetylcholine. All images in this figure were created by Aljoscha Nern.

### Using behavioral genetics to elucidate neuronal function

In order to determine the functional role of wide-field neurons in early visual processing, we used the GAL4-UAS expression system to ectopically express neural effectors in wide-field neurons. Because all available GAL4 lines also expressed in other cell types throughout the nervous system, we used the split-GAL4 technique (Luan et al., 2006; Pfeiffer et al., 2010) to

build two GAL4 driver lines with expression restricted exclusively to wide-field neurons (Fig. 3.1C). We then examined the role of wide-field neurons in visual behavior by neuronal silencing and activation. First, we silenced wide-field neurons by expression of an inwardly rectifying potassium channel: *kir2.1* (Baines et al., 2001). This manipulation effectively silenced wide-field neurons, as demonstrated through electrophysiological recordings from wide-field neurons expressing gfp-tagged *Kir2.1* (see Chapter 4). Second, we activated wide-field neurons through expression of the temperature-gated cation channel *dTRPA1* (Hamada et al., 2008). We studied the effects of these manipulations on visually-guided behavior in a virtual reality flight simulator (Fig. 3.2A; Reiser and Dickinson, 2008).

Behavioral genetics experiments are susceptible to many sources of experimental noise. In order to minimize these effects, we took several precautions. First, all transgenes were located at specific insertion sites in the fly genome, typically *attP2* and *attP40* (Pfeiffer et al., 2008). Second, all behavior experiments were performed on flies with similar genetic background: all flies tested were F1 hybrids of GAL4 lines (made from the same fly stock), crossed to the same effector line (e.g., *w+;DL;UAS-kir2.1*). Because expression of a single split-GAL4 transgene (e.g., a GAL4 AD alone) does not drive UAS transcription, we used flies possessing one split-GAL4 half as controls for comparison. Whenever possible, transgene expression was verified by visualization of fluorescently-tagged effectors. GAL4 expression in the ventral nerve cord and in the larvae was also ruled out by imaging expression of a fluorescent reporter molecule at several stages of development.

For all experiments described below, we compared multiple experimental and control flies to determine whether an observed result was significant. We used two split-GAL4 lines that

expressed exclusively in lamina wide-field neurons; these two lines had comparable expression levels and penetrance (Aljoscha Nern, personal communication). For each behavioral trial, we tested both split-GAL4 lines and compared their responses to two control lines (single split-GAL4 transgenes). A result was considered significant only if both split-GAL4 lines were statistically different from the mean of the control behavior ( $P<0.01$ ). This conservative criterion was used to ensure that we focus on the most salient and repeatable experimental effects. Mean values and standard deviations for integrated turn amplitudes are shown in Table 3.1.

### **Wide-field optomotor behavior**

We first tested basic optomotor behavior- the fly's tendency to follow the rotation of a striped grating. The amplitude of a fly's optomotor response depends on the temporal frequency of the rotating stimulus (Gotz, 1964). We found that fly turning responses increased up to a peak of ~9 Hz (Fig. 3.2B, top row). Silencing wide-field neurons with kir2.1 did not dramatically affect the amplitude of optomotor responses across a range of spatial and temporal frequencies (Fig. 3.2B).

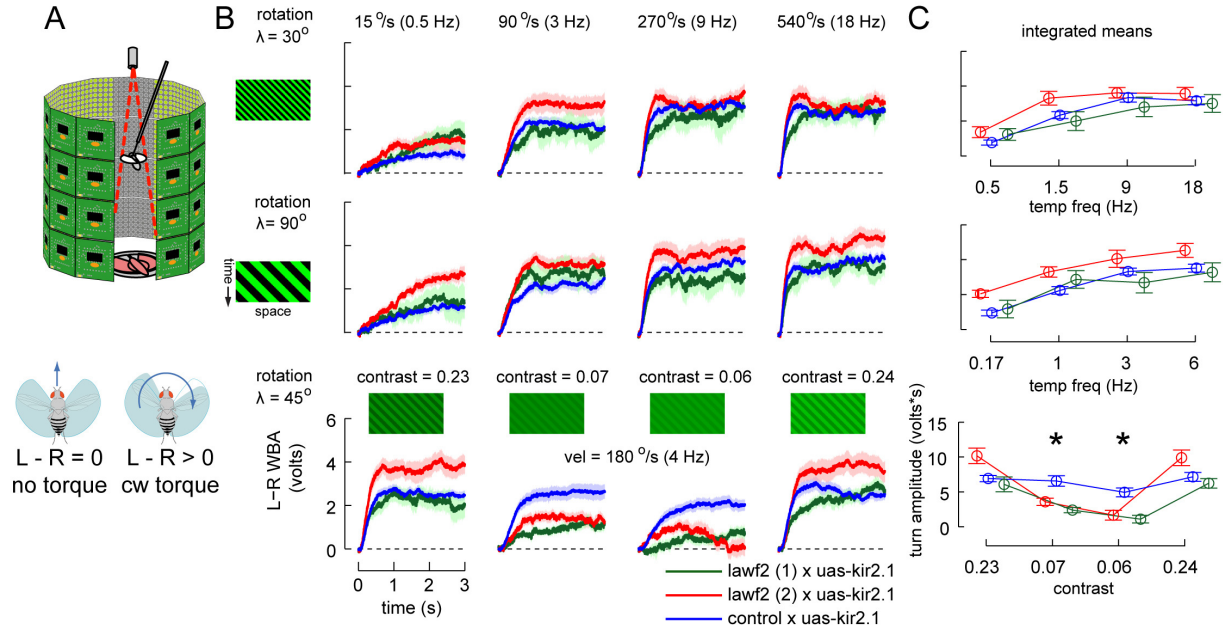


**Fig. 3.2.** Tethered flight experiments identify a behavioral role for wide-field neurons. **(A)** The fly is suspended within a virtual flight arena where the amplitude and frequency of each wingbeat is tracked by an optical detector. The difference between the two wingbeats (L-R WBA) is proportional to yaw torque. For example, when the amplitude of the left wingbeat is greater than the right, the fly is attempting to steer to the right with clockwise torque. **(B)** Silencing wide-field neurons specifically decreases fly responses to low-contrast optomotor stimuli. Flies were tested with rotating square-wave striped gratings across a range of stimulus velocities, spatial wavelengths, and contrasts. Each time series is the mean turning response ( $\pm$  s.e.m) of 12 flies for each genotype. **(C)** Mean turn amplitudes were calculated by integrating the area under each turn response, and are plotted as means  $\pm$  s.e.m. Asterisks indicate that both experimental genotypes are significantly different from the control (black signifies  $P<0.01$ , gray  $P<0.05$ ).

We next measured flight steering responses to low contrast optomotor stimuli. Flies will follow optomotor patterns across a range of stimulus contrasts, with weaker responses to lower contrast stimuli (Duistermars et al., 2007a). We found that flies with silenced wide-field neurons responded more weakly to low contrast optomotor stimuli (Fig. 3.2B,C bottom row). Specifically, when the stimulus contrast was less than 0.1, flies with silenced wide-field neurons were significantly impaired. This effect did not depend on the mean luminance of the optomotor stimulus, as flies responded to both high and low luminance stimuli normally.

## **Motion nulling**

To further explore the temporal properties of the two phenotypes described above, we employed a psychophysical technique known as motion nulling (Cavanagh and Anstis, 1991; Smear et al., 2007), in which two optomotor stimuli (striped gratings) are superimposed—a reference grating moving in one direction, and a test grating moving in the opposite direction. When presented with such conflicting optomotor stimuli moving at different speeds, we found that flies turn in the direction of the faster stimulus, even if it is lower contrast. We therefore tested the ability of flies to distinguish between high and low contrast motion stimuli by varying the velocity and contrast of the test grating across trials (Fig. 3.3A).

We quantified contrast sensitivity as a function of stimulus velocity by computing the “null contrast” at each test speed. The null contrast is the contrast of the test stimulus needed to perceptually cancel, or null, the constant reference stimulus. In practice, the null contrast was determined by fitting a line through the fly response amplitudes to three test contrasts at each test velocity (Fig. 3.3B). The zero-crossing of this line corresponds to the point at which the test and reference stimuli are perceptually equivalent—the null contrast. The lower the null contrast, the more sensitive a fly is to low contrasts at that particular speed. An important advantage of using this null contrast metric is that it does not depend on absolute turning amplitudes. In other words, the nulling technique distinguishes between flies with general motor deficits vs. flies with altered visual sensitivity.

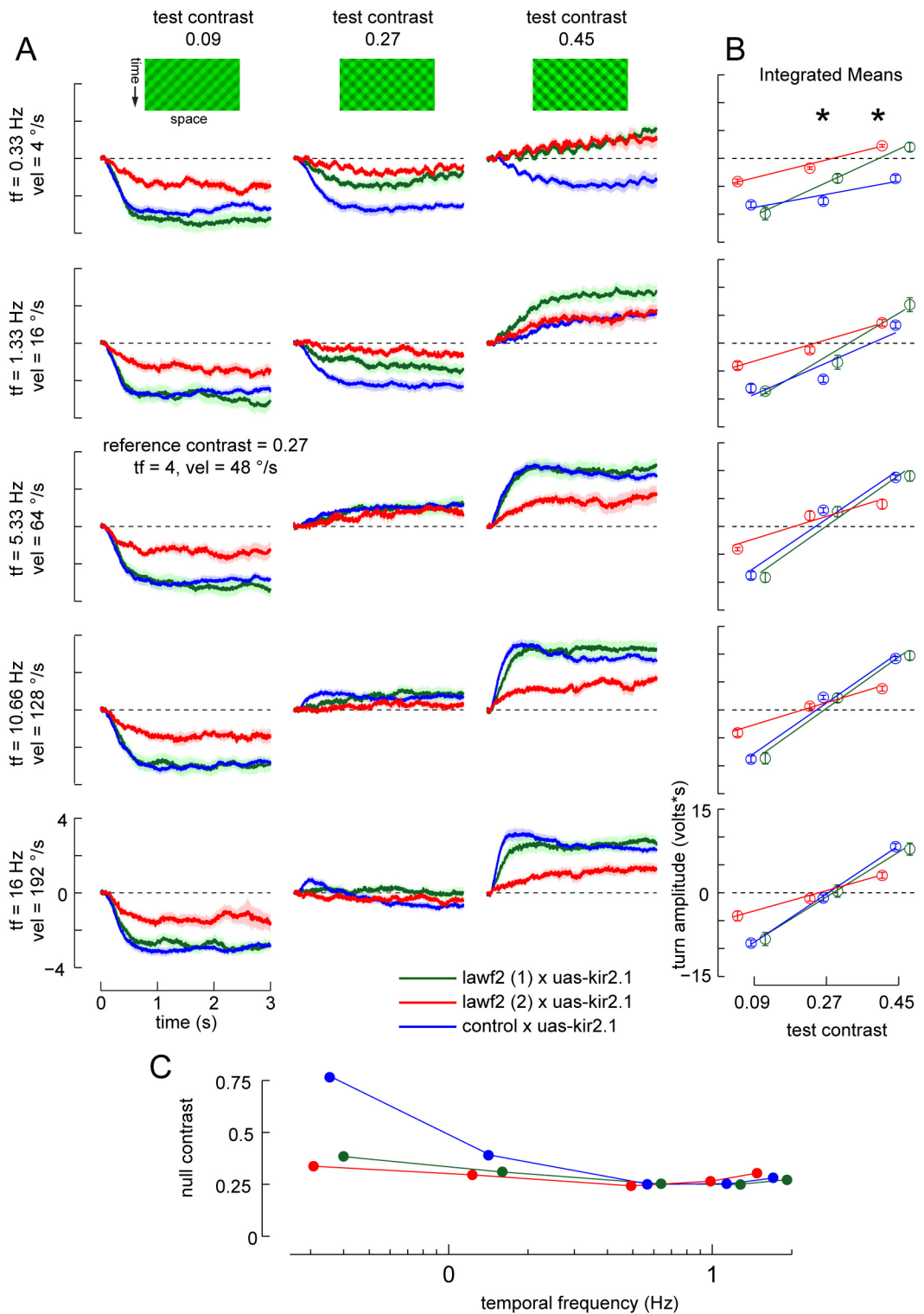


**Fig. 3.3.** Silencing wide-field neurons specifically alters contrast discrimination at low velocities  
**(A)** Mean turning behavior of 12 flies of each genotype ( $\pm$  s.e.m) in response to open-loop rotation of two superimposed square-wave gratings ( $\lambda = 45^\circ$ ): a constant reference stimulus,

**Fig. 3.3. (continued)** and a test stimulus whose contrast is varied across trials. At low test contrast, flies turn in the direction of the reference stimulus ( $L-R\ WBA > 0$ ); at high test contrast, flies attempt to follow the reference stimulus ( $L-R\ WBA < 0$ ). Space-time diagrams are for reference and test stimuli moving at the same velocity, to emphasize contrast differences. **(B)** Mean integrated responses of the behavioral time series at left. A line is fit through each series of tests contrasts to determine the “null contrast”—the contrast of the test stimulus needed to cancel, or null, the reference stimulus. Asterisks indicate that both experimental genotypes are significantly different from the control ( $P < 0.01$ ). **(C)** Tuning curve of the null contrast measured over a range of test stimulus speeds. The null contrast provides an index of contrast sensitivity at a given temporal frequency. The black asterisk signifies  $P < 0.01$ .

Plotting null contrast as a function of the test stimulus speed revealed that contrast discrimination depends on stimulus speed, peaking at around 10 Hz temporal frequency (Fig. 3.3C). Importantly, this tuning curve verifies that flies exhibit the highest contrast sensitivity for stimuli that evoke a maximum behavioral response (Fig. 2.4).

Silencing lawf2 neurons significantly decreased the range of contrasts over which flies could discriminate between fast and slow optomotor stimuli (Fig. 3.3A). Specifically, null contrasts at the lowest test speeds were significantly lower (Fig. 3.3C). This phenotype could occur because either (1) flies became less sensitive to the faster reference stimuli, or (2) flies became more sensitive to the slower test stimuli. Close examination of the data revealed that the second option was correct—flies followed the higher contrast test stimulus even if when it was moving very slowly. In other words, silencing wide-field neurons increased visual sensitivity to low frequency motion stimuli. This observation agrees with the one significant condition in the previous set of experiments—that silencing wide-field neuron increased fly optomotor responses to 1 Hz rotation (Fig. 3.2B).

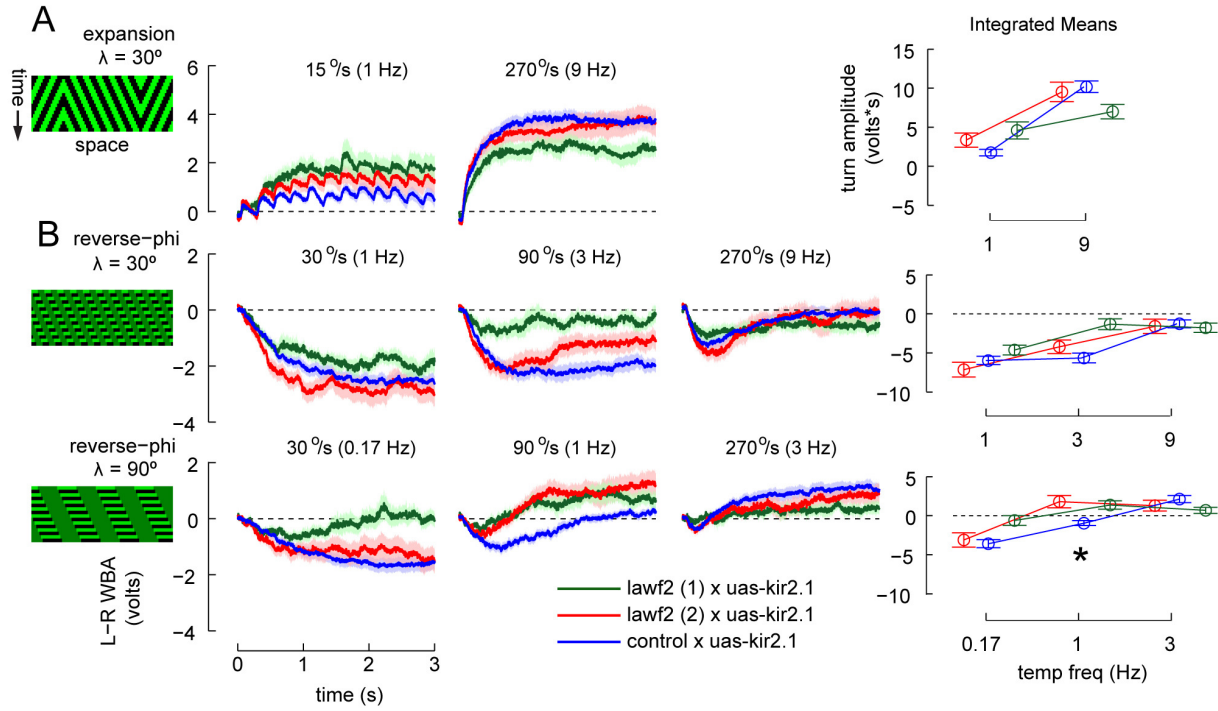


**Fig. 3.4.** Other optomotor behaviors are largely unaffected by silencing wide-field neurons. **(A)** Mean turning behavior of 12 flies ( $\pm$  s.e.m) in response to open-loop expansion of a square-wave grating at two speeds. The expansion stimulus is similar to wide-field rotation, except the front and rear of the arena move in opposite directions, creating a lateral focus of expansion. Flies will typically turn away from this focus of expansion. **(B)** Steering responses to rotation of a reverse-phi stimulus across three velocities and two spatial wavelengths. As shown previously, reverse-phi responses invert at high stimulus velocities. **(C)** As before, mean turn amplitudes were calculated by integrating individual turn responses, and asterisks indicate that both experimental genotypes are significantly different from the control (black signifies  $P < 0.01$ , gray  $P < 0.05$ ).

### Other optomotor behaviors

A previous study suggested that selectivity for translation and rotation stimuli first emerges in the lamina; specifically, that L2 underlies responses to translational motion (Katsov and Clandinin, 2008). We therefore studied fly responses to a full-field expansion stimulus (Fig. 3.4A), which was identical to the rotating optomotor stimulus except the frontal and rear hemispheres of the arena rotated in opposite directions (Tammero et al., 2004). Silencing wide-

field neurons did not significantly change fly responses to expansion at the two velocities tested (Fig. 3.4C).

Flies were also tested with rotating reverse-phi motion stimuli at several speeds and spatial wavelengths (Fig. 3.4B). Silencing wide-field neurons did not greatly affect the sign or amplitude of reverse-phi responses (Fig. 3.4C). Under one condition ( $\lambda = 90^\circ$ , 1 Hz temporal frequency), wide-field neuron inactivation increased the rapid inversion of reverse optomotor behavior. Interestingly, the spatial and temporal parameters of this reverse-phi stimulus were identical to the condition in which a significant difference was observed for basic optomotor behavior (Fig. 3.2B). In both cases, silencing wide-field neurons caused an increase in response amplitude.

It was previously suggested that L1 and L2 are specialized for detection of front-to-back vs. back-to-front motion (Rister et al., 2007). To test this possibility, we presented flies with monocular front-to-back and back-to-front motion (Fig. 3.5). Flies responded strongly to front-to-back motion, with steering behavior that resembled full-field stimulation. Back-to-front clockwise (CW) motion triggered weak counterclockwise (CCW) steering responses at low velocities. At higher speeds, a short CCW transient was followed by turning in the CW direction. Silencing wide-field neurons with kir2.1 did not alter fly responses to monocular back-to-front or front-to-back motion across this range of stimulus speeds (Fig. 3.5B).

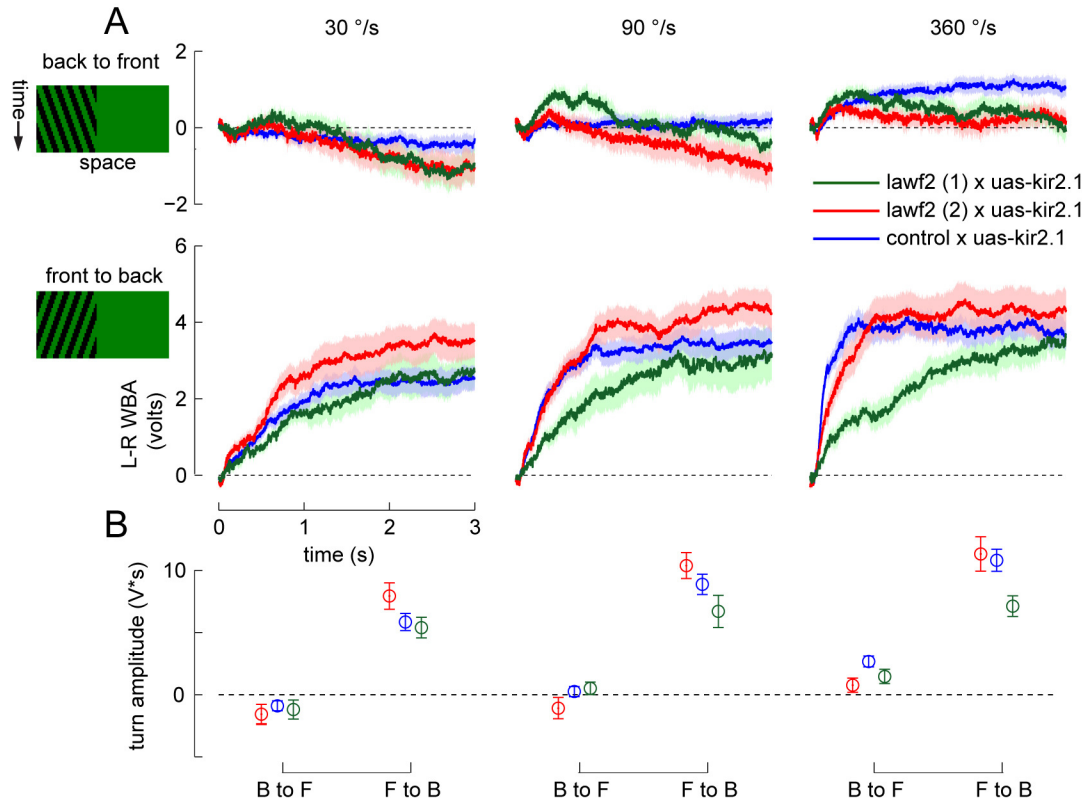


**Fig. 3.5.** Flight steering responses to monocular optomotor stimuli **(A)** Mean turning behavior of 12 flies ( $\pm$  s.e.m) in response to open-loop rotation of a square-wave grating restricted to one eye (120° wide, centered laterally, 30° spatial period). Stimuli rotated from anterior to posterior (front-to-back) or posterior to anterior (back-to-front) at 3 speeds. Responses to counter-clockwise motion were inverted and averaged with clockwise stimuli—all data are plotted for clockwise motion. Front-to-back rotation evoked much larger steering turning responses than back to front; at low speeds, back-to-front responses inverted so that the fly was turning against the direction of stimulus motion. **(B)** Integrated mean responses to bilateral motion stimuli.

To probe visual behavior unrelated to visual motion, we investigated the fly's tendency to orient toward a flickering stimulus (Pick, 1974). This stimulus was a striped grating restricted to 120° of the fly's visual field, which flickered between bright and dark at 40 Hz (Fig. 3.6A). After a transient response in the opposite direction, flies weakly oriented toward the flickering grating (Fig. 3.6B). This response looked similar to that evoked by back-to-front monocular motion.

Inactivating wide-field neurons did not affect the tendency of flies to orient toward a stationary flickering stimulus (Fig. 3.6C).

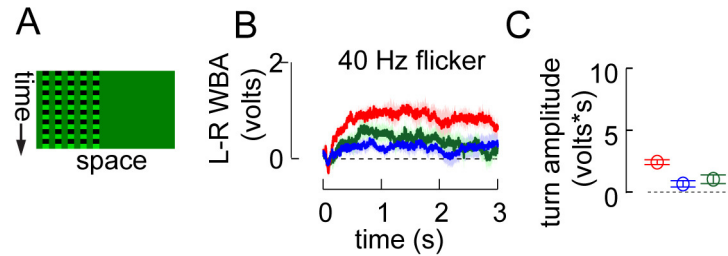


**Fig. 3.6.** Flies orient toward a flickering visual stimulus. **(A)** Space-time diagram for the lateral flickering stimulus. **(B)** Mean flight steering responses ( $\pm$  s.e.m;  $n = 12$  flies) toward a striped grating located within a lateral  $90^\circ$  window. Trials with the stimulus to the fly's left were inverted and averaged with those when the stimulus was on the right. The grating had a spatial period ( $\lambda$ ) of  $30^\circ$  and flickered between dark and bright at 40 Hz. **(C)** The integrated mean turn amplitudes of flicker orientation responses.

### Small-field motion

Flying flies will actively track the position of moving stripe under both open- and closed-loop conditions (Reichardt and Wenking, 1969). A previous behavioral study that compared fly responses to oscillating motion stimuli found that large-field optomotor steering responses peak at low frequency, while small-field responses persist under high frequency conditions (Duistermars et al., 2007b). These data, as well as previous experiments with *Drosophila* vision mutants (Heisenberg and Wolf, 1984), suggest that large- and small-field motion pathways are functionally segregated. We were therefore interested in comparing the dynamic responses of flies to large- and small-field motion stimuli.

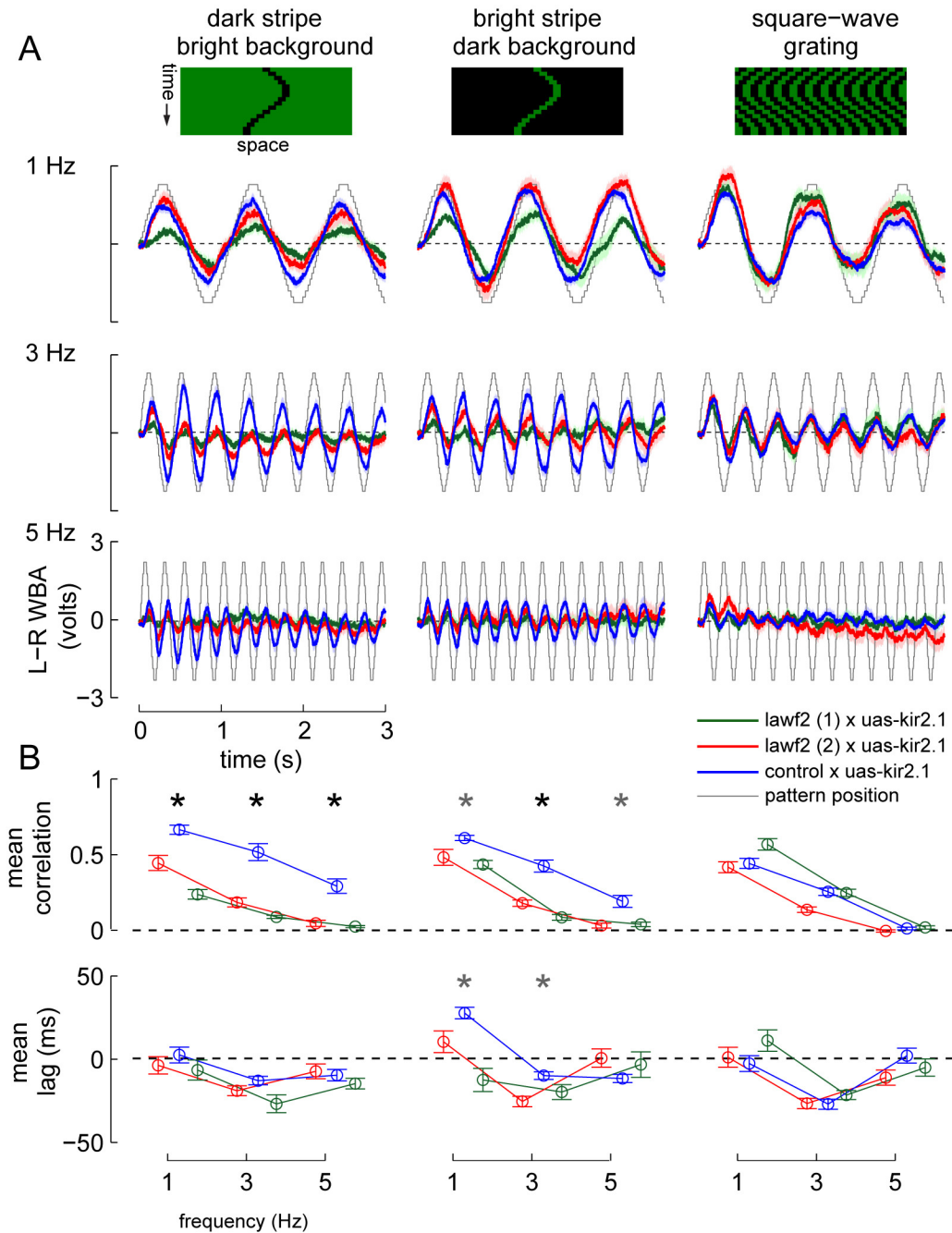


**Fig. 3.7.** Fly responses to open-loop oscillations of small- and large-field visual stimuli **(A)** Time series are mean flight steering responses ( $\pm$  s.e.m;  $n = 12$  flies). Three visual patterns, a  $15^\circ$  wide dark stripe, an equivalent bright stripe, and a square-wave grating ( $\lambda = 30^\circ$ ), oscillated at 3 frequencies. Each stimulus started out at the center of the fly's visual field, and moved  $\pm 37.5^\circ$  (stimulus position is plotted in gray). Stimuli that initially moved CCW were inverted and averaged with stimuli that initially moved CW. **(B)** The correlation and phase lag between the fly's steering (L-R WBA) and the stimulus position were calculated on a trial-by-trial basis. The black asterisk signifies  $P < 0.01$ , gray  $P < 0.05$ .

We measured the flight responses of flies to three oscillating motion stimuli: a dark stripe on a bright background, a bright stripe on a dark background, and a full-field square-wave grating (Fig. 3.7A). Instead of comparing mean turn amplitudes, we computed the cross-correlation between the L-R WBA and the position of the visual stimulus in the arena, resulting in a mean correlation coefficient and phase lag for each stimulus condition (Fig. 3.7B).

Flies respond to the position of small-field objects with strong steering responses at very minimal temporal delay; under certain conditions, control flies appear to actually lead the position of the stripe by up to 30 ms (e.g., the bright stripe, 1 Hz condition in Fig. 3.7). This tight stripe-following behavior is reduced in flies with silenced wide-field neurons. Silencing wide-field neurons decreased the mean correlation coefficient for all small-field stimuli tested, and increased the response phase lag for two conditions: bright stripes oscillating at 1 and 3 Hz (Fig. 3.7B). However, manipulating wide-field neurons did not significantly affect the tracking of the wide-field grating at this particular range of spatial and temporal parameters. These data show that wide-field neurons are important for the detection of small, fast moving objects. Although removing wide-field neuron activity does not abolish object orientation, it significantly decreases the ability of a fly to accurately track small-field motion stimuli.

### **Optic flow translation and rotation**

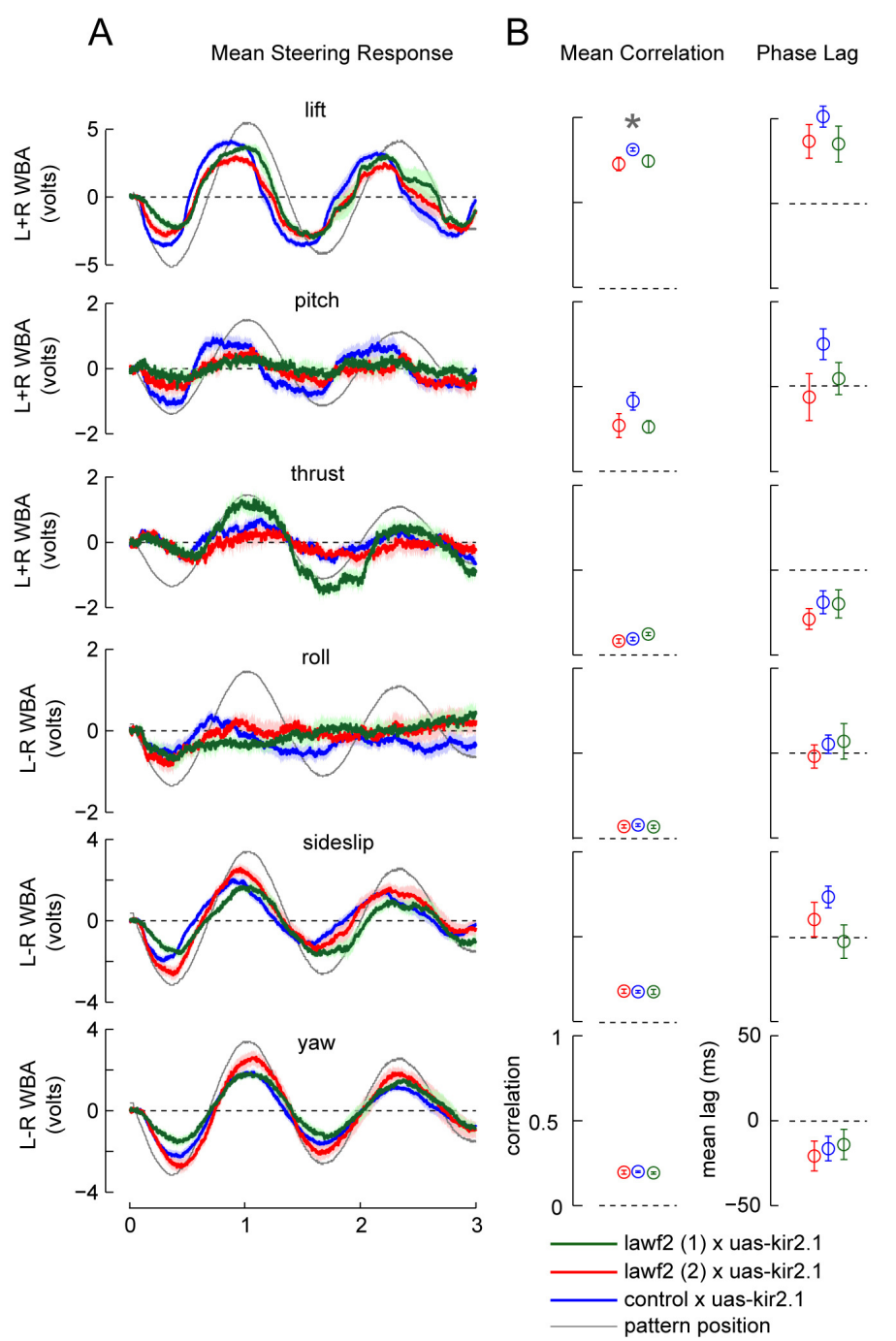
During flight, flies react to unplanned perturbations in course control with compensatory steering reactions. Flies experiences rotational or translational motion around or along the three cardinal axes, and they distinguish between these movements by measuring optic flow on the retina. Evidence for this comes from experiments with tethered flying flies, which exhibit distinct behavioral responses to different optic flow fields (Theobald et al., 2010). In addition,

motion-sensitive neurons in the third optic ganglion, the lobula plate, have receptive fields that closely match patterns of optic flow (Krapp and Hengstenberg, 1996). This network of neurons, the lobula plate tangential cells (LPTCs), may be important for effective course control during flight.

Selectivity for different patterns of optic flow could emerge very early in the visual system. For example, a previous study concluded that silencing L2 differentially affected behavioral responses to rotation and expansion stimuli (Katsov and Clandinin, 2008). We tested this hypothesis by measuring fly responses to oscillating random-dot optic flow fields: translational stimuli that mimicked lift, thrust, and sideslip, and rotational stimuli that mimicked yaw, roll, and pitch (Fig. 3.8). As for the small-field stimuli, we calculated the cross-correlation between the stimulus position and the fly's steering behavior (Fig. 3.8B). For conditions that elicited bilateral changes in WBA (lift, pitch, and thrust), we used the sum of the wingbeat amplitude ( $L+R$  WBA) instead of the difference ( $L-R$  WBA) as a measure of flight steering.

Overall, silencing wide-field neurons did not grossly affect the ability of flies to track sinusoidal displacement of optic flow fields: the peak correlation coefficient between fly steering and pattern position was lower for the lift condition alone (Fig. 3.8B). Given that the optic flow patterns were of high contrast, these data are consistent with the result shown above that silencing wide-field neurons does not have a strong effect of tracking of high contrast optomotor patterns.

**Fig. 3.8. Fly**  
 responses to  
 oscillating patterns  
 of simulated optic  
 flow (A) Mean fly  
 responses to  
 oscillating optic  
 flow fields (mean  $\pm$   
 s.e.m;  $n = 12$  flies).  
 Optic flow stimuli  
 consisted of  
 random dot fields  
 that simulated  
 translational  
 (sideslip, pitch,  
 thrust) or rotational  
 (roll, yaw, lift)  
 movements along  
 the three cardinal  
 axes. Several optic  
 flow stimuli  
 produced  
 symmetric flight  
 responses (lift,  
 pitch, thrust), and  
 for these cases the  
 sum of the  
 wingbeat  
 amplitudes were  
 quantified. Each  
 stimulus oscillated  
 at 0.5 Hz (position  
 plotted in gray),  
 and symmetric  
 conditions were  
 inverted and  
 averaged. (B) The



correlation and phase lag between the fly's steering (L-R or L+R WBA) and the stimulus position were calculated on a trial-by-trial basis to produce a mean correlation and phase lag. The gray asterisk signifies  $P < 0.05$ .

## **ON vs. OFF selectivity**

In the outer plexiform layer of the mammalian retina, luminance signals are rectified at photoreceptor-bipolar cell synapses, forming so-called ON and OFF pathways (Werblin and Dowling, 1969). This does not appear to be the case in the fly lamina: fly LMCs respond to both ON and OFF signals (Laughlin and Hardie, 1978). However, a recent study that recorded from LPTCs while synaptically silencing L1 and L2 concluded that L1 is required for LPTC responses to ON stimuli, while L2 is necessary for OFF selectivity (Joesch et al., 2010). A complementary series of experiments using behavior in walking flies proposed that silencing L1 and L2 produced different effects when flies were tested with moving edges that inverted contrast as they moved (reverse-phi motion stimuli; Clark et al., 2011).

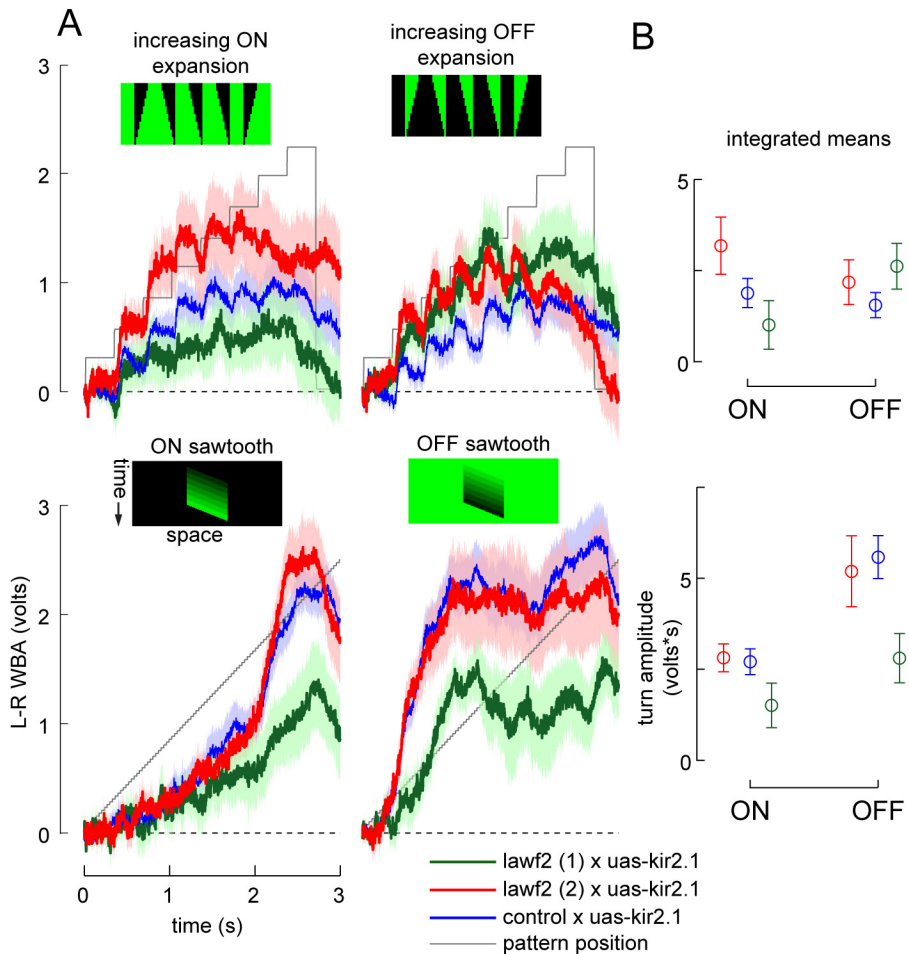


**Fig. 3.9.** Fly responses to ON and OFF visual stimuli. **(A)** Flight steering responses (mean  $\pm$  s.e.m;  $n = 12$  flies) to open-loop visual stimuli that contained luminance changes of a single polarity. The OFF or ON expansion stimulus started as a standard striped grating; each bar then slowly expanded or contracted (at  $9.4^\circ/\text{s}$ ) until the arena was uniformly illuminated. The ON and OFF sawtooth stimuli were luminance gradients that swept across a  $90^\circ$  window of the fly's frontal visual field. Sawtooth stimuli rotated at  $120^\circ/\text{s}$ , completing one full sweep in 3 s. **(B)** Integrated mean responses to ON and OFF motions stimuli, calculated on a trial-by-trial basis.

The visual stimuli used in these 2 previous studies were moving bright or dark edges that swept across the fly's visual field. However, in addition to moving edges, these stimuli also contained asymmetric changes in mean luminance, which flies could react to in a directed manner. We designed 2 alternative visual stimuli that tested the fly's ability to detect luminance increments and decrements. The first stimulus started as a standard striped grating, followed by expansion

of either the dark or bright bars until the arena was uniformly illuminated. The second stimulus was a sawtooth-shaped luminance gradient that swept across the frontal visual field of the fly. Although the sawtooth stimulus also contained asymmetric luminance changes, one would expect that flies with ON vs. OFF deficits would nonetheless react differently to these stimuli. Both of these stimuli triggered strong flight steering responses. The first set, ON and OFF expansion, elicited strongly phase-locked responses to individual motion steps of either polarity (Fig. 3.9A). The ON and OFF sawtooth stimuli evoked steering responses with very different time courses; flies responded earlier to the OFF stimulus, although the peak amplitude of the two responses were similar. Silencing wide-field neurons did not significantly change responses to any of these stimuli, indicating that wide-field neurons are not directly required for processing luminance changes of a single polarity (Fig. 3.9B).

### **Activating wide-field neurons**

In addition to neuronal silencing experiments, there are several methods to conditionally activate neurons by expression of light- or heat-gated ion channels. One of the more effective is the thermally-gated cation channel dtrpA1, which causes tonic firing at 27° C but not at temperatures below 25° (Hamada et al., 2008; Pulver et al., 2009). We tested the effects of activating wide-field neurons with dtrpA1 by measuring tethered flight behavior at 21° vs. 29° C. Because flies do not sustain flight for very long at temperatures above 27°, we tested these flies with a shorter behavioral protocol, and examined only a single split-GAL4 line. We selected a subset of the wide-field optomotor stimuli described above, including front-to-back vs. back-to-front motion, high and low contrast rotation, and reverse-phi motion. Small-field responses were also tested as before, but at a single oscillation frequency (3 Hz).

	control 1 means	control 1 sds	control 2 means	control 2 sds	lawf2(1) means	lawf2 (1) sds	lawf2 (2) means	lawf2 (2) sds
Fig. 3.2								
0.5 Hz	1.67	1.60	2.15	1.79	3.40	2.83	3.08	2.66
3 Hz	5.75	2.42	5.95	2.40	8.26	3.52	4.99	4.21
9 Hz	8.66	3.42	8.04	2.53	9.04	2.71	7.01	4.42
18 Hz	7.31	2.99	8.47	2.23	8.92	3.18	7.52	4.00
0.17 Hz	1.72	1.65	3.04	2.03	5.11	1.89	2.93	3.95
1 Hz	6.59	2.94	4.61	1.77	8.24	2.71	7.16	4.00
3 Hz	8.46	2.55	8.14	2.21	10.13	4.47	6.70	4.63
6 Hz	6.99	2.43	6.81	1.85	10.17	4.02	6.08	3.33
contrast = 0.23	7.17	3.48	5.95	3.77	3.57	1.89	2.39	1.19
contrast = 0.07	5.33	2.58	4.52	3.41	1.65	2.52	1.08	1.73
contrast = 0.06	7.12	3.30	7.17	2.82	9.88	4.09	6.22	2.21
contrast = 0.24	8.89	2.95	8.69	2.54	11.33	3.62	8.19	4.28
Fig. 3.3								
tf = 0.33, tc = 0.09	-7.99	1.96	-6.95	2.41	-8.83	3.72	-3.72	1.27
tf = 0.33, tc = 0.27	-7.79	2.16	-6.02	2.58	-3.20	2.49	-1.55	0.67
tf = 0.33, tc = 0.45	-4.14	2.92	-2.36	2.99	1.84	1.56	2.03	1.90
tf = 1.33, tc = 0.09	-7.74	1.99	-6.80	2.62	-7.72	3.97	-3.62	1.67
tf = 1.33, tc = 0.27	-6.35	2.93	-5.29	2.67	-3.08	2.74	-1.10	0.81
tf = 1.33, tc = 0.45	2.53	1.83	3.24	2.02	6.17	3.04	3.27	2.34
tf = 5.33, tc = 0.09	-8.71	2.27	-7.08	2.56	-8.21	3.31	-3.64	1.85
tf = 5.33, tc = 0.27	2.63	1.08	2.57	2.01	2.39	2.62	1.73	1.23
tf = 5.33, tc = 0.45	8.59	2.77	7.27	1.72	8.10	3.82	3.58	2.51
tf = 10.66, tc = 0.09	-8.38	2.09	-7.48	2.61	-7.80	3.58	-3.70	1.49
tf = 10.66, tc = 0.27	2.37	2.54	1.65	2.22	1.91	2.22	0.58	1.20
tf = 10.66, tc = 0.45	8.80	2.52	7.72	2.45	8.71	3.92	3.39	1.48
tf = 16, tc = 0.09	-8.78	1.11	-7.37	2.46	-7.42	2.70	-3.72	2.30
tf = 16, tc = 0.27	-0.57	2.41	-1.12	1.84	0.27	1.63	-0.89	0.74
tf = 16, tc = 0.45	7.92	2.53	6.96	2.77	7.04	3.37	2.80	1.57
Fig. 3.4								
1 Hz expansion	1.59	2.36	1.90	1.49	3.35	3.26	4.59	3.41
9 Hz expansion	9.07	4.38	11.26	2.01	9.51	4.47	6.99	2.90
1 Hz reverse-phi	-5.19	2.67	-6.74	2.01	-7.15	3.40	-4.62	1.94
3 Hz reverse-phi	-5.47	3.27	-5.83	2.66	-4.22	3.11	-1.33	2.20
9 Hz reverse-phi	-1.86	2.48	-0.68	2.18	-1.59	3.34	-1.77	1.87
0.17 Hz reverse-phi	-3.76	2.67	-3.42	2.30	-3.11	3.33	-0.61	1.96
1 Hz reverse-phi	-1.16	1.28	-0.76	1.61	1.78	2.83	1.36	1.69
3 Hz reverse-phi	1.17	1.78	3.07	2.19	1.29	2.49	0.67	1.22
Fig. 3.5								
30 deg/s b2f	-0.99	2.43	-0.81	1.19	-1.57	2.88	-1.20	2.42
90 deg/s b2f	-0.17	1.69	0.66	2.12	-1.08	3.06	0.51	1.59
360 deg/s b2f	2.61	2.49	2.73	1.60	0.76	2.08	1.46	1.80
30 deg/s f2b	6.72	3.14	4.97	3.13	7.94	3.84	5.39	2.61
90 deg/s f2b	10.07	4.06	7.67	3.33	10.38	3.75	6.70	4.09
360 deg/s f2b	11.01	5.11	10.61	3.11	11.32	5.00	7.12	2.62
Fig. 3.6								
40 Hz flicker	0.62	1.27	0.84	0.84	2.41	0.66	1.03	1.13
Fig. 3.9								
ON expansion	1.23	1.71	2.47	1.89	3.18	2.83	1.01	2.10
OFF expansion	0.84	0.75	2.20	1.93	2.18	2.22	2.62	1.99
ON sawtooth	2.31	1.16	3.07	2.01	2.81	1.38	1.51	1.94
OFF sawtooth	6.26	3.28	4.96	2.16	5.19	3.51	2.80	2.14

**Table 3.1.** Means and standard deviations of mean integrated turning responses. All values are computed from the mean behavior of at least 10 individual flies.

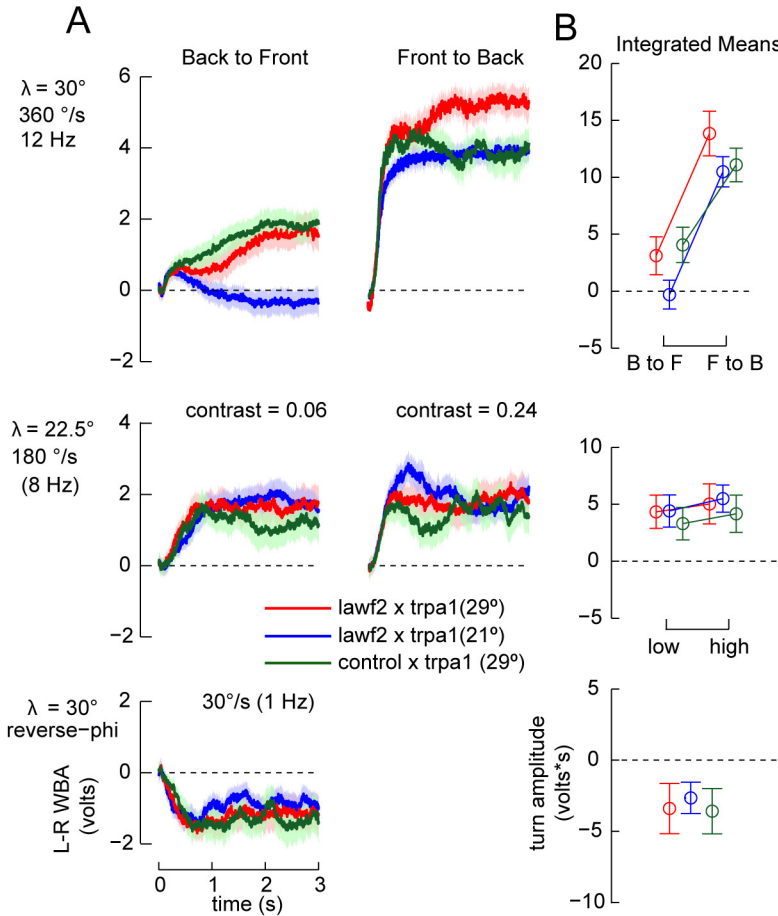


**Fig. 3.10.** Activating wide-field neurons with trpA1 does not alter basic optomotor responses  
**(A)** Mean fly responses to several optomotor behaviors (mean  $\pm$  s.e.m.;  $n = 9$  flies). Flies were tested with bilateral motion (front-to-back vs. back-to-front), high and low contrast optomotor stimuli, and reverse-phi motion. The experimental conditions (lawf2 x trpA1 at 29°) were compared to two controls: the experimental genotype at 21°, and a control genotype at 29°.  
**(B)** Integrated mean responses of the five behavioral conditions in **A**. In no case were experimental flies different from the two controls.

We tested control (11d03AD alone) and experimental (11D03AD;19c10DBD) flies crossed to UAS-dtrpA1 at both permissive (21°) and restrictive (29°) temperatures. The temperature shift significantly affected several behaviors, reducing steering amplitudes to back-to-front motion (Fig. 3.10A) and decreasing tracking of a bright stripe on a dark background (Fig. 3.11B). To

avoid potential confounding effects of the temperature shift, we compared the experimental flies at the restrictive temperature (29°) to the behavior of both experimental flies at 21° and control flies at 29°. Activation of wide-field neurons with dtrpA1 did not significantly alter steering responses for any of the stimuli we tested.

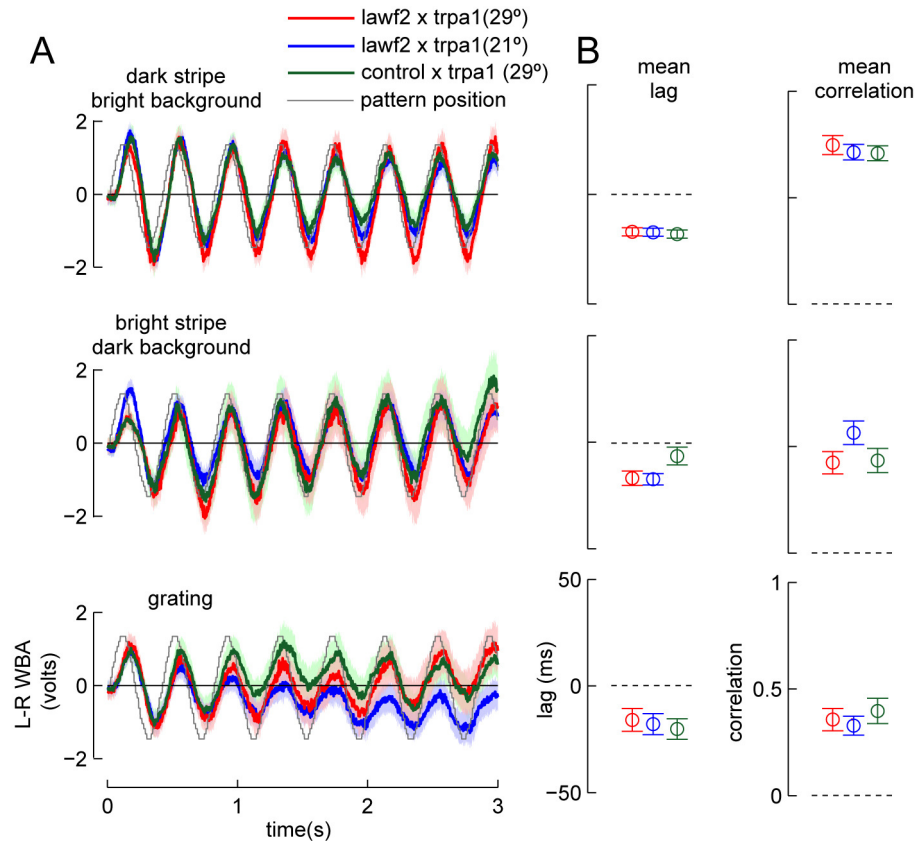


**Fig. 3.11.** Activating wide-field neurons with trpA1 does not alter tracking of small- and large-field motion. **(A)** Mean flight steering responses ( $\pm$  s.e.m;  $n = 9$  flies) to visual stimuli oscillating at 3 Hz. Three visual patterns were tested, a 15° wide dark stripe, an equivalent bright stripe, and a square-wave grating ( $\lambda = 30^\circ$ ). As in Fig. 3.7, each stimulus started out at the center of the fly's visual field, and moved  $\pm 37.5^\circ$  (stimulus position is plotted in gray). **(B)** The correlation and phase lag between the fly's steering (L-R WBA) and the stimulus position were calculated on a trial-by-trial basis. Experimental flies were not different from the two control lines.

## Discussion

The well-being of a fly depends critically on being able to detect subtle changes in the contrast and spatial position of objects in the environment. Flies perform such discriminations across diverse lighting conditions and visual environments. Consequently, visual neurons must rapidly adapt to local and global statistics of visual scenes.

Rapid, local adaptation is known to exist within and between neighboring cartridges in the fly lamina (Laughlin and Hardie, 1978). However, correlations in natural scenes exist across multiple spatial and temporal scales. The spectral power of static natural images(van der Schaaf and van Hateren, 1996) and natural time series(van Hateren, 1997) both decrease according to a power law (e.g.,  $1/\text{frequency}^2$ ), such that natural scenes are dominated by low frequencies. Moving natural scenes are also dominated by low spatial and temporal frequencies (Dong and Atick, 1995). In order to increase sensitivity, the visual system might actively filter out low frequency signals. One method to accomplish this is through efferent feedback from more central brain regions.

The anatomical profile of wide-field neurons suggest that they provide feedback from the medulla to the lamina. Lamina wide-field neurons receive multi-columnar input from layers M1 and M9 of the medulla, and project back into the most distal layers of the lamina. Based on examination of unassigned multi-columnar processes within an individual reconstructed column, it is likely that wide-field neurons form synapses with most cell types in the lamina (Rivera-Alba et al., 2011).

Our behavioral experiments suggest that feedback from wide-field neurons enhances sensitivity of peripheral visual circuits. Silencing wide-field neurons by expression of the ion channel kir2.1 produced several general phenotypes. First, fly responses to low contrast optomotor stimuli were significantly weaker. Second, fly tracking of small-field objects was reduced; this was true for both dark and bright stripes, but not a square-wave grating, across a range of oscillation frequencies. Importantly, behavioral responses to all of these stimuli were not completely abolished. Rather, the absence of wide-field neuron activity decreased the salience of particularly challenging stimuli, such as fast moving stripes and low contrast wide-field motion. This suggests that wide-field neurons play a general role in sharpening visual perception.

More specific clues about wide-field neuron function arose from fly responses to very slow motion. Silencing wide-field neurons significantly increased behavioral responses to slow (1 Hz) optomotor patterns. Overall, flies with silenced wide-field neurons consistently responded more strongly to very slow (<2 Hz) visual motion patterns (both rotation and expansion). These results suggest that wide-field neurons are not directly involved with detecting moving visual stimuli, but rather modulate motion circuits by suppressing sensitivity to low frequencies.

This hypothesis is supported by the most striking and specific phenotype we observed, from the motion nulling experiments. When presented with superimposed high and low velocity stimuli, control flies reliably follow the faster stimulus, even if it is lower contrast. Silencing wide-field neurons dramatically reversed this behavior, causing flies to reliably track the low velocity (1 Hz) stimulus. Remarkably, these flies were indistinguishable from control across the remainder of the velocity range, indicating that the deficit was specific to low speeds.

An intriguing possibility is that wide-field neurons provide adaptive feedback to the lamina, actively suppressing visual sensitivity to low frequency visual signals. Low frequency, subtractive feedback would result in increased sensitivity to faster motion stimuli, perhaps contributing to the characteristic temporal frequency tuning that fly optomotor responses exhibit. However, although our experiments focused primarily on behaviors evoked by visual motion, there is little reason to assume that lawf2 neurons contribute specifically to optomotor responses.

Activating wide-field neurons with trpA1 did not produce any measurable effect. This could be due to the fact that we tested a very small number of behavioral conditions, and that the majority of flies were unwilling to participate in our experiments at temperatures above 25° C. Overall, kir2.1 was a more reliable effector because it produced strong and repeatable behavioral phenotypes, and we could verify its efficacy by recording from gfp-tagged kir2.1-expressing neurons (see Chapter 4). Future experiments using alternative silencing and activation effectors should provide additional insight into the function of wide-field neurons.

### **Materials and methods**

*Drosophila melanogaster* were reared on standard fly medium on a 14 h:10 h light:dark cycle. Flies expressing kir2.1 were reared at 25° C, while trpA1-expressing flies were reared at 18°C. All flies were tested 0-4 hours before the onset of their fictive night. Gravid females, 3-4 days old, were cold-anesthetized and tethered to a 0.1 mm tungsten wire with UV-activated glue. After at least 15 minutes of recovery, flies were placed within a cylindrical electronic flight simulator. Within the arena, the position of the wings was monitored using a wingbeat analyzer (Gotz, 1987) . The wingbeat amplitudes, frequency, and signals encoding the positions of the display

stimuli were sampled at 1 kHz by a DigiData 1440A (Axon Instruments). All data analysis was performed offline in MATLAB (Mathworks, Natick, MA) and MySQL. In all figures showing flight behavior, we follow a convention of plotting the turning response of flies as the left minus right wing beat amplitude (L-R WBA), a measure which is directly proportional to yaw torque (Tammero et al., 2004).

The visual arena consisted of a 32x88 array of green LEDs covering 330° in azimuth and 120° in elevation (Reiser and Dickinson, 2008). The maximum pixel size of each LED is below the inter-ommatidial distance of *Drosophila* (Heisenberg and Wolf, 1984), so single pixel jumps between consecutive frames simulate continuous motion to the fly (except when motion is very slow).

The arena had a linear intensity scale from 0 to 72 cdm<sup>-2</sup>.

All of the flight behavior experiments used a protocol in which 3 second open-loop trials were interleaved with 3.5 seconds of closed-loop 'stripe fixation,' during which the fly actively controlled the position of a 30° dark stripe against a bright background. The stripe fixation epochs ensured that the flies were actively steering at the onset of each open-loop condition. If the fly stopped flying during a trial, a small fan automatically delivered a brief wind stimulus to encourage her to resume flight. Trials in which the flight stopped were excluded from subsequent analysis. Within an experiment, each set of conditions was presented as random blocks repeated three times. Trials in which the fly stopped flying were repeated at the end of each block. Therefore, each fly completed each condition at least three times.

For each open-loop condition, the mean response during the 50 ms previous to stimulus onset was subtracted from the subsequent turning response. Half of the conditions (e.g., CCW rotation) were inverted and averaged with the corresponding symmetric conditions (e.g., CW

rotation). These data were averaged on a per-fly basis to produce a mean turning response for each pair of symmetric conditions, and then plotted as the mean  $\pm$  s.e.m. across flies. The convention in all behavior figures is that rotation is CW.

Mean response amplitudes were calculated by integrating the area under the L-R WBA time-series for each trial, and averaging these values on a per-fly basis. Where appropriate, correlation coefficients and phase lags were also calculated for each trial from the cross-correlation of the visual stimulus position and the wingbeat modulations of the fly, either L-R or L+R WBA. Cross-correlation was performed using the *xcorr* function in Matlab. To determine statistical significance, un-paired t-tests were performed on the mean correlation values, mean phase lags, and mean turning amplitudes for each fly.

## Chapter 4

### **Electrophysiological characterization of a wide-field neuron in the *Drosophila* lamina**

#### **Abstract**

Peripheral visual circuits are highly adapted for efficient coding of image contrast. However, the mechanisms by which retinal circuits maintain sensitivity across diverse luminance conditions are not well understood. We previously identified a new class of wide-field feedback neurons in the fly lamina (wide-field) that provide feedback from the medulla to the distal lamina and are essential for the perception of low contrast visual stimuli. Here, we use targeted whole-cell patch-clamp recordings *in vivo* to show that wide-field neurons encode low frequency luminance fluctuations, and that their excitability increases when the fly is flying. Application of the neuromodulator octopamine mimicked flight conditions, indicating that octopamine release during flight alters the coding properties of wide-field neurons. These data suggest that wide-field neurons enhance visual sensitivity by providing low-frequency feedback to the lamina, and that the quality of this feedback depends on the behavioral state of the fly.

#### **Introduction**

A general problem sensory neurons face is encoding a wide range of inputs within a limited range of cellular responses (Barlow, 1961a; Laughlin, 1981; Srinivasan et al., 1982). For example, the visual system must operate over an enormous range of light conditions, from bright sunlight to dim starlight (Rieke and Rudd, 2009). The retina deals with this variability by adjusting its sensitivity, or adapting, to the statistical features of light inputs, such as mean light intensity and contrast, a measure of variability about the mean (Laughlin, 1989; Shapley and

Enroth-Cugell, 1984). In the retina, adaptation is known to occur on a local scale, such as within and between individual photoreceptors (Laughlin and Osorio, 1989; Shapley and Enroth-Cugell, 1984). However, local adaptation mechanisms are susceptible to noise from both light signals and the stochasticity of neural processing (Laughlin, 1989). Adaptation over a larger spatial scale could exploit convergence to obtain more reliable estimates of relevant scene statistics.

In the previous chapter, we described a novel class of wide-field neurons (lawf2) which provide feedback to the *Drosophila* lamina. Wide-field neurons tile the fly retina, receiving dendritic input from large regions of visual space in the medulla, and supplying synaptic output to equivalently sized regions of the more peripheral lamina. The anatomy of these neurons suggests that they could play a role in adapting the eye over a larger spatial scale than previously described local interactions such as local lateral inhibition. Our behavioral genetics experiments provide evidence that wide-field neurons play a role in adaptation by providing feedback from the medulla to the lamina. Silencing wide-field neurons by expression of kir2.1 decreases fly responses to low contrast optomotor stimuli, and increases responses to very slow motion stimuli. These results suggest that feedback from wide-field neurons suppresses low-frequency visual signals, and that removal of this feedback impairs the fly's ability to track challenging visual patterns. However, a more detailed understanding of wide-field neuron requires knowledge of these neurons' electrophysiological response properties.

## Results

### Whole-cell patch-clamp recordings from wide-field neurons

We developed a preparation in which we could perform whole-cell patch clamp recordings from the peripheral visual system of *Drosophila* (Fig. 4.1A). A split-GAL4 driver line restricted to wide-field neurons was used to drive expression of GFP, permitting visual targeting of wide-field neuron somata in the cell body rind of the medulla. Adult flies were immobilized in a custom-milled stainless steel holder and the dorsal head cuticle and perineural sheath were dissected away to visualize the dorsal surface of the medulla. Individual neurons were patched using oblique infrared illumination and fluorescence to identify wide-field neuron cell bodies (Fig. 4.1B).

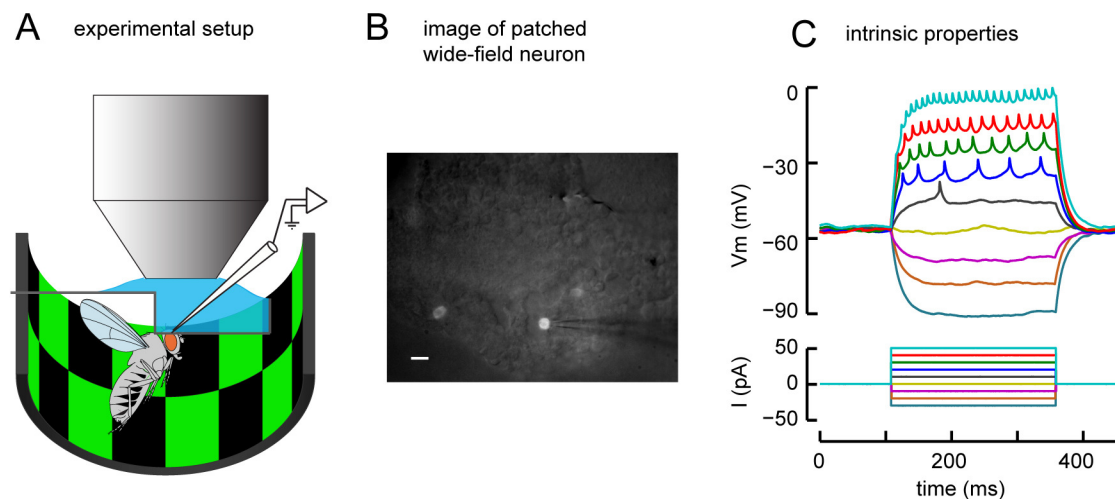


**Fig. 4.1.** Whole-cell patch clamp recordings from wide-field neurons. **(A)** The head of the fly is fixed in a thin stainless steel holder, while patch clamp recordings are visually targeted to GFP-labeled wide-field cell bodies in the medulla. The eye is stimulated with a green LED arena that covers  $180^\circ \times 60^\circ$  of the fly's visual field. **(B)** Merged image of oblique infrared illumination and GFP fluorescence. Scale bar at left is equal to  $5 \mu\text{m}$ . **(C)** Injected current steps, and measured voltage responses of a wide-field neuron recorded in current clamp ( $R_{\text{input}} = 1.09 \pm 0.064 \text{ G}\Omega$ ,  $n = 24$  cells).

We were surprised to find that wide-field is a spiking neuron, the first identified by intracellular recordings in the fly lamina (Fig. 4.1C). This discovery is remarkable given that physiologists have been using sharp-electrodes to record from the fly lamina for over 50 years. The fact that no spikes have been recorded from the lamina is likely due to the strong selection bias of sharp micropipettes and the diminutive size of wide-field neuron axonal processes in the lamina.

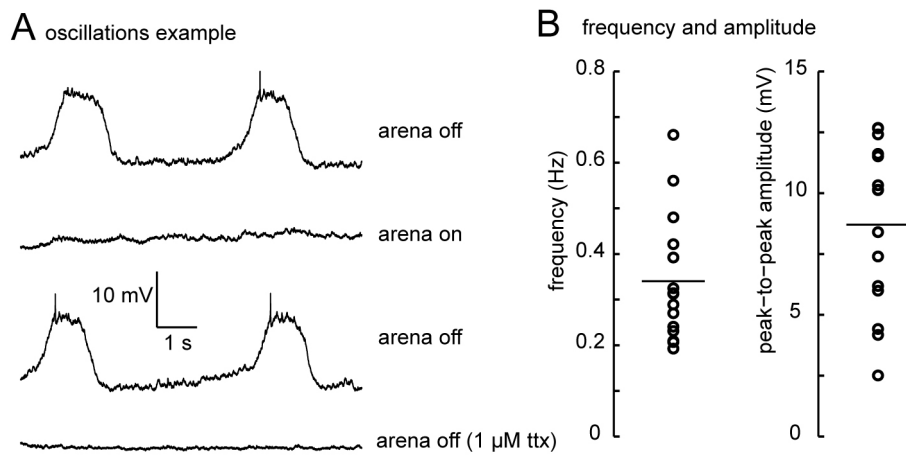


**Fig. 4.2.** Spontaneous oscillations in wide-field neurons. **(A)** Out of 24 cells recorded, 15 exhibited slow oscillations greater than 2.5 mV peak-to-peak. In all cases, oscillations were abolished by light exposure, or application of 1  $\mu$ M TTX. **(B)** Distributions of oscillation frequency and amplitude. The mean oscillation frequency (horizontal bar) was  $0.35 \pm 0.04$  Hz, and the mean peak-to-peak amplitude was  $8.70 \pm 0.88$  mV. Frequency and amplitude estimates of spontaneous oscillations were made by low-pass filtering 10 s windows of spontaneous activity, and fitting a sine function to the data using least-squares.

Injecting current at the wide-field neuron cell body elicited spikes of 5-10 mV amplitude, similar to recordings from projection neurons in the *Drosophila* antennal lobe (Wilson et al., 2004). These spikes were heavily filtered (Fig. 4.1B), presumably due to the electrotonic distance between the cell body and the spike initiation zone, which is presumably located in the initial segment of the axon (Gouwens and Wilson, 2009). This filtering is aggravated by the tiny size of *Drosophila* neurons and the absence of voltage-gated conductances between the cell body and

other processes. A secondary consequence of these properties is that effective voltage clamp is not possible (data not shown); therefore, all recordings were made in current clamp.

Though wide-field neurons were typically silent at rest, 15 out of 24 cells exhibited slow (< 1 Hz) spontaneous oscillations in darkness (Fig. 4.2). These oscillations were eliminated by illuminating the eye or blocking sodium channels through bath application of 1  $\mu$ M tetrodotoxin (TTX).

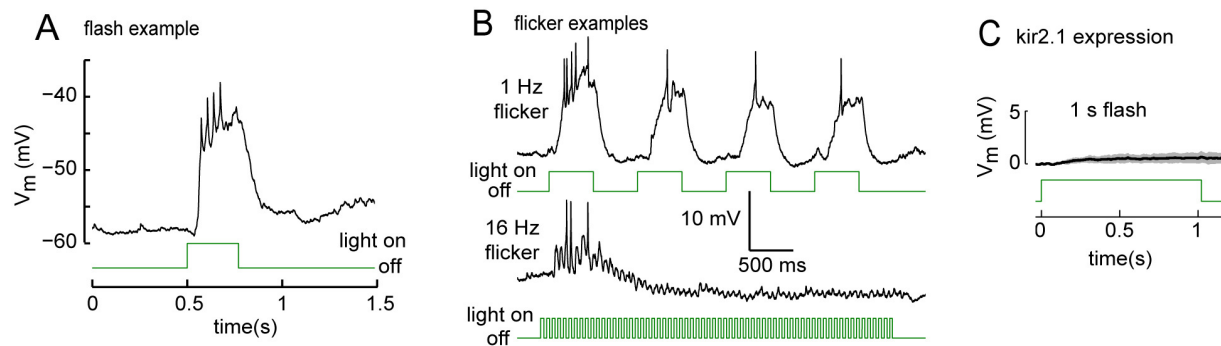


**Fig. 4.3.** Basic light-evoked response properties of wide-field neurons. **(A)** Light-evoked responses of a wide-field neuron to a maximum intensity ( $72 \text{ cd m}^{-2}$ ) full-field flash (1 s). **(B)** Response of a wide-field neuron to a dynamically flickered luminance stimulus. At low flicker frequencies (1 Hz), wide-field neurons phase-lock to light onset, while at higher flicker frequencies (16 Hz), the neuron does not cross threshold after an initial transient burst of spikes. See Fig. 4.8 for group data. **(C)** Whole-cell patch clamp recordings were targeted to neurons expressing UAS-kir2.1-GFP. Traces show mean membrane potential responses of lawf2 neurons expressing kir2.1 to brief full-field light flashes (mean  $\pm$  s.e.m.,  $n = 4$  cells).

### Light-evoked responses of wide-field neurons

We used a green LED arena similar to that used in behavioral experiments to stimulate the eye of the fly while recording from wide-field neurons in restrained flies (i.e., the legs and wings were glued to prevent movement). In response to a 1 second full-field luminance flash, wide-field neurons depolarized and fired small bursts of spikes (Fig. 4.3A). The delay from light ON to the first spike was very large (60 +/- 8 ms) compared to the response latencies of other neurons

recorded in the lamina of larger flies (e.g. *Musca* LMC's: 5-10 ms (Scholes, 1969)). Such a fixed response delay should have an effect on the ability of the neuron to encode fast luminance modulations. Consistent with this, we found that  $V_m$  did not phase-lock to the light stimulus and that neurons did not cross threshold at higher flicker frequencies (Fig. 4.3B and see below). We also verified the efficacy of our genetic manipulations in the previous chapter by recording from wide-field neurons expressing GFP-tagged kir2.1. Neurons expressing kir2.1 did not depolarize or fire action potentials in response to full-field light flashes (Fig. 4.3C), confirming that this manipulation had the desired effect of silencing wide-field cell output. Kir2.1 expression also decreased the average input resistance ( $0.500 \pm 0.159 \text{ G}\Omega$  vs.  $1.09 \pm 0.064 \text{ G}\Omega$ ), as previously reported in other fly neurons (Kazama and Wilson, 2008).

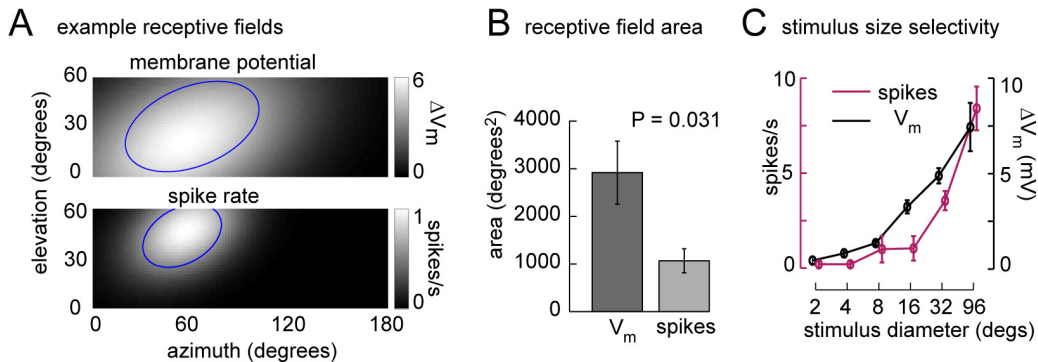


**Fig. 4.4.** Spatial receptive fields of wide-field neurons. **(A)** A typical wide-field neuron receptive field, fit with an elliptical Gaussian. See Fig. 4.5 for population comparison. **(B)** Receptive fields measured by subthreshold activity are significantly larger than those measured by spike rate ( $P = 0.031$ ,  $n = 10$  cells). **(C)** Spike rates and membrane potential depolarizations evoked by square light stimuli of increasing diameter. All stimuli were centered on the peak of the receptive field.

Next, we mapped the spatial receptive fields of wide-field neurons by randomly illuminating large regions ( $30^\circ \times 30^\circ$ ) of the fly's visual field (Fig. 4.4A)—these receptive field maps were well fit with elliptical Gaussians (e.g., Fig. 4.5A). Wide-field spatial receptive fields extended

across multiple ommatidial columns (Fig. 4.4B), and subthreshold receptive fields were bigger (~50° diameter) than receptive fields measured by spiking activity (~30°; Fig. 4.4B). Wide-field neurons responded preferentially to stimuli that excited large portions of their receptive fields, and there we did find any evidence for the existence of an inhibitory surround (Fig. 4.4C).

Physiologically mapped receptive-field sizes qualitatively matched the size of the dendritic arborizations in the medulla, confirming that wide-field neurons receive input from large regions of visual space. However, across the entire population of neurons for which we examined spatial characteristics ( $n = 10$ ), receptive fields were significantly elongated along the azimuth (Fig. 4.5B, C). This asymmetry was consistent for both subthreshold and spiking receptive fields (Fig. 4.5C).

In the previous chapter, we used moving visual stimuli to characterize the behavioral effects of silencing wide-field neurons. Although motion sensitivity is thought to arise postsynaptic to the lamina, wide-field neurons could provide direction-selective feedback to the lamina. To test this possibility, and to characterize the response of wide-field neurons to motion stimuli like those used in our behavioral experiments, we examined wide-field responses to rotating full-field motion stimuli. Wide-field neurons responded robustly to slowly rotating motion stimuli, though motion responses were weaker than those elicited by full-field flicker (Fig. 4.4A). We did not find any specific direction or motion selectivity: wide-field neurons responded equally to motion in all 4 directions tested (Fig. 4.4B). In other words, wide-field neurons responded to slow motion stimuli as predicted from their spatial and temporal receptive fields, without any indication of specific motion sensitivity.

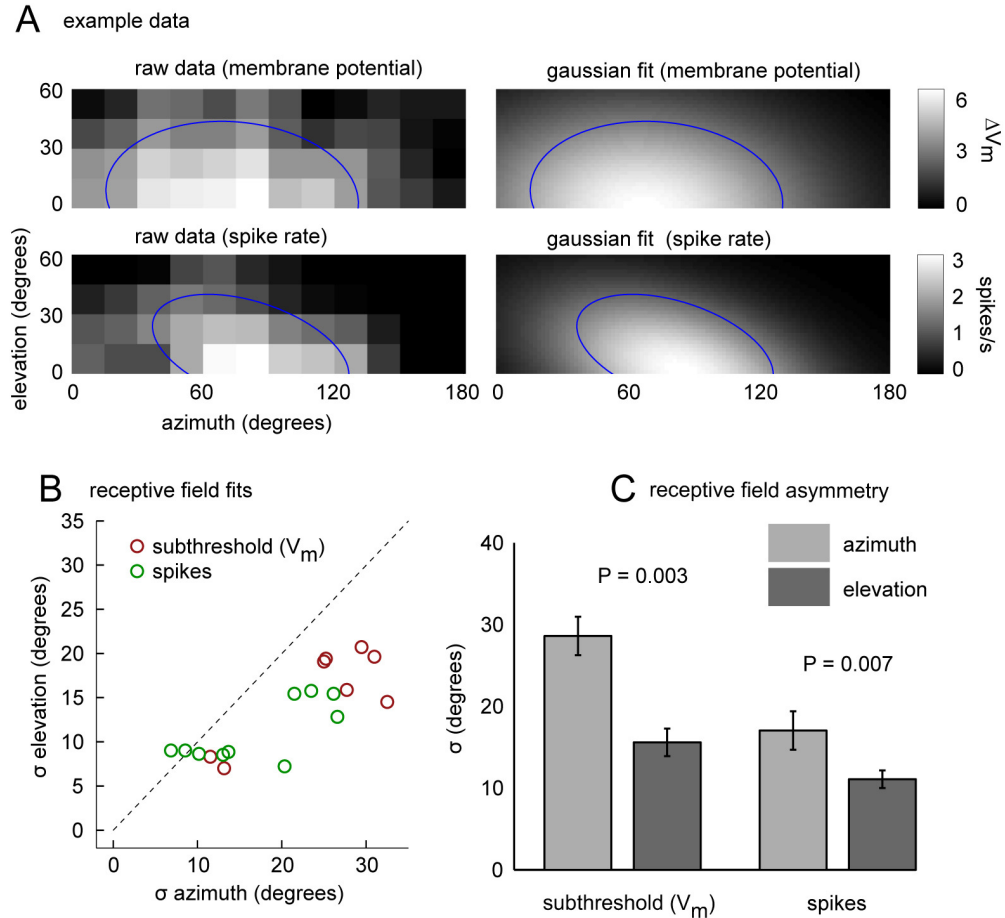


**Fig. 4.5.** Population comparison of receptive fields. **(A)** Receptive fields were mapped by flashing bright square stimuli ( $30^\circ \times 30^\circ$ ) at 33 overlapping locations in the arena, and calculating the mean depolarization and spike rate at each point. The spatial profile of each cell was fitted by a two-dimensional Gaussian, characterized by the long and short axis of an ellipse at 1 s.d. ( $\sigma$ ), and an orientation angle ( $\theta$ ). Left: raw data for means and spike rates of a typical wide-field neuron. Right: Gaussian fits. In both panels, the blue ellipse represents 1 s.d. of the fit Gaussian. **(B)** Distribution of receptive field sizes along the azimuth and elevation of the fly's visual field. **(C)** Measured receptive fields were significantly wider in azimuth than elevation, as measured with both subthreshold activity and spike rate. However, this effect may be due to the dimensions of the arena used to map receptive fields ( $180^\circ$  wide  $\times 30^\circ$  high).

Overall, wide-field neurons signal luminance changes within large regions of the fly's visual field, and are neither sensitive to local fluctuations nor directionally-selective. These properties are consistent with the idea that wide-field neurons provide low frequency, wide-field feedback to the lamina.

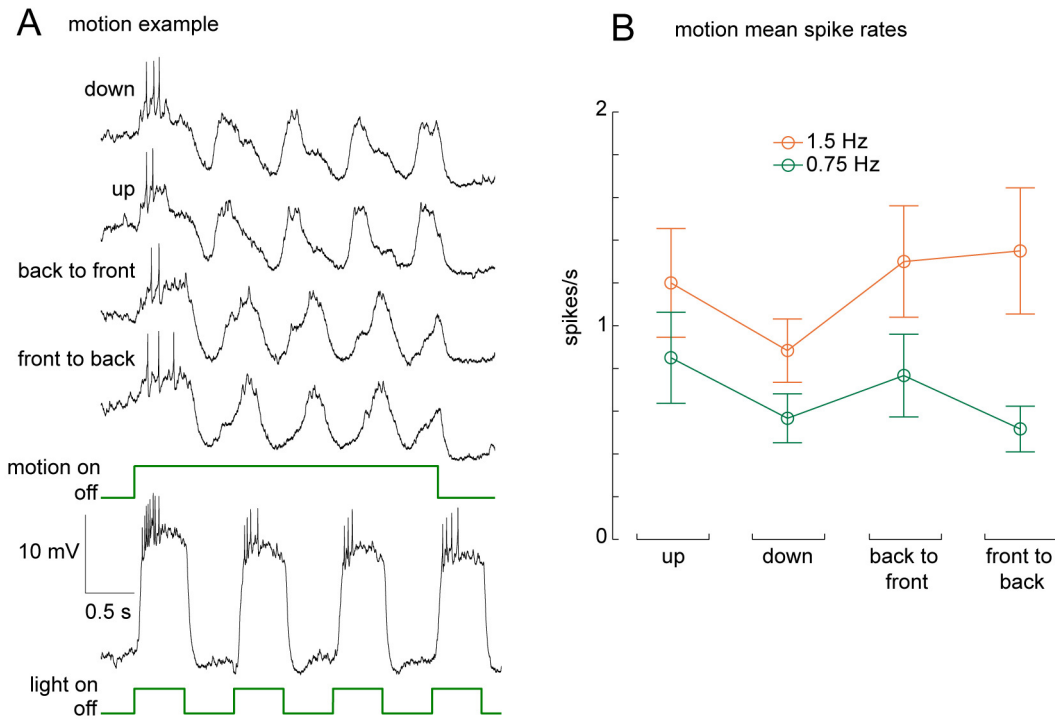


**Fig. 4.6.** Wide-field neurons are not selective for a particular direction of motion. **(A)** Example traces of a wide-field neuron to motion in four directions. The stimulus consisted of  $30^\circ \times 30^\circ$  alternating bright and dark blocks that moved at 1.5 Hz ( $45^\circ/\text{s}$ ). For comparison, the lower trace shows the response of the same cell to 1 Hz wide-field flicker. **(B)** Mean spike rates to motion (3 s) along the 4 cardinal axes of the eye ( $n = 5$  cells). Spike rates were not significantly different for any particular direction of motion (pairwise  $t$  tests).

### Flight state affects wide-field neuron excitability

Recent investigations of the activity of motion-sensitive neurons in the fly lobula plate have shown that their response properties depend critically on the behavioral state of the animal. In particular, the response gain of these neurons increases when the fly is walking (Chiappe et al., 2010) or flying (Jung et al., 2011; Maimon et al., 2010). Similar effects have been observed when an agonist of the neuromodulator octopamine is applied to the blowfly brain (Jung et al., 2011; Longden and Krapp, 2009), suggesting that modulation could be at least partly due to octopamine release during behavior. Octopamine is a biogenic amine structurally related to

noradrenaline. It is found in high concentrations throughout the invertebrate nervous system, and serves as a neuromodulator for many sensory neurons (Farooqui, 2007).

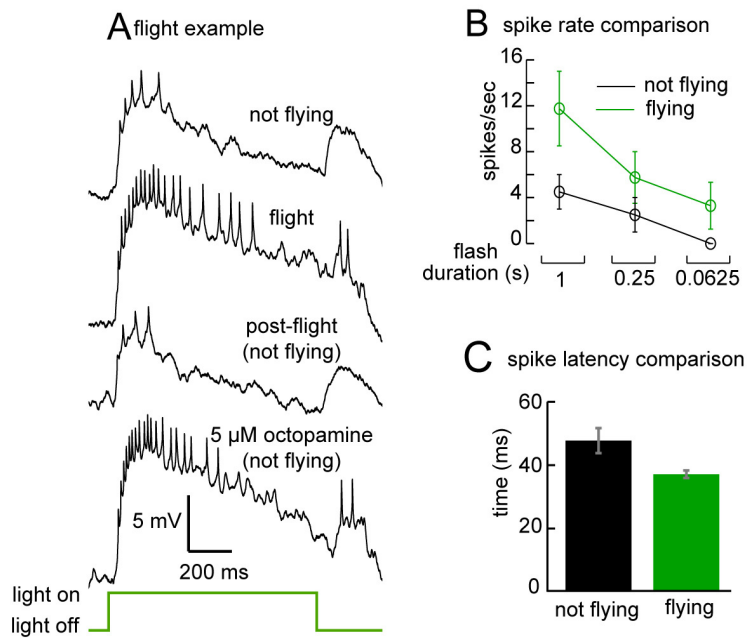


**Fig. 4.7.** Flight increases wide-field excitability. **(A)** Example wide-field responses to a 1 s light flash before, during, and after flight. Application of the neuromodulator octopamine mimicked the effects of flight. **(B)** Comparison of mean spike rates to light flashes of three different durations under flying and non-flying conditions ( $n = 4$ ). **(C)** Latency to the first spike following a 1 second light flash under flying and non-flying conditions ( $P = 0.035$ , 4 cells). Although neurons depolarized slightly during flight (see text), spontaneous activity remained unchanged (mean s.d. of  $V_m$ :  $2.8 \pm 0.9$  mV flying vs.  $2.9 \pm 0.1$  mV not flying;  $P = 0.97$ ).

In order to test whether behavioral state affects wide-field neuron activity, we allowed the fly to initiate and maintain flight during the recording. Similar to a previous study (Maimon et al., 2010), we were able to maintain stable whole-cell recordings during flight while measuring wingbeat activity with an infrared-sensitive camera (Fig. 4.7A). When the fly was flying, brief light flashes evoked larger spike rates (Fig. 4.7B), and decreased the latency of the first stimulus-evoked spike (Fig. 4.7C). Flight also depolarized the resting membrane potential ( $V_m$ ) slightly, though not significantly ( $-61.5 \pm 0.8$  mV not flying vs.  $-58.6 \pm 0.58$  mV flying;  $P = 0.12$ ).

Bath application of 5  $\mu$ M octopamine mimicked the effects of flight (Fig. 4.7A), suggesting that wide-field activity is altered during flight due to release of the neuromodulator octopamine.

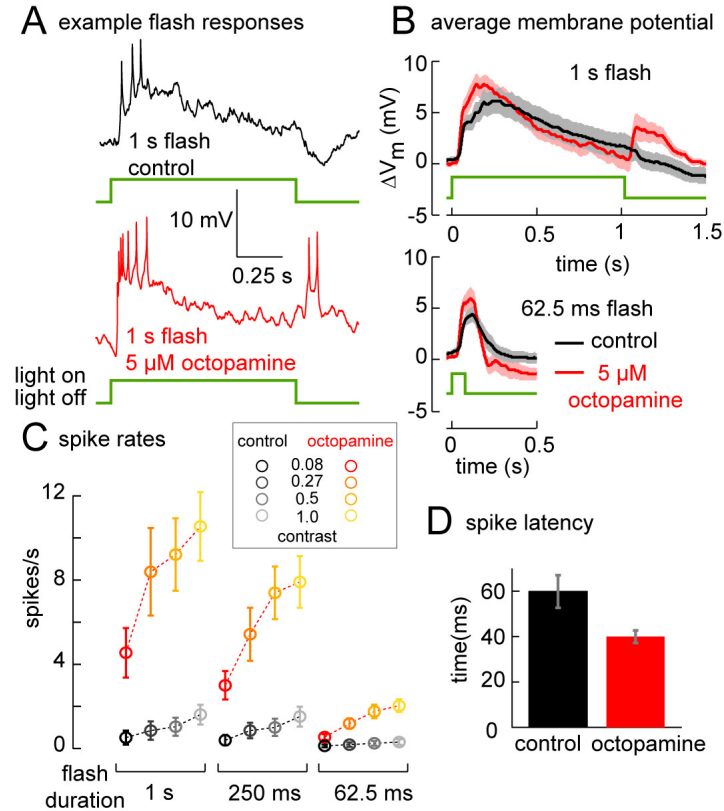


**Fig. 4.8.** The neuromodulator octopamine increases wide-field neuron excitability. **(A)** Example responses of a wide-field cell to a 1 s light flash with and without 5  $\mu$ M octopamine in the bath. **(B)** Average membrane potential responses of wide-field neurons to brief light flashes (mean  $\pm$  s.e.m, 11 cells). Spikes were removed by low-pass filtering prior to averaging. **(C)** Spike rates across contrast conditions and flash durations. **(D)** Latency to the first spike following a 1 second light flash under octopamine and control conditions ( $P = 0.035$ , 8 cells).

#### Wide-field neuron activity is altered by the neuromodulator octopamine

We next examined neuromodulation of wide-field neuron activity by recording from restrained flies (i.e., the wings and legs were glued) in the presence of 5  $\mu$ M octopamine (Fig. 4.8A). As in flight, the amplitude (Fig. 4.8B) and spike rate (Fig. 4.8C) of light-evoked responses increased, spike latency decreased (Fig. 4.8D), and the resting potential depolarized ( $-61.0 \pm 0.9$  mV vs. -

$57.6 \pm 1.4$  mV with octopamine;  $P = 0.05$ ). These data closely parallel the effects of behavioral state modulation shown above, suggesting that octopamine release during flight alters the coding properties of wide-field neurons.

Octopaminergic neurons originating in the central brain project to many parts of the *Drosophila* visual system, including the medulla, but they do not innervate the lamina (Busch et al., 2009). It is therefore unlikely that octopaminergic neuromodulation of wide-field neurons could be originating within the lamina. However, wide-field neurons could receive inputs from the medulla that experience efferent octopaminergic modulation. It is therefore important to ask whether the neuromodulatory effects of octopamine are intrinsic to wide-field neurons, or a result of modulation elsewhere in the circuit.

To test the effects of octopamine on intrinsic neuronal properties, we injected a series of current steps and measured voltage deflections in current clamp. Current injection evoked consistently higher spike rates when octopamine was present (Fig. 4.9). This effect was likely not due to the overall depolarizing effects of octopamine, because each neuron was held at the same resting potential (-60 mV) throughout the experiment. Although spiking activity changed dramatically, octopamine did not affect the input resistance across the population of recorded wide-field neurons ( $1.07 \pm 0.08$  G $\Omega$  (control) vs.  $1.02 \pm 0.06$  G $\Omega$  (octopamine);  $P = 0.63$ , 14 cells), as would be expected if octopamine increased overall neuronal conductance. However, the input resistance measured at the cell body may not reflect conductance changes in electrotonically distant compartments of the neuron. These data suggest that octopaminergic neuromodulation acts directly on wide-field neurons, but do not rule out additional contributions from other elements of the circuit.

### A current-evoked spike rates

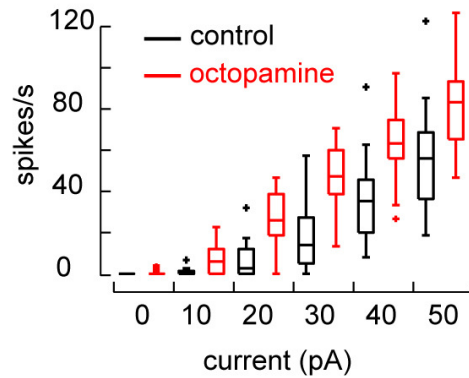


**Fig. 4.9.** Octopamine increases spiking probability. **(A)** Spike rates evoked by brief (250 ms) current steps ( $P = 0.0007$ , 14 cells). Box plots indicate the median value (center line), 25<sup>th</sup> and 75<sup>th</sup> percentiles (boxes), the data range (whiskers), and outliers (crosses). There was no difference in input resistance between the two conditions ( $1.07 \pm 0.08 \text{ G}\Omega$  (control) vs.  $1.02 \pm 0.06 \text{ G}\Omega$  (octopamine);  $P = 0.63$ , 14 cells) or in baseline synaptic activity (mean s.d. of  $V_m$ :  $2.8 \pm 1.6 \text{ mV}$  vs.  $2.19 \pm 1.3 \text{ mV}$ ;  $P = 0.24$ ).

Octopamine application dramatically increased wide-field neuron spike rates across a range of flash durations and contrasts; with octopamine present, wide-field neurons robustly responded to even the weakest contrasts tested (Fig. 4.8C). Another consequence of octopaminergic modulation was an increased response to light offset (Fig 4.10A, B). Under control conditions, wide-field neurons weakly depolarized to darkening stimuli, particularly after long periods of light adaptation. However, this phenomenon was greatly enhanced when octopamine was present, resulting in significant spike rates at light termination (Fig. 4.10C).

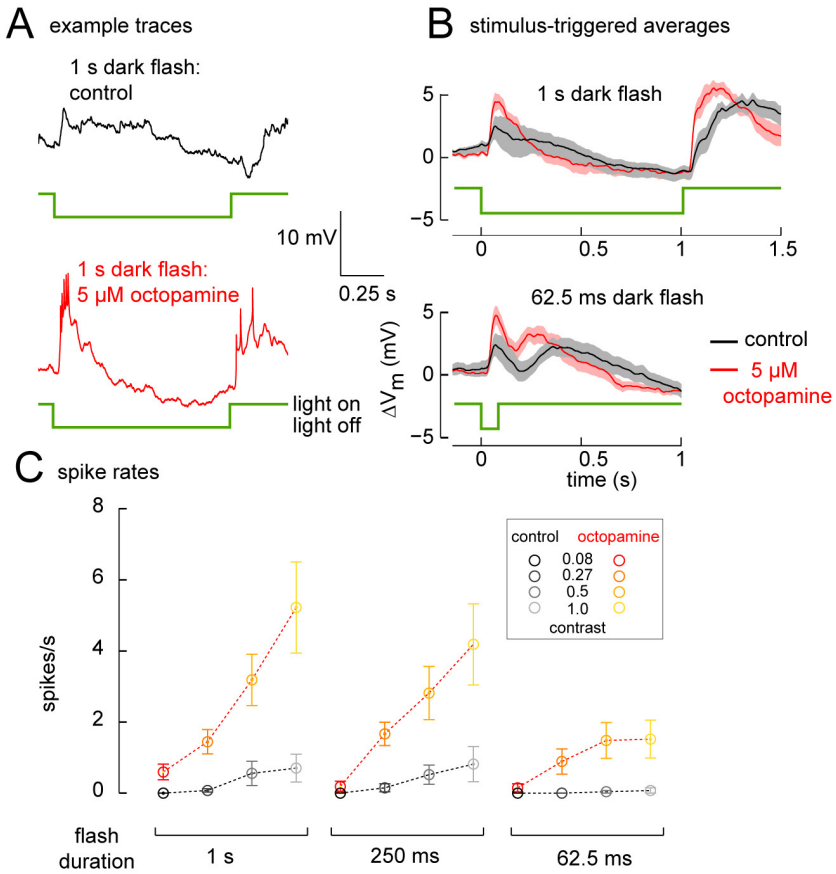


**Fig. 4.10.** Responses to light off increase when octopamine is present. **(A)** Example traces of a wide-field cell to a 1 s light decrement with and without 5  $\mu$ M octopamine in the bath (same cell as in the example of Fig. 4.8a). **(B)** Average membrane potential responses of wide-field neurons to brief light decrements (mean  $\pm$  s.e.m.,  $n = 9$  cells). Spikes were removed by low-pass filtering prior to averaging. **(C)** Spike rates across contrast conditions and flash durations.

We also investigated the effects of adaptation by dark-adapting the eye for different lengths prior to a 1 s light flash. Wide-field neurons fired more spikes after longer periods of dark adaptation, and octopamine significantly increased spiking activity (Fig. 4.11). Octopamine also augmented the *rate* of dark-adaptation, indicated by the slope of the fit line in Fig. 4.11. This change in adaptation rate should have dramatic effects on the coding of dynamic luminance patterns, which we explore below.

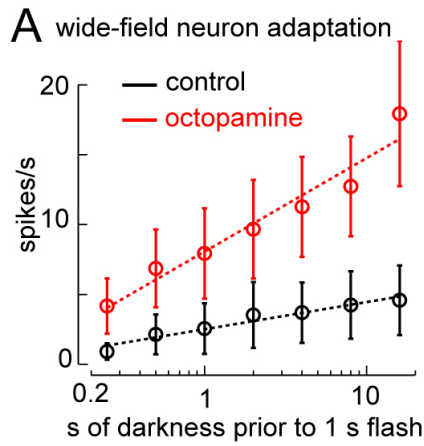


**Fig. 4.11.** Octopamine increases rate of adaptation. **(A)** Spike rates evoked by 1 s light flashes following different periods of dark adaptation ( $n = 6$  cells). Dotted lines are least-squares linear fits, indicating the rate of adaptation for each experimental condition.

#### Octopamine changes the frequency coding of wide-field neurons

Due to self motion, an actively behaving fly is exposed to a higher range of temporal frequencies than a stationary fly. The visual system could take advantage of this relationship by adjusting the frequency sensitivity of visual neurons depending on behavioral state; this strategy could serve to match the dynamic range of visual neurons to the statistics of the visual environment, and save energy by reducing spontaneous neural activity while at rest.

To test whether octopamine alters the frequency coding of wide-field neurons, we measured responses to full-field luminance flicker (Fig. 4.12A). We then calculated the power of the membrane potential ( $V_m$ ) at the fundamental luminance flicker frequency. Under control conditions,  $V_m$  followed low frequency flicker patterns (1-2 Hz), but at higher frequencies (>4 Hz)  $V_m$  power at the flicker frequency decreased to zero (Fig. 4.12B). When octopamine was present, this frequency distribution shifted, and neurons responded with more power at higher frequencies (4-8 Hz). The spike rates in the octopamine condition were greater across a range

of flicker frequencies and contrast conditions, demonstrating that the measured membrane potential fluctuations impact postsynaptic targets of wide-field neurons (Fig. 4.12C). That octopamine increases selectivity for higher frequency luminance fluctuations suggests that wide-field neurons are more sensitive to higher frequencies during flight.

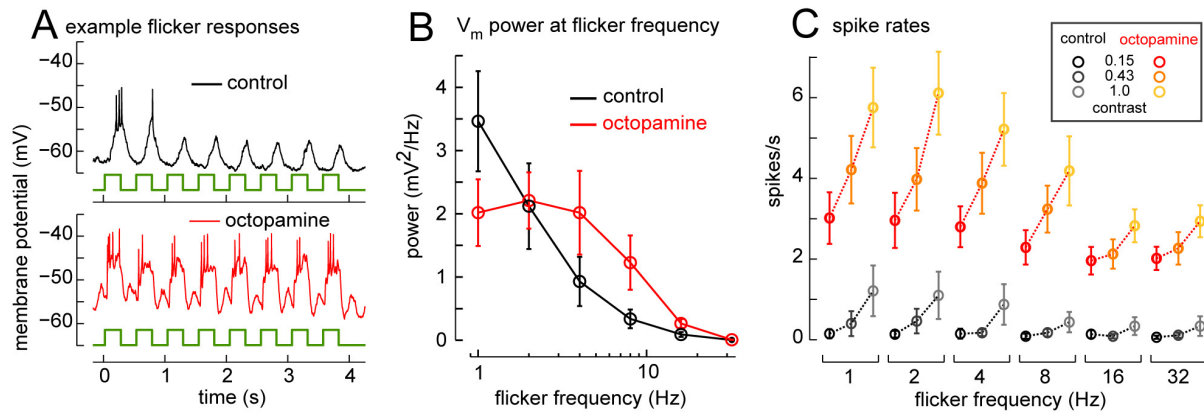


**Fig. 4.12.** Octopamine alters wide-field frequency sensitivity. **(A)** Example traces of a wide-field neuron to a full-field flicker stimulus (2 Hz). **(B)** Power of membrane potential fluctuations at the flicker frequency for the highest contrast tested ( $n = 11$  cells). Each trial was 4 s long, and repeated twice for each cell. Power spectra of individual traces were calculated using multi-taper spectral estimation, and averaged on a per-cell basis. See Methods for additional details about spectral analysis. **(C)** Spike rates across contrast conditions and flicker frequencies.

#### Wide-field neuron model

Natural scenes are dominated by low frequency signals, such that the power spectral density of natural images follows a  $1/f$  distribution (van der Schaaf and van Hateren, 1996; van Hateren, 1997). A significant challenge for the visual system is maintaining sensitivity across the range of frequencies encountered in nature. One way that early visual neurons might accomplish this is by filtering out the predominant low frequency signals through adaptation.

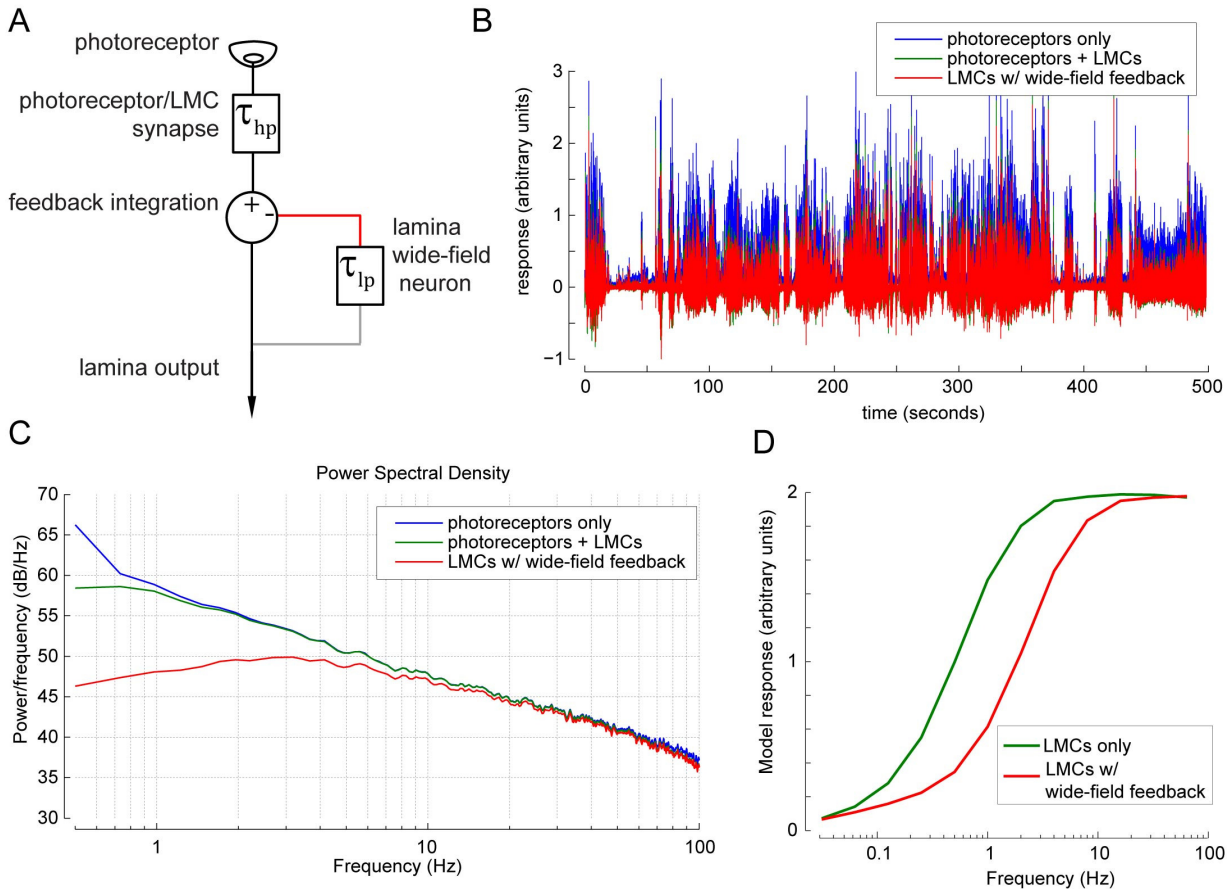


**Fig. 4.13.** Low-pass feedback suppresses low frequency signaling. **(A)** Schematic of the lamina wide-field neuron model. Low-pass filtered feedback, designed to mimic wide-field neurons (cutoff frequency = 0.25 Hz), is subtracted from luminance signals low-pass filtered by the photoreceptors (cutoff = 200 Hz) and high-pass filtered by the lamina monopolar cells (cutoff frequency = 0.4 Hz). **(B)** Model responses to natural luminance time series from van Hateren (1997). Results from the feedback model are compared to a model with photoreceptors alone, and photoreceptors with LMC high-pass filtering. See methods for model details. **(C)** Power spectral density of model responses to natural luminance time series. Low-pass feedback decreases the power density at low frequencies (<10 Hz). **(C)** Simulated response of two lamina models to a rotating grating like those used in behavioral experiments ( $\lambda = 90^\circ$ ). Low-pass feedback shifts motion sensitivity toward higher frequencies.

In order to understand the contributions of wide-field neuron signaling to adaptation, we studied the effects of low frequency feedback on a simple model of lamina processing (Fig. 4.13A). We used previously measured time constants for the photoreceptors (Juusola and Hardie, 2001) and lamina monopolar cells (Juusola et al., 1995) to simulate the output of lamina

neurons to naturalistic luminance time series (Fig. 4.13B). We then compared the output of reduced photoreceptor and LMC models to a model in which low frequency signals were subtracted from the LMCs through a feedback filter designed to mimic the wide-field neuron.

We found that, compared to a model without feedback, wide-field neuron feedback greatly reduced the encoding of low frequency luminance fluctuations, (Fig. 4.13C). Wide-field neuron feedback suppressed the predominant low frequency signals present in a natural time series of luminance fluctuations, resulting in a flatter frequency distribution across the spectral range. Finally, when tested with rotating gratings like those used in behavioral experiments, wide-field neuron feedback shifted lamina sensitivity toward higher motion speeds (Fig. 4.13D). This effect was similar to the behavioral phenotype we observed when silencing wide-field neurons: without wide-field neuron feedback, flies become more sensitive to low frequency motion patterns (Chapter 3).

## Discussion

### **Contribution of wide-field neurons to lamina processing**

The well-being of a fly depends critically on being able to detect subtle changes in the contrast and spatial position of objects in the environment. Flies perform such discriminations across diverse lighting conditions and visual environments. Consequently, visual neurons must rapidly adapt to local and global statistics of visual scenes (Laughlin, 1989; Rieke and Rudd, 2009). The anatomy and physiology of wide-field neurons suggests that their role is to provide low frequency feedback to the lamina. For example, wide-field feedback may sharpen the sensitivity of lamina neurons to higher frequencies by subtracting out, or adapting to, low frequency

background signals. This functional role may be similar to some wide-field amacrine cells in the vertebrate retina (Lin and Masland, 2006).

### **Electrophysiological properties of wide-field neurons**

Wide-field neurons respond to slow changes in mean luminance. Under dark-adapted conditions, light flashes evoke large depolarizations and small bursts of action potentials. These neurons also depolarize, though more weakly, to light decrements. Longer periods of adaptation to a constant intensity stimulus increased responses to both ON and OFF stimuli. Adaptation was also apparent on the time scale of short flashes—after 1 second of light exposure, the membrane potential returned to the resting level. This adaptation is likely related to the low-pass characteristics of the neuron in response to flickering stimuli. The time-scale of adaptation (~1 s) is far too slow to follow luminance modulations at higher flicker frequencies.

Wide-field neurons are the first spiking neurons identified in the fly lamina. However, action potentials have been recorded extracellularly in the chiasm between the lamina and medulla of the blowfly (Arnett, 1972; Jansonius and van Hateren, 1991; Jansonius and van Hateren, 1993a; Jansonius and van Hateren, 1993b). These recording were of two types, corresponding to a “sustaining unit” and an “on-off unit”. Although there has been speculation that these cells correspond to the lamina monopolar cells L4 and L5 (Jansonius and van Hateren, 1993a; Jansonius and van Hateren, 1993b), their identity remains unknown. The on-off units have some features in common with wide-field neurons, including low contrast sensitivity, selectivity for low frequency luminance fluctuations, and spiking responses to both positive and negative contrasts (Jansonius and van Hateren, 1991). However, major differences in the spatial receptive fields (Jansonius and van Hateren, 1993a) and specific temporal response

characteristics(Jansonius and van Hateren, 1991) suggest that wide-field neurons are not the on-off units first described by Arnett(Arnett, 1972).

### **Sources of behavioral state modulation**

A series of recent studies have demonstrated that active behavior modulates the coding properties of motion sensitive LPTC neurons in the fly lobula plate(Chiappe et al., 2010; Jung et al., 2011; Maimon et al., 2010), and that this modulation may be due to release of the neuromodulator octopamine (Jung et al., 2011; Longden and Krapp, 2009). Octopaminergic neurons project from the central brain to many parts of the visual system, including the lobula complex and the medulla, but not the lamina (Busch et al., 2009; Sinakevitch and Strausfeld, 2006). Therefore, it not known whether the effects of octopamine on lobula plate neurons are due to intrinsic neuromodulation, or act through modulation of upstream neurons in the medulla.

Our characterization of the wide-field neuron suggests that behavioral state modulation affects neural coding at the earliest stages of visual processing, and that this modulation is due to release of the neuromodulator octopamine. Both flight and octopamine application increased the amplitude of stimulus-evoked responses, and decreased spike latency. Although octopamine did not significantly alter passive input resistance measured at the soma, spike rates evoked by current injection significantly increased, suggesting that at least some of the behavioral state changes we observed are due to intrinsic neuromodulation of wide-field neurons. However, it is unlikely that wide-field neurons are the sole contributor to behavioral state modulation of visual circuits. Octopaminergic neurons densely innervate the fly optic lobes(Busch et al., 2009), and play an important role in many sensory systems (Farooqui, 2007).

### **Structure of potential feedback circuits**

Wide-field neurons receive input from layers M1 and M9 of the medulla, and project back into the most distal layers of the lamina. Based on examination of unassigned multi-columnar processes within an individual reconstructed column, it is likely that wide-field forms synapses with most cell types in the lamina (Rivera-Alba et al., 2011). The primary lamina inputs to motion circuits, L1 and L2, are sign-inverted with respect to the photoreceptors—they hyperpolarize in response to transient luminance increases. Wide-field neurons depolarize to light ON, and may release acetylcholine. Therefore, excitatory, cholinergic feedback of wide-field onto L1 and L2 would shunt ON-type hyperpolarizing responses. If correct, this circuit would represent a unique form of excitatory feedback.

An apparent contradiction to this feedback model is that wide-field neurons also depolarize to light OFF, particularly following prolonged periods of light adaptation and when octopamine is present. However, excitatory responses to light OFF were always significantly weaker than to light ON, and flickering luminance stimuli evoked spiking responses primarily during the light ON phase of the flicker cycle. Our data indicate that wide-field feedback is strongest following increases in mean luminance. However, direct measurement of the feedback effects on lamina neurons will be needed to explicitly test this model.

### **Behavioral state modulation through feedback**

Rapid, local adaptation is known to exist within and between neighboring cartridges in the fly lamina(Laughlin and Hardie, 1978). However, correlations in natural scenes exist across multiple spatial and temporal scales. The spectral power of static natural images(van der Schaaf and van

Hateren, 1996) and natural time series(van Hateren, 1997) both decrease according to a power law (e.g.,  $1/\text{frequency}^2$ ), such that natural scenes are dominated by low frequencies. Moving natural scenes are also dominated by low spatial and temporal frequencies(Dong and Atick, 1995). A simple model of wide-field neuron feedback (Fig. 4.13) suggests that feedback could act to filter low frequency signals, increasing sensitivity to frequencies that are less common but more behaviorally relevant. Several unique features of wide-field neurons make them well-suited to this purpose.

First, their spatial and temporal receptive fields are larger and slower than the primary lamina neurons L1 and L2. Averaging over a large window in both space and time is a desirable feature of a robust feedback signal, providing resistance to local noise. The contrast sensitivity of wide-field neurons is also comparatively low—under control conditions, neurons respond only weakly (< 1 spike/s) to contrasts under 10%. This weak sensitivity would not, however, prevent wide-field neurons from responding under natural conditions, because contrast distributions in natural scenes are typically high (Frazor and Geisler, 2006; Land and Nilsson, 2002; Laughlin, 1981).

A second noise-reducing feature of this neuron is the spiking nonlinearity. A spike threshold provides a mechanism for differentiation (i.e., signaling luminance changes) without responding to transient input fluctuations.

Finally, the frequency tuning of wide-field neurons depends on the behavioral activity of the animal. When they are walking or flying, animals encounter higher temporal frequencies due to self-motion. Wide-field feedback from the medulla provides a pathway by which behavioral state could modify frequency coding at the earliest stages of visual processing in the lamina.

## Materials and methods

### Fly stocks

For electrophysiology experiments, the split-GAL4 line 11d03AD;19c10DBD was crossed to pJFRC7-20XUAS-IVS-mCD8::GFP or pJFRC12-10XUAS-IVS-myR::GFP (no differences were observed between the two). For neural silencing experiments, the split-GAL4 line was crossed to  $w^+$ ; tubP-GAL80<sup>ts</sup>; UAS-Kir2.1-GFP flies, which were backcrossed ten generations into a wild-type genetic background (Ofstad et al., 2011). Unlike the intact GAL4, GAL80<sup>ts</sup> does not suppress transcriptional activation of UAS transgenes by split-GAL4 (Aljsocha Nern, unpublished data). All flies for behavior and electrophysiology were kept in a 25° incubator on a 14 h:10 h light:dark cycle.

### Electrophysiology

2-3 day old female flies were anesthetized on a Peltier device at 2°C and fixed to a custom-milled stainless steel holder with UV-activated glue. The proboscis was fixed to the head capsule with a tiny drop of glue. After manual dissection of a small region of the dorsal cuticle with fine forceps, the perineural sheath covering the medulla was ruptured by local application of collagenase diluted in extracellular saline (0.5 mg ml<sup>-1</sup>), similar to a previously described technique (Maimon et al., 2010). In brief, a small patch of the sheath was sucked into a micropipette (2-4  $\mu$ m tip) containing collagenase solution for ~30 seconds, while the bath was held at 29°C. When positive pressure was applied to the pipette, the sheath would rupture, exposing the underlying cell bodies. At this point, the bath temperature was lowered to 20 °C for the remainder of the experiment.

The brain was continuously perfused (at a rate of 1 mL/min) with an extracellular saline solution containing (in mM): 103 NaCl, 3 KCl, 5 N-Tris(hydroxymethyl)methyl-2-aminoethane-sulfonic acid, 8 trehalose, 10 glucose, 26 NaHCO<sub>3</sub>, 1 NaH<sub>2</sub>PO<sub>4</sub>, 1.5 CaCl<sub>2</sub>, and 4 MgCl<sub>2</sub>, adjusted to 267–269 mOsm (Wilson and Laurent, 2005). The saline was bubbled with 95% O<sub>2</sub>/5% CO<sub>2</sub> gas for a final pH of 7.3. Pressure-polished (Goodman and Lockery, 2000) patch-clamp electrodes (9–12 MΩ) contained (in mM) 140 potassium-aspartate, 1 KCl, 10 HEPES, 1 EGTA, 0.5 Na<sub>3</sub>GTP, and 4 MgATP, adjusted to pH 7.3, 265 mOsm (Wilson and Laurent, 2005). We sometimes included 10 μM Alexa 568–hydrazide-Na (Invitrogen) in the intracellular solution for visualization purposes. Stock solutions of octopamine hydrochloride (Sigma) and tetrodotoxin (TTX; Sigma) were added to the saline reservoir to achieve final concentrations of 5 μM and 1 μM, respectively.

Recordings were obtained from wide-field somata under visual control using a Nikon Eclipse FN1 microscope with a 60X water-immersion objective and a 2X magnification tube. The sub-stage optics were removed to position the visual arena, and high contrast images of the brain were attained with diffuse illumination via an adjustable infrared LED placed below the fly (Maimon et al., 2010); this same LED was also used to illuminate the fly during flight experiments. The fly was precisely positioned with two cameras (Firefly MV 0.3 MP; Point Grey), one of which was also used to monitor behavior during flight. Online image processing (at 60 Hz) to detect flight was performed with custom Matlab code and recorded simultaneous with electrophysiological data.

To prevent fly movement and reduce neural response variability, the legs and wings were glued in all experiments except those when the fly was flying. The fact that the legs were not glued during recordings from flying flies likely contributed to the increased gain of responses during

non-flight epochs (e.g., Fig. 4.7A). Overall, neurons recorded from unrestrained flies had a higher response gain than those from restrained flies (e.g., the spike latency of unrestrained flies (Fig. 4.7C) was lower than that of restrained flies (Fig. 4.8D)).

Current-clamp recordings were low-pass filtered at 2 kHz and acquired at 10 or 20 kHz with an Axoclamp-2A amplifier, and either a DigiData 1440A data acquisition board (DAQ) and Axoscope software (Molecular Devices) or a National Instruments DAQ (X-series, USB-6343) and custom Matlab code. All traces are corrected for an experimentally measured liquid junction potential of 12 mV. In most cells, we injected a small constant hyperpolarizing current (0–20 pA) to compensate for seal conductance and bring the membrane potential to an initial value of -62 mV (Gouwens and Wilson, 2009; Wilson and Laurent, 2005). Current injection experiments were executed with Matlab control of the National Instruments DAQ. No spikes were detectable in the loose-patch configuration, so we were unable to compare cell-attached and whole-cell firing rates (Gouwens and Wilson, 2009). Capacitance compensation and bridge balance were used. All recordings included in our analysis were made from the right side of the brain.

The display used in electrophysiology experiments was a half-cylinder variant of the green LED arena described previously (Reiser and Dickinson, 2008). In the physiology arena, each of the 96 x 32 LEDs subtended an angle of ~1.875° on the fly eye. The maximum intensity of the arena (16/16) was approximately  $72 \text{ cdm}^{-2}$  and minimum intensity (0/16) was  $0 \text{ cdm}^{-2}$ , with 16 intermediate grayscale values distributed linearly within this range. Arena PCB designs and controller code is available at <http://flypanels.org/>.

All analyses of electrophysiology data, including spike extraction, were performed with custom Matlab scripts. In Fig. 4.8B, spikes were removed by low-pass filtering to produce a smoothed stimulus-triggered average. In Fig. 4.12B, power at the flicker frequency was calculated using multitaper spectral estimation procedures implemented with the Chronux toolbox for Matlab (Bokil et al., 2010). Statistical tests are paired *t* tests, unless otherwise indicated. Because wide-field neurons did not respond to small spots (Figs. 4 and 5), receptive fields were mapped by flashing small square stimuli (30° x 30°) at 33 overlapping locations in the arena (0.5 s flashes at a rate of 1 Hz), and calculating the mean depolarization and spike rate at each point in the arena (Fig. 4.5). The spatial profile of each cell was fitted by a two-dimensional Gaussian, characterized by the long and short axis of the ellipse at 1 s.d. ( $\sigma$ ), and an orientation angle ( $\theta$ ). Receptive fields were very large, often extending beyond the boundaries of the visual arena. For the analysis in Fig. 4.5, we used only those cells in which the receptive field peak was limited to the visual extent of the arena. For the experiments in Figure 4D, in which stimuli of different sizes were used to examine size selectivity, each stimulus was centered on the previously mapped receptive field.

### **Lamina model**

We created a simple reduced model of a lamina circuit consisting of photoreceptors, lamina monopolar cells, and wide-field neuron feedback. The photoreceptor contained simple compound eye optics identical to those used in Chapter 2, and an additional 1<sup>st</sup> order low-pass filter with a cutoff frequency of 200 Hz, designed to match the temporal filtering properties of *Drosophila* photoreceptors (Juusola and Hardie, 2001). LMC's were 1<sup>st</sup> order high-pass filters

with a cutoff frequency of 0.4 Hz (Juusola et al., 1995). Wide-field neurons were modeled with 1<sup>st</sup> order low-pass filters with a cutoff frequency of 0.5 Hz. High- and low-pass Butterworth filters were designed with the MATLAB Signal Processing Toolbox and imported into Simulink. The input to this model was a 500 s time series of natural luminance values, kindly provided by Hans van Hateren; details about this dataset are included in van Hateren (1997). In Fig. 4.13D, we simulated model responses to a rotating square-wave grating using ray tracing methods identical to those described in Chapter 2.

Comparisons were made between models consisting of photoreceptors alone, photoreceptors/LMCs, and photoreceptors/ LMCs /wide-field neuron feedback. Spatial integration of LMCs onto wide-field neurons did not qualitatively change the model results under these reduced conditions. The power spectral density of the model output was calculated via Welch's method with overlapping Hamming windows of 250 ms.

## **Chapter 5**

### **Concluding remarks**

In this thesis, I used a combination of genetic, behavioral, and electrophysiological techniques to study the function of neural circuits in the fly visual system. Chapter 2 described behavioral and physiological responses to a visual illusion called reverse-phi motion. Chapter 3 combined behavioral experiments with genetic manipulation of a single class of neurons in the fly lamina. Chapter 4 described electrophysiological recordings from this same neuron type *in vivo*. Below, I will review the main findings presented in the thesis, discuss the collective significance of these results, and speculate about future directions

## **Chapter 2**

Visual illusions reflect the computational properties of underlying neural circuits and have contributed greatly to our understanding of the brain. An historically important motion illusion is "phi" or "apparent" motion, discovered by the Viennese physiologist Sigmund Exner (e.g., Exner, 1875). Exner found that sequential flashes at neighboring spatial positions cause humans to perceive motion in the direction of the second flash. Thirty years later, Max Wertheimer (Wertheimer, 1912) investigated this same illusion in a paper that laid the foundation for the Gestalt school of psychology (Steinman et al., 2000). An illusion related to the phi phenomenon is so-called "reverse-phi" motion (Anstis, 1970). Like phi motion, the reverse-phi illusion relies on sequential brightness changes to evoke a motion percept. However, in the reverse-phi stimulus, the brightness changes are of opposite sign—when the contrast of a stripe is inverted

as it moves from left to right, human subjects report that leftward motion has occurred (Anstis and Rogers, 1975) .

Similar phenomena have also been investigated in other species. Hassenstein and Reichardt (Hassenstein and Reichardt, 1956) used apparent motion stimuli consisting of two adjacent stripes to study the optomotor response of a beetle. They found that when the polarity of sequential brightness changes were the same, beetles exhibited a positive optomotor response—they turned in the direction of stimulus succession. However, when the polarity of the brightness steps was reversed, beetles turned in the opposite direction. They concluded that the relationship between the visual stimulus and the beetle's behavior involved an algebraic multiplication. This observation led to the formulation of the correlation-type motion detector—the first theoretical model of visual motion detection (Reichardt, 1961).

Since the 1960's, the Hassenstein-Reichardt elementary motion detector (HR-EMD), has received a great deal of attention as a simple, intuitive, and potentially testable model for a basic computation performed by the nervous system (reviewed by Borst et al., 2010). The primary reason for this focus is that the HR-EMD reconciles a wide range of experimental phenomena, such as temporal frequency tuning (Gotz, 1964) and motion adaptation (Borst et al., 2005). For this reason, most results in the field of fly vision are interpreted within the framework of the EMD model.

In Chapter 2, we follow this pattern by showing that the behavior of flies to reverse-phi motion is well-described by the HR-EMD. However, further experiments using combinations of motion and flicker revealed unexpected behavior not predicted by the model. Specifically, when flicker rates were very high, reverse-phi optomotor responses inverted. This behavior was also visible

in the calcium signals of motion-sensitive lobula-plate tangential cells, suggesting that the inversion originates within or upstream of motion detection. We reconcile these differences by suggesting specific modifications to the EMD model: asymmetric summation of motion signals and a discrete temporal delay, instead of smooth filtering. These two slight modifications account for the major discrepancies we observed between fly behavior and the predictions of the EMD model.

What is ignored by our model, however, is the dynamic nature of reverse-phi steering behavior. The inversion of reverse-phi steering we observed had very particular temporal dynamics, with the amplitude of the inversion increasing over time as a function of the flicker rate. Higher flicker rates produced stronger, more rapid steering inversions. This inversion was greatest when the spatial frequency of the stimulus was very low. It also disappeared when the motion stimulus was restricted to a small window of the fly's visual field.

Taken together, these results do not provide a clear picture of the origin or functional significance of the reverse-phi inversion. The dynamic nature of the inversion indicates that temporal adaptation mechanisms must be involved. The spatial properties of this phenomenon suggest that such adaptation might operate over a scale greater than neighboring EMDs. However, our extensive attempts to model the inversion with adaptive feedback onto existing nodes of the HR-EMD, such as the delay time constant, were not successful. Alternative models, such as recent proposed variants of the EMD (Clark et al., 2011; Eichner et al., 2011), were also not sufficient.

Although these experiments do not negate the previous body of evidence in support of the HR-EMD, they do suggest that additional mechanisms contribute to the processing of motion in the

fly visual system. This is not surprising, given the anatomical complexity of the fly optic lobes, but it does contradict the prevailing view that the computational nodes of the EMD, the delay line and multiplier, map on to individual cell types in the fly retina. It is becoming increasingly clear that the EMD is an emergent property of a very complex circuit, with contributions from dozens, if not hundreds, of neuronal cell types. The collective filtering properties of these neuron populations, instead of a single time constant implemented by a single cell, is what gives rise to the behavioral and physiological phenomena described by the EMD. Further insight into the neuronal basis of motion detection in the fly must recognize and contend with the obvious complexity of peripheral visual processing.

### **Chapter 3**

Several behavioral studies have used the GAL4-UAS ectopic expression system in *Drosophila* to silence lamina neurons and look for deficits in visual behaviors. The first of these studies demonstrated that L1 and L2 are necessary and sufficient for stable optomotor responses (Rister et al., 2007): silencing either one or the other cell class impaired, but did not abolish, optomotor behavior. Other groups attempted to differentiate between the contributions of L1 and L2 with behavior (Clark et al., 2011), or recording from downstream neurons (Joesch et al., 2010). However, the contributions of other lamina cell classes to visual behavior are completely unknown. This absence of information is largely due to the lack of clean GAL4 drivers in the *Drosophila* visual system, as well as other technical difficulties described in Chapter 1.

In Chapter 3, I described our efforts to overcome this gap by using the split-GAL4 technique (Luan et al., 2006; Pfeiffer et al., 2010) to target neuronal effectors to single neuron classes in the *Drosophila* visual system. We developed a series of tethered flight experiments to test for

behavioral deficits following silencing or activation of specific cell types in the fly lamina. The goal of these experiments was two-fold: (1) to have a standardized set of behavioral metrics to compare the behavioral function of neurons in the fly lamina, and (2) to understand the behavioral function of a novel class of wide-field feedback neurons in the lamina.

The first goal was achieved by designing visual stimuli to explore as many aspects of fly visual behavior as possible. For example, we adapted a psychophysics technique often used to quantify visual perception in human infants (e.g., Pereverzeva et al., 2002), called motion nulling. The nulling paradigm allowed us to quantify “contrast sensitivity” as a function of stimulus velocity. Future studies of *Drosophila* vision could also draw from the extensive literature of human psychophysics, which provided the impetus for many of the visual stimuli used in this thesis.

In addition to developing new measures of visual perception, we used many stimuli intended to test extant theories of peripheral visual processing, or replicate previous results from wild-type flies. For example, we designed two patterns that contained only luminance increases and decreases, to test the recent proposal that L1 and L2 comprise segregated ON and OFF channels (Joesch et al., 2010). These stimuli will be used in the future to examine the effects of silencing or activating each of the 12 cell types in the fly lamina.

The wide-field neuron was an interesting test case to look for specific effects of manipulating a single cell type. This class of neurons had never been described, despite a century of Golgi studies in the fly optic lobes. Their unique anatomical profile distinguishes them from other columnar neurons of the fly lamina, suggesting that they could provide feedback on a larger

spatial scale than previously described local mechanisms of lateral inhibition (Laughlin and Hardie, 1978).

We examined the role of wide-field neurons by expressing an inwardly-rectifying K<sup>+</sup> channel, kir2.1, which effectively silenced wide-field neurons (as shown by targeted electrophysiology in Chapter 4). Silencing wide-field neurons had several effects on fly visual behavior. Although basic optomotor responses were largely intact, flies responded more weakly to challenging visual stimuli, such as low contrast optomotor patterns and oscillating stripes. An important and surprising phenotype we observed was increased responsiveness to very slow optomotor stimuli. This was further clarified by the motion nulling paradigm, in which flies with silenced wide-field neurons more readily followed very slow optomotor stimuli. Together, these data suggest that wide-field neurons act to suppress low-frequency luminance signals, and that this enhances the fly's ability to discern small-field and low contrast stimuli.

In contrast to the neuronal silencing experiments, activation of wide-field neurons by expression of the temperature-gated cation channel trpA1 had negligible effects on visual behavior. Given the conceptual role of wide-field neurons described above, one would expect that activation of these feedback neurons would tonically suppress signaling in lamina output neurons. However, because trpA1 is not tagged with GFP, we were unable to record from neurons to confirm the efficacy of the manipulation. It is possible that trpA1 expression either had no effect on wide-field neuron output, or that persistent firing of wide-field neurons does not disrupt visual processing. Another caveat of the activation experiments is that we were unable to test the same range of visual behaviors as in the silencing experiments, because flies are indisposed to fly at the higher temperatures required to open trpA1 channels. More

detailed behavioral experiments, testing a greater range of stimuli, might reveal more subtle effects of wide-field neuron activation.

Several features of these experiments provide encouragement that future behavioral genetics studies of lamina function should be feasible. First, we were able to get reliable and robust behavior from flies in the flight arena, enough to quantify several dozen visual behaviors. This was made possible by the use of UAS transgenes crossed into a wild-type background. Second, the effect of manipulating wide-field neurons was consistent across time and reagents. Fly behavior experiments are known for their fickleness: a single ingredient in the food or a shift in humidity can alter the result of a behavioral result (e.g., Xia et al., 1997). Our experiments were repeated many times over a period of several months, and no large variations were observed. We also used multiple split-GAL4 lines to confirm that our phenotypes were not the result of the specific enhancer fragments used to drive GAL4 expression. As controls, we used single Split-GAL4 transgenes to control for the toxicity of GAL4 expression. Overall, the specificity and repeatability of these experiments suggest that future studies using similar methods should produce behavioral phenotypes that are detectable above experimental noise.

## **Chapter 4**

The *Drosophila* visual system is a promising model for investigating early sensory processing. Advanced genetic tools for transgene expression and cell-type specific manipulations have led to a detailed understanding of many developmental processes in the fly visual system (Clandinin and Feldheim, 2009). Many of these tools can now be applied to understanding the contribution of genetically-defined neuron types to behavior (Olsen and Wilson, 2008; Simpson, 2009). A diverse suite of fly visual behaviors have been intensively studied for over 80

years(Hecht and Wald, 1933), and methods have been developed for quantifying visual behaviors in both fixed (Gotz, 1964; Reiser and Dickinson, 2008) and freely moving animals (Schilstra and Hateren, 1999; Straw et al., 2011). Finally, the anatomy of the visual system is known in exquisite detail (Cajal and Sanchez, 1915; Fischbach and Dittrich, 1989), to the point of complete synaptic connectivity maps in some regions(Meinertzhagen and O'Neil, 1991; Takemura et al., 2008).

Despite all of these advantages, however, a significant obstacle to understanding visual coding in *Drosophila* has been the inability to record electrophysiologically from the tiny neurons of the peripheral visual system. Each lamina cartridge contains 12 cell types, including the 5 lamina monopolar cells (LMCs). Only two lamina cell types of these cell types, L1 and L2, have been characterized with physiological recordings in larger flies (Laughlin and Hardie, 1978; Laughlin et al., 1987; Laughlin and Osorio, 1989) and more recently in *Drosophila* (Clark et al., 2011; Reiff et al., 2010; Zheng et al., 2006). The electrophysiological properties of the other columnar and multi-columnar neurons in the fly visual system are not well understood, primarily due to the technical difficulty of obtaining stable recordings.

For the past 50 years, the primary method of intracellular recording *in vivo* has been the sharp electrode. Sharp recordings are subject to strong selection bias and mechanical instability. However, new methods for visually targeted whole-cell patch clamp recordings offer the possibility of targeting genetically-labeled neurons for stable, high quality recording (Wilson et al., 2004). In Chapter 4, we described the first recordings from the fly lamina using the whole-cell patch-clamp technique.

Recordings from lamina wide-field neurons revealed that they have large spatial receptive fields and are tuned to detect low frequency luminance fluctuations. The excitability of lawf2 neurons depended on the behavioral state of the fly: flight increased lawf2 sensitivity to higher frequency luminance fluctuations. Application of the neuromodulator octopamine mimicked the effects of flight on lawf2 activity. Most surprisingly, octopamine shifted the distribution of frequencies encoded by wide-field neurons, indicating that behavioral state influences sensory coding at the earliest stages of visual processing in the lamina. A simple computational model demonstrated that wide-field neurons could enhance sensitivity to higher frequency components of natural luminance patterns through low frequency feedback onto lamina monopolar cells.

The electrophysiological properties of wide-field neurons are largely consistent with the behavioral phenotypes associated with inactivation experiments. Specifically, the selectivity of wide-field neurons for low frequency luminance fluctuations explains the tendency of flies to follow low velocity optomotor stimuli when wide-field neurons are silenced. A working model for this circuit's function is that acetylcholine release from wide-field neurons subtracts low frequency luminance signals from the primary motion pathway, consisting of L1 and L2. Because L1 and L2 hyperpolarize in response to light increases, excitatory (i.e., cholinergic) feedback from wide-field neurons would effectively constitute a form of reverse feedback-inhibition.

There were several other behavioral phenotypes that were not directly related to the electrophysiological characterization, for example the impaired stripe tracking and weak responses to low contrast optomotor patterns. These secondary phenotypes may be indirect

effects of eliminating wide field neuron feedback. In other words, low frequency, subtractive feedback could enhance the sensitivity of lamina neurons to detect moving stripes or low contrast motion patterns. Further experiments are required to directly assess the effect of wide-field neuron silencing on motion processing. Ideally, one would like to record directly from the primary motion pathways (L1 and L2) during wide-field neuron inactivation. These experiments are not immediately viable, due to the large number of transgenes required to silence one class of cells while recording from another, but should be possible within the near future.

One advantage of studying neural circuits in a genetic model organism is the capacity to repeatedly target the same class of neurons. For example, the fact that past lamina recordings did not encounter wide-field neurons is probably due to the inherent sampling bias of the sharp electrode technique. Although visually-targeted whole-cell recordings from small neurons in the *Drosophila* brain can be challenging, the advantage of this approach is being able to reliably record from the same neuron type across multiple animals. Similarly, the fact that this neuron was not identified by any of the myriad Golgi studies performed in the fly visual system demonstrates the advantage of using genetic techniques to study nervous system anatomy, and suggests that there are still cell types awaiting discovery, even in heavily studied brain regions. The ability to return to the same neuron type in multiple animals, and to perturb that neuron type selectively, will allow us to interrogate the function of many classes of neurons as we have done here for the lamina wide-field neuron. A more challenging task will be to understand how assemblies of neuronal cell types act in concert to produce the complex behaviors we observe in the natural world.

## References

- Adelson, E. H. and Bergen, J. R.** (1985). Spatiotemporal energy models for the perception of motion. *J Opt Soc Am A* **2**, 284-99.
- An, X., Armstrong, J. D., Kaiser, K. and O'Dell, K. M.** (2000). The effects of ectopic white and transformer expression on *Drosophila* courtship behavior. *J Neurogenet* **14**, 227-43,271.
- Anstis, S. M.** (1970). Phi movement as a subtraction process. *Vision Res* **10**, 1411-30.
- Anstis, S. M. and Rogers, B. J.** (1975). Illusory reversal of visual depth and movement during changes of contrast. *Vision Res* **15**, 957-61.
- Arendt, D.** (2003). Evolution of eyes and photoreceptor cell types. *Int J Dev Biol* **47**, 563-71.
- Arnett, D. W.** (1971). Receptive field organization of units in the first optic ganglion of diptera. *Science* **173**, 929-31.
- Arnett, D. W.** (1972). Spatial and temporal integration properties of units in first optic ganglion of dipterans. *J Neurophysiol* **35**, 429-44.
- Autrum, H., Zettler, F. and Jarvilehto, M.** (1970). Postsynaptic potentials from a single monopolar neuron of ganglion opticum I of blowfly *Calliphora*. *J Comp Physiol A* **70**, 414-8.
- Baier, A., Wittek, B. and Brembs, B.** (2002). *Drosophila* as a new model organism for the neurobiology of aggression? *J Exp Biol* **205**, 1233-40.
- Baines, R. A., Uhler, J. P., Thompson, A., Sweeney, S. T. and Bate, M.** (2001). Altered electrical properties in *Drosophila* neurons developing without synaptic transmission. *J Neurosci* **21**, 1523-31.
- Barlow, H. B.** (1961a). The coding of sensory messages. In *Current problems in animal behavior*, eds. W. H. Thorpe and G. J. Mitchison). Cambridge: Cambridge University Press.
- Barlow, H. B.** (1961b). Possible principles underlying the transformation of sensory messages. In *Sensory Communication*, pp. 217-234. Cambridge, MA: MIT Press.
- Barlow, H. B. and Levick, W. R.** (1965). The mechanism of directionally selective units in rabbit's retina. *J Physiol* **178**, 477-504.
- Benzer, S.** (1967). Behavioral mutants of *Drosophila* isolated by countercurrent distribution. *Proc Natl Acad Sci U S A* **58**, 1112-1119.
- Bokil, H., Andrews, P., Kulkarni, J. E., Mehta, S. and Mitra, P. P.** (2010). Chronux: a platform for analyzing neural signals. *J Neurosci Methods* **192**, 146-51.

**Borst, A. and Bahde, S.** (1988). Visual information processin gin the fly's landing system. *J Comp Physiol A* **163**, 167-173.

**Borst, A. and Egelhaaf, M.** (1989). Principles of visual motion detection. *Trends Neurosci* **12**, 297-306.

**Borst, A., Flanagin, V. L. and Sompolinsky, H.** (2005). Adaptation without parameter change: Dynamic gain control in motion detection. *Proc Natl Acad Sci U S A* **102**, 6172-6.

**Borst, A., Haag, J. and Reiff, D. F.** (2010). Fly Motion Vision. *Annu Rev Neurosci*.

**Borst, A., Reisenman, C. and Haag, J.** (2003). Adaptation of response transients in fly motion vision. II: Model studies. *Vision Res* **43**, 1309-22.

**Bours, R. J., Kroes, M. C. and Lankheet, M. J.** (2009). Sensitivity for reverse-phi motion. *Vision Res* **49**, 1-9.

**Braitenberg, V.** (1967). Patterns of projection in the visual system of the fly. I. Retina-lamina projections. *Exp Brain Res* **3**, 271-98.

**Brand, A. H. and Perrimon, N.** (1993). Targeted gene expression as a means of altering cell fates and generating dominant phenotypes. *Development* **118**, 401-15.

**Buchner, E.** (1976). Elementary Movement Detectors in an Insect Visual System. *Biol Cybern* **24**, 85-101.

**Buchner, E.** (1984). Behavioural Analysis of Spatial Vision in Insects. In *Photoreception and Vision in Invertebrates*, (ed. M. Ali), pp. 561-619. New York: Plenum.

**Buchner, E., Gotz, K. G. and Straub, C.** (1978). Elementary detectors for vertical movement in visual system of *Drosophila*. *Biol Cybern* **31**, 235-242.

**Busch, S., Selcho, M., Ito, K. and Tanimoto, H.** (2009). A map of octopaminergic neurons in the Drosophila brain. *J Comp Neurol* **513**, 643-67.

**Cajal, S. R.** (1910). Nota sobre la retina de los muscidos. *Madrid Boletin de la Sociedad Espanola* **1910**.

**Cajal, S. R. and Sanchez, D.** (1915). Contribucion al conocimiento de los centros nerviosos del los insectos. *Trab Lab Invest Biol* **13**, 1-167.

**Carandini, M., Demb, J. B., Mante, V., Tolhurst, D. J., Dan, Y., Olshausen, B. A., Gallant, J. L. and Rust, N. C.** (2005). Do we know what the early visual system does? *J Neurosci* **25**, 10577-97.

**Card, G. and Dickinson, M.** (2008a). Performance trade-offs in the flight initiation of Drosophila. *J Exp Biol* **211**, 341-53.

**Card, G. and Dickinson, M. H.** (2008b). Visually mediated motor planning in the escape response of Drosophila. *Curr Biol* **18**, 1300-7.

**Carpenter, F. W.** (1905). The reactions of the pomace fly (Drosophila ampelophila Loew) to light gravity, and mechanical stimulation. *American Naturalist* **39**, 157-171.

**Cavanagh, P. and Anstis, S.** (1991). The contribution of color to motion in normal and color-deficient observers. *Vision Res* **31**, 2109-48.

**Chi, C. and Carlson, S. D.** (1980). Membrane specializations in the first optic neuropil of the housefly, *Musca domestica* L. I. Junctions between neurons. *J Neurocytol* **9**, 429-49.

**Chiappe, M. E., Seelig, J. D., Reiser, M. B. and Jayaraman, V.** (2010). Walking Modulates Speed Sensitivity in Drosophila Motion Vision. *Curr Biol* **20**, 1470-5.

**Chklovskii, D. B., Vitaladevuni, S. and Scheffer, L. K.** (2010). Semi-automated reconstruction of neural circuits using electron microscopy. *Curr Opin Neurobiol* **20**, 667-75.

**Clandinin, T. R. and Feldheim, D. A.** (2009). Making a visual map: mechanisms and molecules. *Curr Opin Neurobiol* **19**, 174-80.

**Clark, D. A., Bursztyn, L., Horowitz, M. A., Schnitzer, M. J. and Clandinin, T. R.** (2011). Defining the computational structure of the motion detector in Drosophila. *Neuron* **70**, 1165-77.

**Clifford, C. W. and Ibbotson, M. R.** (2002). Fundamental mechanisms of visual motion detection: models, cells and functions. *Prog Neurobiol* **68**, 409-37.

**Cook, T. and Desplan, C.** (2001). Photoreceptor subtype specification: from flies to humans. *Semin Cell Dev Biol* **12**, 509-18.

**Coombe, P. E. and Heisenberg, M.** (1986). The structural brain mutant Vacuolar medulla of *Drosophila melanogaster* with specific behavioral defects and cell degeneration in the adult. *J Neurogenet* **3**, 135-58.

**David, C. T.** (1978). The relationship between body angle and flight speed in free-flying Drosophila. *Physiol Entomol* **3**, 191-195.

**Dodge, F. A., Jr., Knight, B. W. and Toyoda, J.** (1968). Voltage noise in Limulus visual cells. *Science* **160**, 88-90.

**Dong, D. W. and Atick, J. J.** (1995). Statistics of natural time-varying images. *Network-Computation in Neural Systems* **6**, 345-358.

**Douglass, J. K. and Strausfeld, N. J.** (1995). Visual motion detection circuits in flies: peripheral motion computation by identified small-field retinotopic neurons. *J Neurosci* **15**, 5596-611.

**Dubs, A.** (1982). The spatial integration of signals in the retina and lamina of the fly compound eye under different conditions of luminance. *J Comp Physiol A* **146**, 321-343.

**Dubs, A., Laughlin, S. B. and Srinivasan, M. V.** (1981). Single photon signals in fly photoreceptors and first order interneurones at behavioral threshold. *J Physiol* **317**, 317-34.

**Duistermars, B. J., Chow, D. M., Condro, M. and Frye, M. A.** (2007a). The spatial, temporal and contrast properties of expansion and rotation flight optomotor responses in *Drosophila*. *J Exp Biol* **210**, 3218-3227.

**Duistermars, B. J., Reiser, M. B., Zhu, Y. and Frye, M. A.** (2007b). Dynamic properties of large-field and small-field optomotor flight responses in *Drosophila*. *J Comp Physiol A* **193**, 787-99.

**Edwards, T. N. and Meinertzhagen, I. A.** (2010). The functional organisation of glia in the adult brain of *Drosophila* and other insects. *Prog Neurobiol* **90**, 471-97.

**Egelhaaf, M. and Borst, A.** (1992). Are there separate ON and OFF channels in fly motion vision? *Vis Neurosci* **8**, 151-64.

**Egelhaaf, M., Borst, A. and Reichardt, W.** (1989). Computational structure of a biological motion-detection system as revealed by local detector analysis in the fly's nervous system. *J Opt Soc Am A* **6**, 1070-87.

**Eichner, H., Joesch, M., Schnell, B., Reiff, D. F. and Borst, A.** (2011). Internal structure of the fly elementary motion detector. *Neuron* **70**, 1155-64.

**Emerson, R. C., Citron, M. C., Vaughn, W. J. and Klein, S. A.** (1987). Nonlinear directionally selective subunits in complex cells of cat striate cortex. *J Neurophysiol* **58**, 33-65.

**Exner, S.** (1875). Experimentelle untersuchung der einfachsten psychischen proesse. *Pflugers Arch* **8**, 526-537.

**Exner, S.** (1891). The physiology of the compound eyes of insects and crustaceans. Berlin ; New York: Springer-Verlag.

**Fain, G. L., Hardie, R. and Laughlin, S. B.** (2010). Phototransduction and the evolution of photoreceptors. *Curr Biol* **20**, R114-24.

**Farooqui, T.** (2007). Octopamine-mediated neuromodulation of insect senses. *Neurochem Res* **32**, 1511-29.

**Fermi, G. and Reichardt, W.** (1963). Optomotor reactions of the fly, *Musca domestica*. Dependence of the reaction on wave length, velocity, contrast and median brightness of periodically moved stimulus patterns. *Kybernetik* **2**, 15-28.

**Fischbach, K. F. and Dittrich, A. P.** (1989). The optic lobe of *Drosophila melanogaster*. I. A Golgi analysis of wild-type structure. *Cell Tissue Res* **258**, 441-475.

**Franceschini, N.** (1972). Pupil and pseduopupil in the compound eye of *Drosophila*. In *Information Processing in the Visual Systems of Arthropods*, (ed. R. Wehner), pp. 72-85. Berlin Heidelberg New York: Springer-Verlag.

**Franceschini, N., Riehle, A. and Le Nestour, A.** (1989). Directionally Selective Motion Detection by Insect Neurons. In *Facets of Vision*, eds. D. G. Stavenga and R. C. Hardie), pp. 361-390. Berlin: Springer-Verlag.

**Frazor, R. A. and Geisler, W. S.** (2006). Local luminance and contrast in natural images. *Vision Res* **46**, 1585-98.

**Fuortes, M. G. and Yeandle, S.** (1964). Probability of Occurrence of Discrete Potential Waves in the Eye of Limulus. *J Gen Physiol* **47**, 443-63.

**Gaffron, M.** (1934). Untersuchungen über das Bewegungssehen bei Libellenlarven, Fliegen und Fischen. *Zeitschrift Fur Vergleichende Physiologie* **20**, 299-337.

**Gao, S., Takemura, S. Y., Ting, C. Y., Huang, S., Lu, Z., Luan, H., Rister, J., Thum, A. S., Yang, M., Hong, S. T. et al.** (2008). The neural substrate of spectral preference in *Drosophila*. *Neuron* **60**, 328-42.

**Gavel, L. V.** (1939). Die "kritische Streifenbreite" als Mass der Sehscharfe bei *Drosophila melanogaster*. *Zeitschrift Fur Vergleichende Physiologie* **27**, 80-135.

**Geiger, G. and Nassel, D. R.** (1981). Visual orientation behavior of flies after selective laser-beam ablation of interneurons. *Nature* **293**, 398-399.

**Gengs, C., Leung, H. T., Skingsley, D. R., Iovchev, M. I., Yin, Z., Semenov, E. P., Burg, M. G., Hardie, R. C. and Pak, W. L.** (2002). The target of *Drosophila* photoreceptor synaptic transmission is a histamine-gated chloride channel encoded by *ort* (*hclA*). *J Biol Chem* **277**, 42113-20.

**Goodman, M. B. and Lockery, S. R.** (2000). Pressure polishing: a method for re-shaping patch pipettes during fire polishing. *J Neurosci Methods* **100**, 13-5.

**Gorska-Andrzejak, J., Keller, A., Raabe, T., Kilianek, L. and Pyza, E.** (2005). Structural daily rhythms in GFP-labelled neurons in the visual system of *Drosophila melanogaster*. *Photochem Photobiol Sci* **4**, 721-6.

**Gotz, K. and Wenking, H.** (1973). Visual control of locomotion in the walking fruit fly *Drosophila Melanogaster*. *J Comp Physiol A* **85**, 235-266.

**Gotz, K. G.** (1964). Optomotor studies of the visual system of several eye mutants of the fruit fly *Drosophila*. *Kybernetik* **2**, 77-92.

**Gotz, K. G.** (1987). Course-Control, Metabolism and Wing Interference During Ultralong Tethered Flight in *Drosophila Melanogaster*. *J Exp Biol* **128**, 35-46.

**Gouwens, N. W. and Wilson, R. I.** (2009). Signal propagation in *Drosophila* central neurons. *J Neurosci* **29**, 6239-49.

**Gross, A. O.** (1913). The reactions of arthropods to monochromatic lights of equal intensities. *Journal of Experimental Zoology* **14**, 467-514.

**Guy, R. G. and Srinivasan, M. V.** (1988). Integrative properties of 2nd-order visual neurons - a study of large monopolar cells in the dronefly *Eristalis*. *J Comp Physiol A* **162**, 317-331.

**Hamada, F. N., Rosenzweig, M., Kang, K., Pulver, S. R., Ghezzi, A., Jegla, T. J. and Garrity, P. A.** (2008). An internal thermal sensor controlling temperature preference in *Drosophila*. *Nature* **454**, 217-20.

**Hardie, R. and Postma, M.** (2008). Phototransduction in microvillar photoreceptors of *Drosophila* and other invertebrates. In *Senses: A Comprehensive Reference*, vol. 1, pp. 77-130. Amsterdam; Boston: Elsevier.

**Hardie, R. C.** (1987). Is histamine a neurotransmitter in insect photoreceptors? *J Comp Physiol A* **161**, 201-13.

**Hardie, R. C.** (1989). A histamine-activated chloride channel involved in neurotransmission at a photoreceptor synapse. *Nature* **339**, 704-6.

**Hardie, R. C. and Raghu, P.** (2001). Visual transduction in *Drosophila*. *Nature* **413**, 186-93.

**Hardie, R. C., Voss, D., Pongs, O. and Laughlin, S. B.** (1991). Novel potassium channels encoded by the Shaker locus in *Drosophila* photoreceptors. *Neuron* **6**, 477-86.

**Hardie, R. C. and Weckstrom, M.** (1990). Three classes of potassium channels in large monopolar cells of the blowfly *Calliphora vicina*. *J Comp Physiol A* **167**, 723-736.

**Harris, R. A. and O'Carroll, D. C.** (2002). Afterimages in fly motion vision. *Vision Res* **42**, 1701-1714.

**Hassenstein, V. B. and Reichardt, W.** (1956). Systemtheoretische Analyse der Zeit-, Reihenfolgen und Vorzeichenauswertung bei der Bewegungsperzeption des Russelkafers Chlorophanus. *Z Naturforsch* **11 b**, 513-524.

**Hausen, K. and Wehrhahn, C.** (1983). Microsurgical Lesion of Horizontal Cells Changes Optomotor Yaw Responses in the Blowfly *Calliphora erythrocephala*. *Proc R Soc Lond B Biol Sci* **219**, 211-216.

**Hecht, S., Shlaer, S. and Pirenne, M. H.** (1942). Energy, quanta, and vision. *J Gen Physiol* **25**, 819-40.

**Hecht, S. and Wald, G.** (1933). The Influence of Intensity on the Visual Functions of *Drosophila*. *Proc Natl Acad Sci U S A* **19**, 964-72.

**Hecht, S. and Wald, G.** (1934). The Visual Acuity and Intensity Discrimination of *Drosophila*. *J Gen Physiol* **17**, 517-547.

**Heisenberg, M.** (2003). Mushroom body memoir: From maps to models. *Nature Reviews Neuroscience* **4**, 266-275.

**Heisenberg, M. and Buchner, E.** (1977). The role of retinula cell types in visual behavior of *Drosophila melanogaster*. *J Comp Physiol A* **117**, 127-162.

**Heisenberg, M. and Wolf, R.** (1979). On the fine structure of yaw torque in visual flight orientation of *Drosophila melanogaster*. *J Comp Physiol A* **130**, 113-130.

**Heisenberg, M. and Wolf, R.** (1984). Vision in *Drosophila*: Genetics of Microbehavior. Berlin: Springer-Verlag.

**Heisenberg, M., Wonneberger, R. and Wolf, R.** (1978). Optomotor-blind - *Drosophila* mutant of lobula plate giant neurons. *J Comp Physiol A* **124**, 287-296.

**Higgins, C. M., Douglass, J. K. and Strausfeld, N. J.** (2004). The computational basis of an identified neuronal circuit for elementary motion detection in dipterous insects. *Vis Neurosci* **21**, 567-86.

**Horn, E. and Wehner, R.** (1975). The Mechanism of Visual Pattern Fixation in the Walking Fly, *Drosophila melanogaster*. *J Comp Physiol A* **101**, 39-56.

**Hu, K. G. and Stark, W. S.** (1977). Specific receptor input into spectral preference in *Drosophila*. *J Comp Physiol A* **121**, 241-252.

**Ibbotson, M. R. and Clifford, C. W.** (2001). Interactions between ON and OFF signals in directional motion detectors feeding the NOT of the wallaby. *J Neurophysiol* **86**, 997-1005.

**Jansonius, N. M.** (1990). Properties of the sodium-pump in the blowfly photoreceptor cell. *J Comp Physiol A* **167**, 461-467.

**Jansonius, N. M. and van Hateren, J. H.** (1991). Fast temporal adaptation of on-off units in the first optic chiasm of the blowfly. *J Comp Physiol A* **168**, 631-7.

**Jansonius, N. M. and van Hateren, J. H.** (1993a). On-Off Units in the 1st optic chiasm of the Blowfly .2. Spatial properties. *J Comp Physiol A* **172**, 467-471.

**Jansonius, N. M. and van Hateren, J. H.** (1993b). On spiking units in the 1st optic chiasm of the blowfly. 3. The sustaining unit. *J Comp Physiol A* **173**, 187-192.

**Jarvilehto, M. and Zettler, F.** (1973). Electrophysiological-histological studies on some functional properties of visual cells and second-order neurons of an insect retina. *Zeitschrift Fur Zellforschung Und Mikroskopische Anatomie* **136**, 291-306.

**Jekely, G.** (2009). Evolution of phototaxis. *Philos Trans R Soc Lond B Biol Sci* **364**, 2795-808.

**Joesch, M., Schnell, B., Raghu, S. V., Reiff, D. F. and Borst, A.** (2010). ON and OFF pathways in Drosophila motion vision. *Nature* **468**, 300-4.

**Johnston, A. and Clifford, C. W.** (1995). A unified account of three apparent motion illusions. *Vision Res* **35**, 1109-23.

**Jung, S. N., Borst, A. and Haag, J.** (2011). Flight activity alters velocity tuning of fly motion-sensitive neurons. *J Neurosci* **31**, 9231-7.

**Juusola, M. and Hardie, R. C.** (2001). Light adaptation in Drosophila photoreceptors: I. Response dynamics and signaling efficiency at 25 degrees C. *J Gen Physiol* **117**, 3-25.

**Juusola, M., Uusitalo, R. O. and Weckstrom, M.** (1995). Transfer of graded potentials at the photoreceptor-interneuron synapse. *J Gen Physiol* **105**, 117-48.

**Kalmus, H.** (1943). The optomotor responses of some eye mutants of Drosophila. *Journal of Genetics* **42**, 206-213.

**Kalmus, H.** (1949). Optomotor responses in Drosophila and Musca. *Physiol Comp Ocol Int J Comp Physiol Ecol* **1**, 127-47.

**Katsov, A. Y. and Clandinin, T. R.** (2008). Motion Processing Streams in Drosophila Are Behaviorally Specialized. *Neuron* **59**, 322-335.

**Kazama, H. and Wilson, R. I.** (2008). Homeostatic matching and nonlinear amplification at identified central synapses. *Neuron* **58**, 401-13.

**Kenyon, F. C.** (1897). The optic lobes of the bee's brain in the light of recent neurological methods. *American Naturalist*, 369-376.

**Kirschfeld, K.** (1967). Die projekion der optischen umwelt auf das raster der rhabdomere im komplexauge von *musca*. *Exp Brain Res* **3**, 248-&.

**Kirschfeld, K. and Franceschini, N.** (1969). A mechanism for directing flow of light in rhabdomeres of complex eyes in *Musca*. *Kybernetik* **6**, 13-&.

**Kolodziejczyk, A., Sun, X., Meinertzhagen, I. A. and Nassel, D. R.** (2008). Glutamate, GABA and acetylcholine signaling components in the lamina of the *Drosophila* visual system. *PLoS One* **3**, e2110.

**Krapp, H. G. and Hengstenberg, R.** (1996). Estimation of self-motion by optic flow processing in single visual interneurons. *Nature* **384**, 463-6.

**Krekelberg, B. and Albright, T. D.** (2005). Motion mechanisms in macaque MT. *J Neurophysiol* **93**, 2908-21.

**Kuffler, S. W.** (1953). Discharge patterns and functional organization of mammalian retina. *J Neurophysiol* **16**, 37-68.

**Land, M. F. and Nilsson, D.-E.** (2002). Animal eyes. New York: Oxford University Press.

**Laughlin, S.** (1981). A simple coding procedure enhances a neuron's information capacity. *Z Naturforsch* **36**, 910-2.

**Laughlin, S.** (1984). The Roles of Parallel Channels in Early Visual Processing by the Arthropod Compound Eye. In *Photoreception and Vision in Invertebrates*

**Laughlin, S. B.** (1987). Form and function in retinal processing. *Trends Neurosci* **10**, 478-483.

**Laughlin, S. B.** (1989). The role of sensory adaptation in the retina. *J Exp Biol* **146**, 39-62.

**Laughlin, S. B. and Hardie, R. C.** (1978). Common Strategies for Light Adaptation in the Peripheral Visual Systems of Fly and Dragonfly. *J Comp Physiol A* **128**, 319-340.

**Laughlin, S. B., Howard, J. and Blakeslee, B.** (1987). Synaptic limitations to contrast coding in the retina of the blowfly *Calliphora*. *Proc R Soc Lond B Biol Sci* **231**, 437-67.

**Laughlin, S. B. and Osorio, D.** (1989). Mechanisms for neural signal enhancement in the blowfly compound eye. *J Exp Biol* **144**, 113-146.

**Lettvin, J. Y.** (1968). What the frog's eye tells the frog's brain. *Proc Inst Radio Engr* **47**, 1940-1951.

**Lin, B. and Masland, R. H.** (2006). Populations of wide-field amacrine cells in the mouse retina. *J Comp Neurol* **499**, 797-809.

**Livingstone, M. S., Pack, C. C. and Born, R. T.** (2001). Two-dimensional substructure of MT receptive fields. *Neuron* **30**, 781-93.

**Longden, K. D. and Krapp, H. G.** (2009). State-dependent performance of optic-flow processing interneurons. *J Neurophysiol*.

**Luan, H., Peabody, N. C., Vinson, C. R. and White, B. H.** (2006). Refined spatial manipulation of neuronal function by combinatorial restriction of transgene expression. *Neuron* **52**, 425-36.

**Luo, L., Callaway, E. M. and Svoboda, K.** (2008). Genetic dissection of neural circuits. *Neuron* **57**, 634-60.

**Maimon, G., Straw, A. D. and Dickinson, M. H.** (2008). A simple vision-based algorithm for decision making in flying Drosophila. *Curr Biol* **18**, 464-70.

**Maimon, G., Straw, A. D. and Dickinson, M. H.** (2010). Active flight increases the gain of visual motion processing in Drosophila. *Nat Neurosci* **13**, 393-9.

**Markow, T. A.** (1987). Behavioral and sensory basis of courtship success in *Drosophila melanogaster*. *Proc Natl Acad Sci U S A* **84**, 6200-4.

**Marmarelis, P. Z. and McCann, G. D.** (1973). Development and application of white-noise modeling techniques for studies of insect visual nervous system. *Kybernetik* **12**, 74-89.

**McCann, G. D. and Arnett, D. W.** (1972). Spectral and polarization sensitivity of the dipteran visual system. *J Gen Physiol* **59**, 534-58.

**McEwen, R. S.** (1918). The reactions to light and to gravity in *Drosophila* and its mutants. *Journal of Experimental Zoology* **25**, 49-106.

**Meinertzhagen, I. A. and O'Neil, S. D.** (1991). Synaptic organization of columnar elements in the lamina of the wild type in *Drosophila melanogaster*. *J Comp Neurol* **305**, 232-63.

**Meinertzhagen, I. A. and Pyza, E.** (1999). Neurotransmitter regulation of circadian structural changes in the fly's visual system. *Microsc Res Tech* **45**, 96-105.

**Meinertzhagen, I. A. and Sorra, K. E.** (2001). Synaptic organization in the fly's optic lamina: few cells, many synapses and divergent microcircuits. *Prog Brain Res* **131**, 53-69.

**Mo, C. H. and Koch, C.** (2003). Modeling reverse-phi motion-selective neurons in cortex: double synaptic-veto mechanism. *Neural Comput* **15**, 735-59.

**Niven, J. E., Vahasoyrinki, M., Kauranen, M., Hardie, R. C., Juusola, M. and Weckstrom, M.** (2003). The contribution of Shaker K<sup>+</sup> channels to the information capacity of Drosophila photoreceptors. *Nature* **421**, 630-4.

**Ofstad, T. A., Zuker, C. S. and Reiser, M. B.** (2011). Visual place learning in Drosophila melanogaster. *Nature* **474**, 204-7.

**Olsen, S. R. and Wilson, R. I.** (2008). Cracking neural circuits in a tiny brain: new approaches for understanding the neural circuitry of Drosophila. *Trends Neurosci* **31**, 512-20.

**Orger, M. B., Smear, M. C., Anstis, S. M. and Baier, H.** (2000). Perception of Fourier and non-Fourier motion by larval zebrafish. *Nat Neurosci* **3**, 1128-33.

**Osorio, D. and Bacon, J. P.** (1994). A good eye for arthropod evolution. *Bioessays* **16**, 419-24.

**Pak, W. L., Grossfield, J. and White, N. V.** (1969). Nonphototactic mutants in a study of vision of Drosophila. *Nature* **222**, 351-4.

**Pantazis, A., Segaran, A., Liu, C. H., Nikolaev, A., Rister, J., Thum, A. S., Roeder, T., Semenov, E., Juusola, M. and Hardie, R. C.** (2008). Distinct roles for two histamine receptors (hclA and hclB) at the Drosophila photoreceptor synapse. *J Neurosci* **28**, 7250-9.

**Parsons, M. M., Krapp, H. G. and Laughlin, S. B.** (2010). Sensor Fusion in Identified Visual Interneurons. *Curr Biol*.

**Pereverzeva, M., Hui-Lin Chien, S., Palmer, J. and Teller, D. Y.** (2002). Infant photometry: are mean adult isoluminance values a sufficient approximation to individual infant values? *Vision Res* **42**, 1639-49.

**Pfeiffer, B. D., Jenett, A., Hammonds, A. S., Ngo, T. T., Misra, S., Murphy, C., Scully, A., Carlson, J. W., Wan, K. H., Laverty, T. R. et al.** (2008). Tools for neuroanatomy and neurogenetics in Drosophila. *Proc Natl Acad Sci U S A* **105**, 9715-20.

**Pfeiffer, B. D., Ngo, T. T., Hibbard, K. L., Murphy, C., Jenett, A., Truman, J. W. and Rubin, G. M.** (2010). Refinement of tools for targeted gene expression in Drosophila. *Genetics* **186**, 735-55.

**Pick, B.** (1974). Visual flicker induces orientation behavior in the fly *Musca*. *Z Naturforsch C* **29**, 310-312.

**Pick, B.** (1976). Visual-pattern discrimination as an element of the fly's orientation behavior. *Biol Cybern* **23**, 171-180.

**Pick, S. and Strauss, R.** (2005). Goal-driven behavioral adaptations in gap-climbing Drosophila. *Curr Biol* **15**, 1473-8.

**Poggio, T. and Reichardt, W.** (1976). Visual control of orientation behavior in the fly. Part 2: towards the underlying neural interactions. *Q Rev Biophys* **9**, 377-438.

**Pologruto, T. A., Sabatini, B. L. and Svoboda, K.** (2003). ScanImage: flexible software for operating laser scanning microscopes. *Biomed Eng Online* **2**, 13.

**Pulver, S. R., Pashkovski, S. L., Hornstein, N. J., Garrity, P. A. and Griffith, L. C.** (2009). Temporal dynamics of neuronal activation by Channelrhodopsin-2 and TRPA1 determine behavioral output in Drosophila larvae. *J Neurophysiol* **101**, 3075-88.

**Pyza, E. and Meinertzhagen, I. A.** (1999). Daily rhythmic changes of cell size and shape in the first optic neuropil in Drosophila melanogaster. *J Neurobiol* **40**, 77-88.

**Reichardt, W.** (1961). Autocorrelation, a Principle for the Evaluation of Sensory Information by the Central Nervous System. In *Sensory Communication* (ed. W. A. Rosenblith), pp. 303-317. New York: John Wiley.

**Reichardt, W. and Poggio, T.** (1976). Visual control of orientation behaviour in the fly. Part I. A quantitative analysis. *Q Rev Biophys* **9**, 311-75, 428-38.

**Reichardt, W. and Wenking, H.** (1969). Optical detection and fixation of objects by fixed flying flies. *Naturwissenschaften* **56**, 424-5.

**Reiff, D. F., Plett, J., Mank, M., Griesbeck, O. and Borst, A.** (2010). Visualizing retinotopic half-wave rectified input to the motion detection circuitry of Drosophila. *Nat Neurosci* **13**, 973-978.

**Reiser, M. B. and Dickinson, M. H.** (2008). A modular display system for insect behavioral neuroscience. *J Neurosci Methods* **167**, 127-139.

**Reiser, M. B. and Dickinson, M. H.** (2010). Drosophila fly straight by fixating objects in the face of expanding optic flow. *J Exp Biol* **213**, 1771-81.

**Ribi, W. A.** (1978). Gap junctions coupling photoreceptor axons in the 1st optic ganglion of the fly. *Cell Tissue Res* **195**, 299-308.

**Rieke, F. and Rudd, M. E.** (2009). The challenges natural images pose for visual adaptation. *Neuron* **64**, 605-16.

**Rister, J., Pauls, D., Schnell, B., Ting, C. Y., Lee, C. H., Sinakevitch, I., Morante, J., Strausfeld, N. J., Ito, K. and Heisenberg, M.** (2007). Dissection of the peripheral motion channel in the visual system of Drosophila melanogaster. *Neuron* **56**, 155-70.

**Rivera-Alba, M.** (2011). Wiring economy in the first stage of visual processing in *Drosophila Melanogaster*. In *Facultad de Ciencias*, vol. Phd., pp. 181. Madrid: Universidad Autonoma de Madrid.

**Rivera-Alba, M., Vitaladevuni, S. N., Mischenko, Y., Lu, Z., Takemura, S. Y., Scheffer, L., Meinertzhagen, I. A., Chklovskii, D. B. and de Polavieja, G. G.** (2011). Wiring economy and volume exclusion determine neuronal placement in the *Drosophila* brain. *Curr Biol* **21**, 2000-5.

**Sanes, J. R. and Zipursky, S. L.** (2010). Design principles of insect and vertebrate visual systems. *Neuron* **66**, 15-36.

**Sato, T.** (1989). Reversed apparent motion with random dot patterns. *Vision Res* **29**, 1749-58.

**Schilstra, C. and Hateren, J. H.** (1999). Blowfly flight and optic flow. I. Thorax kinematics and flight dynamics. *J Exp Biol* **202** (Pt 11), 1481-90.

**Schnell, B., Joesch, M., Forstner, F., Raghu, S. V., Otsuna, H., Ito, K., Borst, A. and Reiff, D. F.** (2010). Processing of horizontal optic flow in three visual interneurons of the *Drosophila* brain. *J Neurophysiol* **103**, 1646-57.

**Scholes, J.** (1969). The electrical responses of the retinal receptors and the lamina in the visual system of the fly *Musca*. *Kybernetik* **6**, 149-62.

**Schulz, D. J., Goaillard, J. M. and Marder, E.** (2006). Variable channel expression in identified single and electrically coupled neurons in different animals. *Nat Neurosci* **9**, 356-62.

**Schuppe, H. and Hengstenberg, R.** (1993). Optical properties of the ocelli of *Calliphora erythrocephala* and their role in the dorsal light response. *J Comp Physiol A* **173**, 143-149.

**Scott, E. K., Reuter, J. E. and Luo, L.** (2003). Dendritic development of *Drosophila* high order visual system neurons is independent of sensory experience. *BMC Neurosci* **4**, 14.

**Seelig, J. D., Chiappe, M. E., Lott, G. K., Dutta, A., Osborne, J. E., Reiser, M. B. and Jayaraman, V.** (2010). Two-photon calcium imaging from head-fixed *Drosophila* during optomotor walking behavior. *Nat Methods*.

**Shapley, R. M. and Enroth-Cugell, C.** (1984). Visual Adaptation and Retinal Gain Controls. In *Progress in retinal research* **3**, vol. 3.

**Shaw, S. R.** (1984). Early visual processing in insects. *J Exp Biol* **112**, 225-51.

**Shaw, S. R. and Stowe, S.** (1982). Freeze-fracture evidence for gap-junctions connecting the axon terminals of dipteran photoreceptors. *Journal of Cell Science* **53**, 115-141.

**Shioiri, S. and Cavanagh, P.** (1990). ISI produces reverse apparent motion. *Vision Res* **30**, 757-68.

**Simpson, J. H.** (2009). Mapping and manipulating neural circuits in the fly brain. *Adv Genet* **65**, 79-143.

**Sinakevitch, I. and Strausfeld, N. J.** (2004). Chemical neuroanatomy of the fly's movement detection pathway. *J Comp Neurol* **468**, 6-23.

**Sinakevitch, I. and Strausfeld, N. J.** (2006). Comparison of octopamine-like immunoreactivity in the brains of the fruit fly and blow fly. *J Comp Neurol* **494**, 460-75.

**Single, S. and Borst, A.** (1998). Dendritic integration and its role in computing image velocity. *Science* **281**, 1848-50.

**Skingsley, D. R., Laughlin, S. B. and Hardie, R. C.** (1995). Properties of histamine-activated chloride channels in the large monopolar cells of the dipteran compound eye - a comparative study. *J Comp Physiol A* **176**, 611-623.

**Smear, M. C., Tao, H. W., Staub, W., Orger, M. B., Gosse, N. J., Liu, Y., Takahashi, K., Poo, M. M. and Baier, H.** (2007). Vesicular glutamate transport at a central synapse limits the acuity of visual perception in zebrafish. *Neuron* **53**, 65-77.

**Snyder, A. W.** (1979). Physics of vision in compound eyes. In *Handbook of Sensory Physiology*, (ed. H. Autrum), pp. 225-313. Berlin: Springer.

**Srinivasan, M.** (1993). Even insects experience visual illusions. *Current Science* **64**, 649-655.

**Srinivasan, M. and Dvorak, D. R.** (1980). Spatial Processing of Visual Information in the Movement -Detecting Pathway of the Fly. *J Comp Physiol A* **140**, 1-23.

**Srinivasan, M. V.** (1990). Generalized gradient schemes for the measurement of two-dimensional image motion. *Biol Cybern* **63**, 421-31.

**Srinivasan, M. V., Laughlin, S. B. and Dubs, A.** (1982). Predictive coding: a fresh view of inhibition in the retina. *Proc R Soc Lond B Biol Sci* **216**, 427-59.

**Stange, G.** (1981). The ocellar component of flight equilibrium control in dragonflies. *J Comp Physiol A* **141**, 335-347.

**Steinman, R. M., Pizlo, Z. and Pizlo, F. J.** (2000). Phi is not beta, and why Wertheimer's discovery launched the Gestalt revolution. *Vision Res* **40**, 2257-64.

**Strausfeld, N.** (1976). *Atlas of an Insect Brain*. Berlin: Springer-Verlag.

**Strausfeld, N. J. and Nassel, D. R.** (1980). Neuroarchitecture of brain regions that subserve the compound eyes of crustaceans and insects. In *Handbook of sensory physiology*, vol. VII/6B (ed. H. Autrum), pp. 1-132. Berlin: Springer.

**Straw, A. D., Branson, K., Neumann, T. R. and Dickinson, M. H.** (2011). Multi-camera real-time three-dimensional tracking of multiple flying animals. *J R Soc Interface* **8**, 395-409.

**Takemura, S. Y., Karuppusudurai, T., Ting, C. Y., Lu, Z., Lee, C. H. and Meinertzhagen, I. A.** (2011). Cholinergic circuits integrate neighboring visual signals in a *Drosophila* motion detection pathway. *Curr Biol* **21**, 2077-84.

**Takemura, S. Y., Lu, Z. and Meinertzhagen, I. A.** (2008). Synaptic circuits of the *Drosophila* optic lobe: the input terminals to the medulla. *J Comp Neurol* **509**, 493-513.

**Tammero, L. F., Frye, M. A. and Dickinson, M. H.** (2004). Spatial organization of visuomotor reflexes in *Drosophila*. *J Exp Biol* **207**, 113-22.

**Taylor, C. P.** (1981). Contribution of compound eyes and ocelli to steering of locusts in flight.1. Behavioral analysis. *J Exp Biol* **93**, 1-18.

**Theobald, J. C., Ringach, D. L. and Frye, M. A.** (2010). Dynamics of optomotor responses in *Drosophila* to perturbations in optic flow. *J Exp Biol* **213**, 1366-75.

**Thum, A. S., Knapke, S., Rister, J., Dierichs-Schmitt, E., Heisenberg, M. and Tanimoto, H.** (2006). Differential potencies of effector genes in adult *Drosophila*. *J Comp Neurol* **498**, 194-203.

**Tian, L., Hires, S. A., Mao, T., Huber, D., Chiappe, M. E., Chalasani, S. H., Petreanu, L., Akerboom, J., McKinney, S. A., Schreiter, E. R. et al.** (2009). Imaging neural activity in worms, flies and mice with improved GCaMP calcium indicators. *Nat Methods* **6**, 875-81.

**Ting, C. Y. and Lee, C. H.** (2007). Visual circuit development in *Drosophila*. *Curr Opin Neurobiol* **17**, 65-72.

**Triphan, T., Poeck, B., Neuser, K. and Strauss, R.** (2010). Visual targeting of motor actions in climbing *Drosophila*. *Curr Biol* **20**, 663-8.

**Uusitalo, R. O., Juusola, M., Kouvalainen, E. and Weckstrom, M.** (1995a). Tonic transmitter release in a graded potential synapse. *J Neurophysiol* **74**, 470-3.

**Uusitalo, R. O., Juusola, M. and Weckstrom, M.** (1995b). Graded responses and spiking properties of identified first-order visual interneurons of the fly compound eye. *J Neurophysiol* **73**, 1782-92.

**van der Schaaf, A. and van Hateren, J. H.** (1996). Modelling the power spectra of natural images: statistics and information. *Vision Res* **36**, 2759-70.

**van Hateren, J. H.** (1986). Electrical coupling of neuro-ommatidial photoreceptor cells in the blowfly. *J Comp Physiol A* **158**, 795-811.

**van Hateren, J. H.** (1997). Processing of natural time series of intensities by the visual system of the blowfly. *Vision Res* **37**, 3407-16.

**van Hateren, J. H. and Laughlin, S. B.** (1990). Membrane parameters, signal transmission, and the design of a graded potential neuron. *J Comp Physiol A* **166**, 437-48.

**van Santen, J. P. and Sperling, G.** (1985). Elaborated Reichardt detectors. *J Opt Soc Am A* **2**, 300-21.

**Varija Raghu, S., Reiff, D. F. and Borst, A.** (2011). Neurons with cholinergic phenotype in the visual system of Drosophila. *J Comp Neuro* **519**, 162-76.

**Vigier, P.** (1907). On the photoreceptive endings in the compound eyes of Muscids. *Comptes Rendus Hebdomadaires Des Seances De L Academie Des Sciences* **145**, 532-536.

**Vigier, P.** (1908). Sur l'existence reelle et le role des appendices piriformes des neurones. Le neurone perioptique des Diptera. *Compte Rendu de la Societe de Biologie Paris* **64**.

**Wagner, H.** (1982). Flow-field variables trigger landing in flies. *Nature* **297**, 147-148.

**Wald, G.** (1964). The Receptors of Human Color Vision. *Science* **145**, 1007-16.

**Wang-Bennett, L. T. and Glantz, R. M.** (1987). The functional organization of the crayfish lamina ganglionaris. I. Nonspiking monopolar cells. *J Comp Physiol A* **161**, 131-45.

**Weber, P., Kula-Eversole, E. and Pyza, E.** (2009). Circadian control of dendrite morphology in the visual system of Drosophila melanogaster. *PLoS One* **4**, e4290.

**Weckstrom, M., Juusola, M. and Laughlin, S. B.** (1992). Presynaptic enhancement of signal transients in photoreceptor terminals in the compound eye. *Proc R Soc Lond B Biol Sci* **250**, 83-89.

**Weckstrom, M. and Laughlin, S.** (2010). Extracellular Potentials Modify the Transfer of Information at Photoreceptor Output Synapses in the Blowfly Compound Eye. *Journal of Neuroscience* **30**, 9557-9566.

**Wehrhahn, C. and Hausen, K.** (1980). How is Tracking and Fixation Accomplished in the Nervous System of the Fly? *Biol Cybern* **38**, 179-186.

**Wehrhahn, C., Hausen, K. and Zanker, J. M.** (1981). Is the Landing Response of the Housefly (Musca) Driven by Motion of a Flow Field? *Biol Cybern* **41**, 91-99.

**Wehrhahn, C. and Rapf, D.** (1992). ON- and OFF-pathways form separate neural substrates for motion perception: psychophysical evidence. *J Neurosci* **12**, 2247-50.

**Werblin, F. S. and Dowling, J. E.** (1969). Organization of the retina of the mudpuppy, *Necturus maculosus*. II. Intracellular recording. *J Neurophysiol* **32**, 339-55.

**Wertheimer, M.** (1912). Experimentelle Studien über das Sehen von Bewegung. *Zeitschrift Fur Vergleichende Physiologie* **61**, 161-265.

**White, J. G., Southgate, E., Thomson, J. N. and Brenner, S.** (1986). The structure of the nervous-system of the nematode *Caenorhabditis-Elegans*. *Philos Trans R Soc Lond B Biol Sci* **314**, 1-340.

**Wilson, R. I. and Laurent, G.** (2005). Role of GABAergic inhibition in shaping odor-evoked spatiotemporal patterns in the *Drosophila* antennal lobe. *J Neurosci* **25**, 9069-79.

**Wilson, R. I., Turner, G. C. and Laurent, G.** (2004). Transformation of olfactory representations in the *Drosophila* antennal lobe. *Science* **303**, 366-70.

**Wolf, R. and Heisenberg, M.** (1986). Visual orientation in motion-blind flies is an operant behaviour. *Nature* **323**, 154.

**Xia, S. Z., Liu, L., Feng, C. H. and Guo, A. K.** (1997). Nutritional effects on operant visual learning in *Drosophila melanogaster*. *Physiol Behav* **62**, 263-71.

**Zettler, F.** (1969). Course of output-input ratio in relation to frequency and state of adaptation measured at a single photo-receptor in compound eye of *Calliphora erythrocephala*. *Zeitschrift Fur Vergleichende Physiologie* **64**, 432-&.

**Zettler, F. and Jarvilehto, M.** (1972). Lateral inhibition in an insect eye. *Zeitschrift Fur Vergleichende Physiologie* **76**, 233-&.

**Zettler, F. and Jarvilehto, M.** (1973). Active and passive axonal propagation of non-spiking signals in retina of *Calliphora*. *Zeitschrift Fur Vergleichende Physiologie* **85**, 89-104.

**Zettler, F. and Straka, H.** (1987). Synaptic chloride channels generating hyperpolarizing ON-responses in monopolar neurons of the blowfly visual-system. *J Exp Biol* **131**, 435-438.

**Zheng, L., de Polavieja, G. G., Wolfram, V., Asyali, M. H., Hardie, R. C. and Juusola, M.** (2006). Feedback Network Controls Photoreceptor Output at the of First Layer of Visual Synapses in *Drosophila*. *Journal of General Physiology* **127**, 495-510.

**Zheng, Y., Hirschberg, B., Yuan, J., Wang, A. P., Hunt, D. C., Ludmerer, S. W., Schmatz, D. M. and Cully, D. F.** (2002). Identification of two novel *Drosophila melanogaster* histamine-gated chloride channel subunits expressed in the eye. *J Biol Chem* **277**, 2000-5.

**Zhu, Y., Nern, A., Zipursky, S. L. and Frye, M. A.** (2009). Peripheral Visual Circuits Functionally Segregate Motion and Phototaxis Behaviors in the Fly. *Curr Biol* **19**, 613-619.